Title	An evaluation of orogenic kinematic evolution utilizing crystalline and magnetic anisotropy in granitoids
Author(s)	McCarthy, William J.
Publication date	2013
Original citation	McCarthy, W. J. 2013. An evaluation of orogenic kinematic evolution utilizing crystalline and magnetic anisotropy in granitoids. PhD Thesis, University College Cork.
Type of publication	Doctoral thesis
Rights	**© 2013, William J. McCarthy** http://creativecommons.org/licenses/by-nc-nd/3.0/
Embargo information	No embargo required
Item downloaded from	http://hdl.handle.net/10468/1669

An Evaluation of Orogenic Kinematic Evolution Utilizing Crystalline and Magnetic Anisotropy in Granitoids

---

Volume 2 of 2 (Appendices)

William J. McCarthy

A thesis submitted for the degree of

Doctor of Philosophy

June 2013

Research Supervisors:

Dr. R.J. Reavy

Prof. M.S. Petronis

National University of Ireland, Cork
School of Biological, Earth & Environmental Sciences (Discipline of Geology)
College of Science, Engineering and Food Science
Head of School: Prof. John O'Halloran

Notes On Appendices

Notes on Appendices

Six appendices accompany this thesis. Appendices A, B, C and D are intended to be used in conjunction with the main text and so a hard copy of these is provided here, in Volume 2 of the thesis. Appendix A is the map folder, Appendix B contains details of rock magnetic analytical procedures, Appendix C contains abbreviated data tables and Appendix D contains supplementary information on aspects of rock magnetic remanence, susceptibility and demagnetisation that are not detailed in the main text.

Appendix E contains the original and spread sheet data tables that were compiled during the course of the current work. Appendix F contains copies of open source software which was use to manipulate raw data. As such these two appendices are only provided on a CD (also contains appendices A, B, C and D) which accompanies the hard copy appendix.

The content of these appendices are as follows;

Appendix E (accompanying CD)

- Data Bank
  - Reduced and primary isotopic data and sample attributes
  - Summarised rock magnetic data
    - AMS Data
      - Omey AMS (Original and reduced data)
      - Roundstone AMS (Original and reduced data)
      - Carna AMS (Original and reduced data)
    - Rock Magnetic Experiment Data
      - High temperature low field susceptibility
      - Cryogenic low field susceptibility
      - The Lowrie-Fuller test
      - IRM acquisition and back-field demagnetisation
      - Thermomagnetic analysis of three-component IRM

Appendix F (accompanying CD)

- Open Source Software
  - Isoplot Installation files
  - AMS Software
    - Anisoft43-Install.rar
    - Bodge1.exe
    - Jelanew5.exe
    - Jelanew6.exe
    - Manifig.exe
    - Measaver.exe
    - measuer.exe
    - Pitchrev.exe
    - ERRDOC33.rar (KLY3 setup and trouble shoot)
    - Carteasian_to_Polar.xls
  - Rock Magnetic Experiments
    - CORRECT.txt (correction file for high temperature low field susceptibility exp.)
    - cureval8-install.rar
    - remasoft30-install.rar
    - Ti_X_Compext.xls
    - LowT_datareduction.mbd

Appendix A:

Map Folder

Appendix A: Map Folder

The maps that are contained in the map folder ("Fig.*" below) are intended to be used in conjunction with the text when referred to. Supplementary digital maps Sup. 1, Sup. 2 and Sup. 3 are provided in .pdf format owing to the resolution of data available (see Appendix A on CD).

Fig. 7.2 - New geological map of the Omey Granite.

Fig. 7.30 - AMS data from the Omey Pluton projected based on Shape Anisotropy (Tj).

Fig. 7.31 - Interpreted AMS data from the Omey Pluton with polar and stereonet projections.

Fig. 7.32 - Overlay of AMS stereographic projections from the Omey Pluton.

Fig. 8.21 - AMS data from the Roundstone Pluton projected based on Shape Anisotropy (Tj) with representative stereographic projections.

Fig. 8.22 - Interpreted AMS fabrics from the Roundstone Pluton.

Fig. 9.1 - Modified geological map of the Carna Pluton from new and compiled existing data.

Fig. 9.17 - AMS data from the Carna Pluton projected based on Shape Anisotropy (Tj) with representative stereographic projections.

Fig. 9.18 - Interpreted AMS data from the Carna Pluton with polar and stereonet projections.

Sup. 1 - All AMS from the Omey Pluton plotted onto the map as southern hemisphere stereographic projections.

Sup. 2 - All AMS from the Roundstone Pluton plotted onto the map as southern hemisphere stereographic projections.

Sup. 3 - All AMS from the Carna Pluton plotted onto the map as southern hemisphere stereographic projections.

Appendix B:

Rock Magnetic Analytical Procedures

Anisotropy of Magnetic Susceptibility

A summary of all AMS practices and procedures may be found in Tarling and Hrouda (1993) and Borradaile and Jackson (2004).

Equipment;

Field hammer & chisel, Garman *e*trex H GPS unit, Markers, compass clinometer, drill press, abrasive non-magnetic diamond coring drill bit (24mmØ, 125mm long), abrasive non-magnetic diamond cutting disk, Agico KLY-3S Kappabridge

Field Sampling;

- An orientated block of at least 2000cm^3 was sampled from each sample site.
- Interference between the compass needle and constituent minerals of the rock was tested and found not to be an issue in each case.
- An orientation line was marked directly on to the outcrop using a compass clinometer before the block was removed (left hand rule).
- The sample sites six figure grid reference was recorded using a handheld GPS.

Drilling;

- The orientation line on each block sample was extended across the entire specimen.
- Each block was clapped in position on the drill press table and the pitch of the orientation line relative to horizontal was recorded for reorientation purposes.
- Between 3-5 120mm cores were drilled from each block using a abrasive diamond coring drill bit cooled by re-circulating water.
- Each core was removed from the block sample, dried and an orientation line drawn along the length of the core parallel to the orientation line on the surface of the core, the down hole direction was marked on the right hand side of the core (Fig. B.1).
- Each core was then cut into 24x22cm right-angle cylinders using a non-magnetic abrasive cutting disk cooled by water.
- Each cylinder corresponds to a single sub-specimen, between 7-25 sub-specimens were retrieved from each block sample.

Measuring AMS;

- Each sub-specimen was placed in the Kappabridge sample holder in three mutually orthogonal positions.
- In each position, the sample was lowered into the Kappabridge and rotated through 360° on a single axis as low field magnetic susceptibility was measured across the sub-specimen.
- A bulk susceptibility measurement was taken.
- This process was repeated for each sub-specimen in each block sample.

Data management;

Two data files were compiled for each block sample. The ".ASC" carries the calculated averaged AMS of each sub-sample. The ".RAN" contains irrelevant coded information from the Kappabridge. This data requires further process as follows (open source software in Appendix F) The *.ASC file and recorded orientation data of the sample block (dill table and field) were processed through the bodge1.exe, measure.exe, mesaver.exe, jelanew5.exe, jalenew6.exe and manifig.exe programs to obtain mean normalised and un-normalised AMS data for each sample site in the following way;

1. *.asc file input into bodge1.exe
   enter orientations from the field and drill table
   output - *.out
   (count number of sub-specimens and enter this at end of .txt file)

2. *.out file input into measure.exe
   output - *.lfp
   *.plt
   *.res

3. *.out file input into mesaver.exe (field corrected)
   output - *.ave

4. *.ave file input into jelanew5.exe (mean normalised)
   output - *.cv5
   *.pl5

*.rs5

5. *.ave file input into jelanew6.exe (mean un-normalised)

output - *.cv6

*.pl6

*.rs6

6. Input *.plt, *.pl5 or *.pl6 into manifig.exe or Anisoft42 to output the plotted data as southern hemisphere stereographic projections. Mean K1, K2 and K3 vectors with 95% confidence ellipses or individual sub-specimens may be plotted.

7. Import *.rs5 and *.rs6 into Microsoft Excel spreadsheet to compile, reduce and project (Arc GIS was used for this purpose in this case)

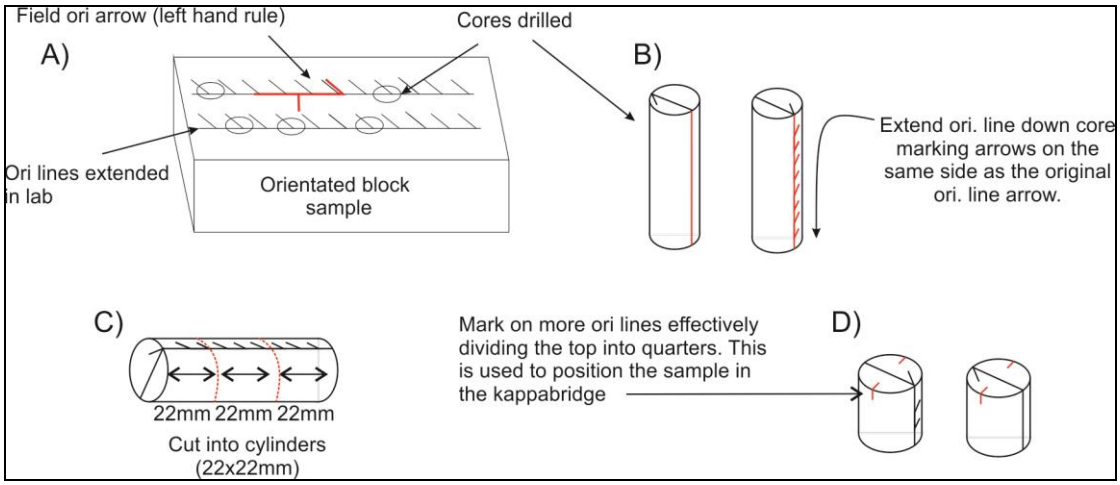

Fig. B.1 Sample preparation for AMS analysis

<u>High temperature low field susceptibility</u>

The principles of the experiment are discussed in Dunlop and Ozdemir (1997)

<u>Equipment;</u>

Porcelain mortar and pestle, scales, 6x200mm quartz test tube, MFK1-A Kappabridge with CS4 attachment with argon atmosphere attachment.

<u>Analytical Process;</u>

- A representative sub-specimen from each block sample was crushed to fine power and homogenised
- 5grams of powder was placed in a sterile quartz test tube
- The CS4 thermometer was inserted into the test tube and the tube flooded with argon
- The sample was placed in the Kappabridge and heated from room temperature to 700°C and cooled back to room temperature at an even rate over ~20mins, a bulk low field magnetic susceptibility reading was taken every ~5 seconds.

Data management;

A single *.CUR file is generated containing the temperature and corresponding bulk susceptibility value. This is imported directly into Cureval 8 (open source software, see Appendix F) for data analysis.

Cryogenic low field susceptibility

The principles of the experiment are discussed in Dunlop and Ozdemir (1997)

Equipment

MFK1-A Kappabridge, Fluke 289 True-rms industrial logging multimeter with thermocouple, epoxy resin (e.g. Ever Build Stick2), high thermo-conductivity paste (e.g. Acrolab Isopaste), diamond tipped abrasive cutting disk, liquid nitrogen.

Analytical Procedure

- A representative sub-specimen was selected from each block sample and submersed in liquid nitrogen for 5min.
- The sub-specimen was removed and immediately placed in the Kappabridge where bulk susceptibly measurements were made over 20 +/-1 seconds intervals until the specimen reached room temperature.
- The sub-specimen was removed and cut half way through with an abrasive cutting disk
- A thermocouple was positioned at the core of the sub-specimen, packed in high conductivity paste and sealed in position with epoxy resin
- The specimen was submerged in liquid nitrogen for 5 minutes
- The sub-specimen was removed from the nitrogen and the time taken for the sub-specimen to warm to room temperature is recorded using a multimeter thermocouple.

Data management;

The data set from the heating - susceptibly and heating only procedures are entered into an access data base which is queered to match the second intervals of each experiment. In this way the temperature at each 20 +/- 1sec interval is attributed to the correct bulk susceptibly value at a particular temperature (custom built Access data base attached in Appendix F).

Data is exported, analysed and graphed in Microsoft Excel.

Lowrie Fuller Test

This experiment follows the procedures of Lowrie and Fuller (1971).

Equipment;

D-tech D-2000 AF demagnetizer, JR-6A dual speed spinner magnetometer, DC impulse electromagnetic coil

Analytical Procedure

A representative sub-specimen was selected and the Natural Remanent Magnetisation (NRM) measured in the spinner magnetometer.

NRM was progressively stripped in an AF-demagnetising field at increments of 0mT, 5mT, 10mT, 15mT, 20mT, 25mT, 30mT, 40mT, 50mT, 60mT, 70mT, 80mT, 90mT, 100mT, 125mT and remanent magnetisation recorded at each interval.

Following AF-demagnetisation, an anhysteretic remanent magnetisation (ARM) (0.1T DC bias and 125mT AF) was induced on the sample along three orthogonal axes.

ARM was measured at intervals during stepwise demagnetisation (same intervals as above).

Following AF-demagnetisation, an IRM was induced along three orthogonal axes of the sub-specimen (1.3T on homemade impulse electromagnetic coil)

IRM was measured at intervals during stepwise demagnetisation (same intervals as above).

Data management;

All data was saved to a *.JR6 file, imported into Microsoft Excel and sorted according to sample number and type of magnetisation (NRM, NRM or IRM). Data was then graphed and analysed accordingly. Analysis of NRM data in Remasoft may also be desirable (Appendix F)

IRM acquisition and back-field demagnetisation

This experiment is based on the concepts discussed in (Neel 1955) and Dunlop and Ozdemir (1997);

Equipment;

D-tech D-2000 AF demagnetizer, JR-6A dual speed spinner magnetometer, DC impulse electromagnetic coil

Analytical Procedure;

- A representative sub-specimen was selected, fully AF cleaned in a field of 125mT and magnetic remanence measured.
- A single axis of the sub-specimen was exposed to progressively increasing DC fields (0, 0.01, 0.03, 0.05, 0.07, 0.1, 0.13, 0.16, 0.2, 0.25, 0.3, 0.4 0.5, 0.7, 0.9, 1.25, 2, 2.5 Tesla) and magnetic remanence measured at each interval.
- The specimen was inverted, placed in the electromagnetic coil and exposed to progressively increasing DC fields i.e. BIRM (0, 0.01, 0.02, 0.03, 0.04, 0.05, 0.06, 0.08, 0.01Tesla), magnetic remanence was measure at each interval.

Data management;

Data was saved to *.JR6 files during the experiment and may be directly imported into Microsoft Excel of data reduction, projection and interpretation.

Thermomagnetic Analysis of Three-Component IRM

This experiment is based on the procedures of Lowrie (1990) and is modified to suite the mineral spectra of the current samples.

Equipment;

D-tech D-2000 AF demagnetizer, JR-6A dual speed spinner magnetometer, DC impulse electromagnetic coil, a ASC TD48 thermal demagnetiser in a zero field

Analytical Process;

- A representative sub-specimen was selected, fully AF cleaned in a field of 125mT and magnetic remanence measured.

- A 3T, 0.3T and 0.03T DC field was imposed parallel to the X, Y and Z axis of the sub-specimen in that order.
- Sub-specimen magnetic remanence was measured.
- Thermal demagnetisation was carried out in a zero field at progressive increments (100°C, 200°C, 300°C, 350°C, 400°C, 450°C, 500°C, 550°C, 575°C, 600°C, 625°C, 650°C), magnetic remanence was measure at each interval.

Data management;

Data was saved to both *.JR6 and *.TXT files. The *.JR6 file contains the magnitude of the magnetic remanence vector for each of the three axes analysed (i.e. X, Y and Z axes) for each sample at each temperature interval. The magnitude of the Modulus vector for each sample at each temperature interval is detailed in the *.TXT file. This data may be ready graphed once all negative magnitude values are converted to positive values. The Modulus value (M) relates to the X, Y and Z component vectors through the equation $SQRT(X^2 + Y^2 + Z^2) = M$.

Appendix C:

Summarised Data Tables

Appendix C: Summarised Data Tables

Guide;

This appendix is a hard copy of summarised magnetic susceptibility and geochronology data that has been applied in the work presented. The data are provided as a short hand reference to the most important data in this thesis. Data pertaining to rock magnetic experiments, including cryogenic and high temperature susceptibility, magnetic remanence and demagnetisation tests, are not included. A full digital data bank of original files and a data base of magnetic remanence, magnetic susceptibility and chronological data is provided in Appendix E which accompanies the thesis on CD.

Section 1 contains summarised geochronology data which was obtained from LA-ICP-MS carried out on resin mounted zircon separates.

Section 2 includes the principal AMS data recovered from each pluton along with the calculated parameters that are most often applied in the current work. Sample identification numbers as well as grid co-ordinates are provided.

Section 1; Isotopic Data

Isotope data from LA-ICP-MS Sample RD1

Sample Run	Approx U PPM	Approx U PPM Int2SE	Approx Th PPM	Approx Th PPM Int2SE	Approx Pb PPM	Approx Pb PPM Int2SE	Final U-Th Ratio	Final U-Th Ratio Int2SE	Final 207-235	Final 207-235 Int2SE	Final 206-238	Final 206-238 Int2SE	Final 207-206	Final 207-206 Int2SE	Error Correlation 6 38vs7 35	Final Age 206-238	Final Age 206-238 Int2SE	Final Age 207-235	Final Age 207-235 Int2SE	Final Age 207-206	Final Age 207-206 Int2SE	Final Disc Percent	Final Disc Percent Int2SE
GG17_1	679	66	359	27	74	4.3	1.754	0.059	0.522	0.012	0.0695	0.0013	0.0553	0.0013	0.4729	432.9	7.6	426.1	8.2	402	39	3.48	0.68
GG17_2	445	18	322	11	60.8	1.6	1.382	0.064	0.521	0.016	0.0685	0.0024	0.0547	0.0022	0.16926	427	15	425	10	452	71	6.5	1.2
GG17_3	499	22	297.5	8.7	57.7	1.3	1.664	0.055	0.518	0.015	0.0683	0.0016	0.0538	0.002	0.14549	425.9	9.7	425.1	9.5	360	56	5.6	1.1
GG17_4	757	66	708	30	140.6	6.3	1.021	0.078	0.546	0.012	0.0703	0.001	0.0559	0.0014	0.28751	438	6.2	442.1	8	469	34	4.04	0.73
GG17_5	700	17	457	13	90.6	2.4	1.551	0.053	0.538	0.014	0.0716	0.0021	0.0542	0.0016	0.47616	446	12	436.5	9.5	378	52	4.84	0.87
GG17_6	529	78	269	32	53.6	5.8	1.87	0.055	0.479	0.014	0.0635	0.0017	0.0546	0.0019	0.47625	397	10	396.9	9.5	405	51	5	1.1
GG17_7	726	60	573	48	113.4	7.4	1.227	0.023	0.546	0.011	0.0714	0.0016	0.0549	0.0015	0.34546	444.3	9.5	441.8	7.4	440	38	3.93	0.79
GG17_8	580	42	424	51	77.4	8.5	1.352	0.077	0.503	0.013	0.0661	0.0014	0.0541	0.0014	0.31161	412.6	8.7	414.3	8.5	394	28	3.94	0.87
GG17_9	543	31	264	12	52.6	2	1.973	0.045	0.529	0.014	0.0693	0.0012	0.0552	0.0017	0.10733	431.8	7.5	433.6	8.5	422	57	4.7	0.87
GG17_10	609	21	154.9	2.8	32.9	1.1	3.91	0.13	0.507	0.015	0.0676	0.0017	0.0533	0.0018	0.29104	421	10	415.9	9.8	364	55	5.45	0.97
GG17_11	899	43	1737	83	323.3	9.4	0.575	0.012	0.529	0.012	0.0681	0.0014	0.0557	0.0015	0.34251	424.6	8.2	431.7	7.8	446	41	3.89	0.85
GG17_12	586	19	458	24	81.2	3.4	1.429	0.04	0.497	0.013	0.0644	0.0012	0.0557	0.0017	0.59599	402.3	7.1	409.2	8.8	443	43	5.3	0.87
GG17_13	910	44	490	34	95.9	6.9	2.014	0.069	0.49	0.013	0.0665	0.0015	0.0539	0.0016	0.39343	415.1	8.8	405.8	8.3	391	40	4.52	0.85
GG17_14	462	25	281	15	52.6	1.6	1.797	0.047	0.517	0.015	0.0676	0.0018	0.0551	0.002	0.11492	422	11	422.6	9.8	425	56	5.3	1.1
GG17_15	1350	150	726	96	142	16	1.998	0.05	0.516	0.012	0.0689	0.0015	0.0546	0.0014	0.29082	429.2	9.1	422	7.7	395	41	4.23	0.77
GG17_16	583	11	281	9.5	54.9	1.9	2.22	0.076	0.488	0.013	0.0668	0.0022	0.0539	0.0017	0.46436	417	13	404.8	9.4	381	52	5.29	0.91
GG17_17	989	41	1039	23	197.8	2.4	1.027	0.033	0.504	0.01	0.0667	0.0013	0.0549	0.0011	0.32232	415.9	8	415.1	6.6	411	28	3.09	0.67
GG17_18	795	56	577	51	109.4	8.5	1.476	0.041	0.513	0.012	0.0671	0.0017	0.0536	0.0017	0.15369	418	10	421.3	8.1	403	59	5.2	1
GG17_19	1039	71	499	42	96.1	6.8	2.2	0.059	0.5193	0.0088	0.0671	0.0017	0.0555	0.0016	0.081111	419	10	424.5	5.9	449	52	4.64	0.95
GG17_20	1181	55	1076	79	214	16	1.158	0.051	0.502	0.011	0.0663	0.0015	0.0545	0.0015	0.28832	413.6	9.1	413.9	7.9	450	42	4.47	0.85
GG17_21	1152	54	721	31	159.5	5.7	1.651	0.046	0.48	0.012	0.0638	0.002	0.0551	0.0021	0.29005	398	12	398.9	8.1	421	65	6.06	0.95
GG17_22	750	53	667	14	135.5	1.9	1.141	0.061	0.523	0.013	0.0687	0.0016	0.0542	0.0019	0.13755	428	9.9	426.4	8.3	383	58	5.29	0.9
GG17_23	1011	71	771	82	157	15	1.467	0.078	0.528	0.013	0.0714	0.0018	0.0538	0.0013	0.36768	445	11	429.8	8.4	403	32	4.19	0.88
GG17_24	441	35	189	27	32.4	1.8	2.44	0.37	0.461	0.029	0.0543	0.0026	0.0591	0.0054	0.17647	341	16	385	21	600	120	7.7	3.1
GG17_25	533	56	181	18	37.3	3.6	3.04	0.11	0.513	0.017	0.0685	0.0014	0.0544	0.0017	0.27873	427	8.7	420	11	426	35	4.15	0.86
GG17_26	1242	42	992	39	207.4	6.5	1.358	0.045	0.531	0.013	0.07	0.0021	0.0545	0.0014	0.53281	436	13	431.8	8.9	413	44	4.68	0.77
GG17_27	1312	89	579	30	118.3	4.6	2.443	0.07	0.519	0.013	0.0688	0.0019	0.0548	0.0017	0.17467	429	11	424.2	8.9	413	47	4.85	0.99
GG17_28	990	60	689	48	145.3	8.6	1.484	0.036	0.517	0.011	0.0695	0.0013	0.054	0.0014	0.21836	433	7.8	422.6	7.4	376	45	3.89	0.78
GG17_29	876	70	674	45	132	7.8	1.367	0.064	0.493	0.018	0.0636	0.0019	0.0558	0.0017	0.5846	397	12	406	12	432	51	4.29	0.97
GG17_30	870	120	515	64	103	13	1.734	0.061	0.504	0.015	0.0686	0.002	0.0552	0.0016	0.42138	428	12	414.1	9.9	422	39	4.3	1
GG17_31	810	100	565	79	111	15	1.462	0.06	0.497	0.014	0.0671	0.0025	0.0536	0.0021	0.19035	419	15	411	10	419	64	6.5	1.4

Isotope data from LA-ICP-MS Sample CN2

Sample Run	Approx U PPM	Approx U PPM Int2SE	Approx Th PPM	Approx Th PPM Int2SE	Approx Pb PPM	Approx Pb PPM Int2SE	Final U-Th Ratio	Final U-Th Ratio Int2SE	Final 207-235	Final 207-235 Int2SE	Final 206-238	Final 206-238 Int2SE	Final 207-206	Final 207-206 Int2SE	Error Correl 6 38vs7 35	Final Age 206-238	Final Age 206-238 Int2SE	Final Age 207-235	Final Age 207-235 Int2SE	Final Age 207-206	Final Age 207-206 Int2SE	Final Disc Percent	Final Disc Percent Int2SE
GG19_1	380	40	205	36	39.9	7.9	1.93	0.12	0.48	0.013	0.0653	0.0013	0.0535	0.0011	0.73858	409	8	399.3	9.1	340	49	5.2	1.1
GG19_2	639	40	381	23	72.4	4.6	1.75	0.11	0.52	0.012	0.0684	0.0011	0.05518	0.00067	0.80136	426.6	6.6	424.6	8.3	417	27	3.71	0.84
GG19_3	620	42	353	25	64.1	5.2	1.788	0.037	0.498	0.01	0.06727	0.00074	0.05359	0.00076	0.55722	419.7	4.5	410.9	7.2	356	34	3.4	0.58
GG19_4	649	58	265	21	48.7	3.1	2.415	0.052	0.504	0.013	0.0667	0.0014	0.05513	0.00074	0.76975	416.2	8.4	413.7	8.8	426	34	3.51	0.77
GG19_5	336	54	198	26	34.3	3.7	1.686	0.038	0.494	0.014	0.0673	0.0013	0.0535	0.0013	0.7486	419.9	7.7	406.7	9.8	336	56	4.9	1.1
GG19_6	535	53	327	38	57.9	5.3	1.719	0.041	0.4884	0.0097	0.06621	0.00085	0.05357	0.00076	0.51559	413.3	5.1	404.7	6.4	361	31	3.72	0.75
GG19_7	831	46	289	17	55.9	3.8	2.911	0.03	0.452	0.012	0.0595	0.0013	0.05425	0.00077	0.90429	372.8	7.7	376	9.6	378	33	5.1	1.2
GG19_8	654	14	332	12	66.3	1.5	1.984	0.041	0.5044	0.0086	0.06685	0.0007	0.05475	0.00067	0.42783	417.1	4.2	414.4	5.8	399	27	3.16	0.55
GG19_9	735	59	592	64	111	12	1.307	0.051	0.436	0.012	0.0591	0.0011	0.0519	0.00095	0.79404	370.3	6.4	366.7	8.6	274	43	4.74	0.94
GG19_10	546	18	362	16	68.6	2.4	1.541	0.036	0.494	0.011	0.06588	0.00096	0.05474	0.00095	0.66078	411.2	5.8	407.6	7.1	402	41	3.89	0.79
GG19_11	443	32	292	22	55.1	4.2	1.562	0.034	0.4963	0.0096	0.06579	0.00096	0.0535	0.0011	0.59903	410.7	5.8	408.9	6.5	343	46	4.21	0.75
GG19_12	469	34	337	22	69	2.8	1.383	0.015	0.481	0.015	0.0635	0.0015	0.05299	0.00098	0.81351	398.1	9.1	398	10	356	35	4.76	0.95
GG19_13	567	51	523	51	96	7.3	1.091	0.019	0.49	0.011	0.06504	0.00071	0.05449	0.00082	0.47677	406.2	4.3	405.8	7	387	34	3.53	0.65
GG19_14	424	76	171	29	33.4	4.8	2.368	0.076	0.512	0.016	0.0692	0.002	0.05471	0.0009	0.80294	431	12	419	10	395	37	5.2	1.1
GG19_15	448	18	233.2	4.4	46.2	1	1.989	0.066	0.506	0.012	0.06801	0.00094	0.05456	0.00093	0.70477	424.1	5.7	415.5	8.4	404	34	4.03	0.69
GG19_16	880	25	814	31	160.6	6.6	1.137	0.051	0.503	0.014	0.0661	0.0011	0.05463	0.00093	0.73514	412.3	6.9	414.5	9	398	37	3.72	0.7
GG19_17	484	32	343	33	66.6	5.9	1.468	0.058	0.509	0.014	0.0663	0.0011	0.05573	0.0008	0.90434	413.6	6.6	417.3	9.3	443	34	4.39	0.73
GG19_18	418	12	384.2	6.8	68	1.9	1.13	0.044	0.461	0.011	0.06164	0.00082	0.05495	0.00073	0.67331	385.6	5	384.8	7.5	413	31	4.23	0.67
GG19_19	344.9	7.1	243.5	7.9	48.4	1.7	1.47	0.039	0.425	0.013	0.0595	0.0011	0.0518	0.0011	0.74349	372.7	6.6	359.4	9.3	264	50	4.92	0.87
GG19_20	549	20	363	20	62.6	3.2	1.534	0.074	0.49	0.011	0.0656	0.001	0.0538	0.001	0.75336	409.9	6.3	404.8	7.8	403	33	4.08	0.78
GG19_21	452	52	187	23	36.4	3.9	2.52	0.042	0.549	0.014	0.0737	0.0011	0.05425	0.00086	0.78093	458.3	6.8	443.8	8.9	377	36	4.41	0.87
GG19_22	558	28	269.6	5	50.2	1.2	2.01	0.11	0.493	0.012	0.06633	0.00085	0.0537	0.0012	0.52741	414	5.2	406.5	8.1	350	50	4.02	0.83
GG19_23	531	67	393	68	78	11	1.539	0.074	0.541	0.014	0.0713	0.0013	0.0543	0.0012	0.73222	444.2	7.7	438.7	9.1	380	53	3.47	0.68
GG19_24	351	27	143	12	30.9	2.7	2.292	0.069	0.477	0.024	0.0656	0.0027	0.0531	0.0013	0.92867	409	16	394	17	320	58	8.1	1.5
GG19_25	291.3	7.4	177.6	3.4	34.4	1	1.562	0.042	0.508	0.012	0.06911	0.00081	0.0528	0.0012	0.48372	430.8	4.9	418.1	7.8	309	52	4.54	0.99
GG19_26	606	28	296	11	52.8	2.2	2.06	0.14	0.4956	0.0096	0.06546	0.00077	0.05445	0.00089	0.57305	408.8	4.6	408.5	6.6	391	36	3.44	0.56
GG19_27	1253	57	742	30	140.3	5.9	1.663	0.07	0.443	0.014	0.0598	0.0015	0.0523	0.0011	0.86198	374.6	9.4	371.9	9.9	296	50	4.06	0.86
GG19_28	691	35	288	12	50.8	2.2	2.391	0.062	0.411	0.011	0.0562	0.0011	0.05252	0.00091	0.96878	352.3	6.5	349.1	8.3	301	41	4.91	0.98
GG19_29	358.5	6.7	327.2	6	64.9	2.3	1.076	0.032	0.498	0.015	0.0683	0.0012	0.053	0.0013	0.72868	425.7	7.3	410	10	325	56	4.52	0.93

Isotope data from LA-ICP-MS Sample CN3

Sample Run	Approx U PPM	Approx U PPM Int2SE	Approx Th PPM	Approx Th PPM Int2SE	Approx Pb PPM	Approx Pb PPM Int2SE	Final U-Th Ratio	Final U-Th Ratio Int2SE	Final 207-235	Final 207-235 Int2SE	Final 206-238	Final 206-238 Int2SE	Error Correlation 6 38vs7 35	Final 207-235 Prop2SE	Final 207-206	Final 207-206 Int2SE	Error Correlation 38 6vs7 6	Final Age 206-238	Final Age 206-238 Int2SE	Final Age 207-235	Final Age 207-235 Int2SE	Final Age 207-206	Final Age 207-206 Int2SE	Final Disc Percent	Final Disc Percent Int2SE
GG20_Z1	896	30	533	11	94.9	1.6	1.619	0.042	0.426	0.012	0.058	0.0016	0.64409	0.046	0.0542	0.0016	0.53924	363.2	9.6	360	8.4	382	48	4.65	0.9
GG20_Z2	614	19	174	15	31	2.8	3.81	0.36	0.406	0.013	0.05539	0.00097	0.45106	0.046	0.0546	0.0017	-0.010187	347.5	5.9	345.6	9.3	387	34	4.39	0.87
GG20_Z3	425	13	231	10	42.2	2	1.832	0.04	0.426	0.012	0.0573	0.001	0.58781	0.046	0.0559	0.0015	0.029371	360.2	6.6	360.1	8.9	434	31	3.85	0.8
GG20_Z4	1082	72	581	53	115	11	1.735	0.07	0.471	0.021	0.0632	0.0026	0.87579	0.049	0.0547	0.0011	0.041084	395	16	390	14	410	35	3.2	0.67
GG20_Z5	709	65	204	12	36.7	2.2	3.42	0.16	0.488	0.015	0.0656	0.0012	0.6725	0.047	0.0532	0.0013	0.13007	409.6	7.2	403	10	358	36	4.22	0.77
GG20_Z6	331	68	184	44	35.3	8	1.74	0.13	0.537	0.024	0.0716	0.0026	0.54789	0.051	0.054	0.0026	0.48992	446	16	435	16	399	59	6.8	1.4
GG20_Z7	196	11	96.4	6.6	18.1	1	2.016	0.032	0.416	0.021	0.0565	0.0011	0.47484	0.049	0.0538	0.0024	-0.063961	354.1	6.9	352	15	386	54	5.8	1.2
GG20_Z8	801	97	355	62	73	11	2.39	0.13	0.434	0.013	0.0595	0.0015	0.74813	0.047	0.0549	0.0014	0.23704	372.2	9.3	365.7	9.2	378	40	4.08	0.73
GG20_Z9	681	26	353	18	66.3	3.4	1.925	0.081	0.496	0.013	0.06519	0.00079	0.14517	0.047	0.055	0.0015	0.37765	407.1	4.8	408.7	9	410	30	4.02	0.71
GG20_Z11	375	25	256	26	52	5.7	1.486	0.083	0.502	0.017	0.06475	0.00095	0.56034	0.048	0.0558	0.0017	0.28579	404.4	5.8	414	11	427	44	4.9	0.88
GG20_Z12	877	70	930	110	180	23	0.945	0.053	0.4356	0.0088	0.0586	0.001	0.28092	0.046	0.0546	0.0014	0.42134	367.9	6.5	366.9	6.2	429	33	3.86	0.76
GG20_Z13	533	60	247	42	48.6	8.2	2.18	0.13	0.472	0.016	0.0643	0.002	0.53658	0.048	0.054	0.0018	0.36058	401	12	392	11	372	53	5.47	0.93
GG20_Z14	185	29	85	17	16.7	2.9	2.14	0.11	0.504	0.027	0.0653	0.0014	0.39243	0.053	0.0558	0.0027	-0.080159	407.8	8.4	413	18	466	64	6.6	1.6
GG20_Z15	549	16	327	28	61.9	5.7	1.8	0.25	0.443	0.013	0.0595	0.0015	0.32221	0.047	0.0553	0.0017	0.40045	372.6	9.1	371.6	9.2	452	39	4.68	0.96
GG20_Z16	740	47	369	42	68.9	8.4	2.05	0.15	0.409	0.011	0.056	0.0013	0.40711	0.046	0.0552	0.0013	0.49109	351.3	7.8	350.1	7.2	426	36	3.55	0.71
GG20_Z17	531	40	337	39	66.5	7.9	1.668	0.081	0.488	0.017	0.0668	0.0019	0.80552	0.048	0.0531	0.0018	0.31105	417	11	402	11	352	45	5.89	0.97
GG20_Z18	525	20	313.2	8.5	56.3	1.5	1.664	0.061	0.478	0.016	0.0632	0.0011	0.84296	0.048	0.0551	0.0016	0.10157	395.2	6.4	396	11	418	40	4.33	0.77
GG20_Z19	495	21	125.6	3.4	25.7	0.75	3.81	0.1	0.492	0.013	0.06567	0.00084	0.0080312	0.047	0.0546	0.0017	0.44496	410	5.1	405.4	8.8	393	50	4.85	0.86
GG20_Z20	443	15	257.4	5.7	47.27	0.63	1.714	0.026	0.431	0.013	0.0583	0.0013	0.51059	0.047	0.055	0.0016	0.25565	365.2	8	363.2	9.5	430	44	3.9	0.87
GG20_Z22	239	14	110.9	9	29.1	1.4	2.098	0.094	0.496	0.021	0.0662	0.0022	0.44186	0.05	0.0559	0.0024	0.31918	413	13	408	14	473	56	5.9	1.3
GG20_Z23	257.6	3.9	110.8	3.6	22	1.3	2.282	0.06	0.491	0.021	0.0659	0.0012	0.16976	0.05	0.0544	0.0023	0.20323	411.4	7.4	407	13	393	59	5.5	1.2
GG20_Z24	658	34	394	60	79	11	1.98	0.25	0.509	0.017	0.0674	0.0018	0.76357	0.048	0.0548	0.0019	0.47647	420	11	417	11	390	51	5.2	1
GG20_Z25	875	79	293	23	59.4	4.5	2.927	0.092	0.457	0.016	0.0628	0.0022	0.59313	0.048	0.0538	0.0018	0.40067	393	14	382	11	384	47	5.06	0.99
GG20_Z26	393	20	217	13	44	2.3	1.84	0.11	0.45	0.015	0.0603	0.0017	0.36462	0.048	0.0558	0.0021	0.46718	377	11	378	10	461	57	5.9	1.1
GG20_Z27	222.7	3.8	139.4	3.6	27.3	1.2	1.623	0.06	0.491	0.02	0.0636	0.001	0.21212	0.05	0.0559	0.0024	0.19569	397.3	6.3	405	14	416	58	6.6	1.2
GG20_Z28	302	17	160	11	31.1	1.2	1.923	0.028	0.454	0.02	0.061	0.002	0.59686	0.05	0.0546	0.002	0.13737	382	12	379	14	407	47	4.9	1.1
GG20_Z29	760	56	352	35	71.2	7.8	2.283	0.063	0.443	0.011	0.0585	0.0013	0.3189	0.047	0.0556	0.0016	0.48253	366.3	7.9	372	7.8	446	49	4.53	0.89
GG20_Z30	290	25	145	28	28.1	4.2	2.59	0.26	0.498	0.018	0.0677	0.0012	0.26397	0.049	0.0542	0.002	0.19507	422	7.3	412	13	407	54	5.1	1.1
GG20_Z31	250	11	115.6	6.4	21.5	1.7	2.208	0.034	0.45	0.019	0.0616	0.00086	0.19159	0.049	0.0521	0.0021	0.13224	385.3	5.2	378	13	382	49	6.5	1.5

Isotope data from LA-ICP-MS Sample CN4

Sample Run	Approx U PPM	Approx U PPM Int2SE	Approx Th PPM	Approx Th PPM Int2SE	Approx Pb PPM	Approx Pb PPM Int2SE	Final U-Th Ratio	Final U-Th Ratio Int2SE	Final 207-235	Final 207-235 Int2SE	Final 206-238	Final 206-238 Int2SE	Final 207-206	Final 207-206 Int2SE	Error Correlation 6 38vs7 35	Final 206-238 Prop2SE	Final Age 206-238	Final Age 206-238 Int2SE	Final Age 207-235	Final Age 207-235 Int2SE	Final Age 207-206	Final Age 207-206 Int2SE	Final 206-204	Final 206-204 Int2SE	Final Disc Percent	Final Disc Percent Int2SE
GG-21-Z1	512	51	332	40	64	8	1.69	0.06	0.487	0.016	0.0630	0.0016	0.0559	0.0022	0.13029	0.0036	394	10	402	11	449	59	260	210	6.6	1.1
GG-21-Z2	538	77	366	69	66	12	1.72	0.09	0.479	0.015	0.0643	0.0020	0.0523	0.0018	0.37642	0.0037	402	12	397	10	344	42	620	830	5.4	1.1
GG-21-Z3	226	6	90	3	19	1	2.61	0.09	0.510	0.027	0.0656	0.0023	0.0561	0.0034	0.074311	0.0039	410	14	419	18	494	70	730	610	8.9	1.7
GG-21-Z4	272	9	122	3	25	1	2.27	0.07	0.486	0.023	0.0651	0.0024	0.0555	0.0031	0.12524	0.004	407	14	403	16	495	67	10	230	8.6	1.6
GG-21-Z5	516	50	333	47	68	8	1.69	0.08	0.509	0.018	0.0666	0.0028	0.0551	0.0025	0.31634	0.0042	416	17	419	13	442	79	180	400	7	1.3
GG-21-Z6	603	61	358	43	81	8	1.76	0.07	0.513	0.014	0.0664	0.0025	0.0550	0.0020	0.43935	0.0041	414	15	422	9	457	61	-40	520	5.9	1.1
GG-21-Z7	308	9	140	6	29	1	2.20	0.08	0.496	0.019	0.0658	0.0029	0.0542	0.0024	0.40133	0.0043	410	17	408	13	432	71	660	230	7	1.4
GG-21-Z8	307	17	130	10	27	2	2.38	0.08	0.491	0.020	0.0654	0.0025	0.0537	0.0023	0.32728	0.0041	408	15	409	14	433	68	-80	220	6.5	1.3
GG-21-Z9	515	41	156	9	32	2	3.31	0.11	0.493	0.016	0.0655	0.0019	0.0553	0.0023	0.028502	0.0037	409	12	406	11	430	70	260	440	6.8	1.1
GG-21-Z10	306	24	154	15	32	2	2.12	0.09	0.482	0.017	0.0679	0.0028	0.0537	0.0030	0.16562	0.0042	423	17	403	12	463	76	-30	240	8.6	1.3
GG-21-Z11	318	13	132	5	28	1	2.23	0.07	0.512	0.023	0.0653	0.0022	0.0570	0.0020	0.54015	0.0039	408	13	418	15	469	56	4.70E+03	7.20E+03	5.5	1.2
GG-21-Z12	447	53	168	25	39	5	2.47	0.13	0.488	0.015	0.0640	0.0020	0.0549	0.0023	0.14335	0.0038	400	12	403	10	454	66	830	780	6.7	1.2
GG-21-Z13	480	11	323	16	73	4	1.38	0.05	0.477	0.014	0.0636	0.0016	0.0537	0.0019	0.11207	0.0036	397	10	397	10	388	59	120	290	5.77	0.98
GG-21-Z14	231	6	90	4	21	1	2.40	0.10	0.509	0.018	0.0665	0.0023	0.0560	0.0024	0.20309	0.0039	415	14	417	12	443	62	930	420	6.9	1.3
GG-21-Z15	547	50	221	20	48	4	2.34	0.08	0.483	0.018	0.0657	0.0024	0.0539	0.0023	0.29516	0.004	410	14	399	12	385	60	620	550	6.2	1.3
GG-21-Z16	255	17	94	6	22	1	2.62	0.09	0.490	0.020	0.0670	0.0024	0.0529	0.0028	0.025217	0.004	418	15	403	14	436	80	40	290	8.4	1.5
GG-21-Z18	910	85	391	36	85	6	2.22	0.07	0.484	0.014	0.0655	0.0020	0.0535	0.0014	0.59053	0.0038	409	12	400	9	335	44	370	890	4.47	0.79
GG-21-Z19	563	28	246	13	52	3	2.21	0.07	0.501	0.013	0.0671	0.0027	0.0543	0.0021	0.39909	0.0042	418	16	412	9	400	66	-210	500	6.2	1.1
GG-21-Z20	599	20	353	11	60	2	1.82	0.05	0.511	0.021	0.0676	0.0025	0.0543	0.0026	0.15831	0.0041	422	15	418	14	441	59	60	120	6.8	1.5
GG-21-Z22	623	28	320	22	55	3	2.01	0.08	0.492	0.019	0.0673	0.0026	0.0533	0.0025	0.24212	0.0042	420	16	405	13	396	70	-30	310	7.4	1.4
GG-21-Z23	850	31	436	14	75	2	1.96	0.07	0.494	0.016	0.0683	0.0026	0.0530	0.0020	0.4755	0.0042	425	16	407	11	374	61	120	280	6.2	1.1
GG-21-Z24	381	8	155	4	28	1	2.48	0.06	0.479	0.021	0.0648	0.0017	0.0537	0.0025	0.28528	0.0036	404	10	396	14	351	56	140	120	6.7	1.3

Section 2; AMS data

AMS Data from the Omey Pluton

Site ID	Facies	East	North	N	K3 Plunge	K3 Trend	K1 Plunge	K1 Trend	Km x10^{-6}(SI)	H (%)	Pj	lnPj	Tj
OM1	G1	057842	256311	11	44	69	34	299	11319	4.1	1.024	0.024	0.06
OM10	G1	057766	256680	16	38	224	49	69	14232	4.7	1.034	0.034	0.70
OM100	G1	054397	257388	11	47	88	34	312	15784	5.8	1.039	0.038	-0.55
OM101	G1	054404	257296	14	24	73	37	323	10109	5.3	1.037	0.036	-0.64
OM102	G1	054940	257399	15	33	65	36	306	3186	6.8	1.040	0.039	-0.09
OM103	G1	054806	258208	14	50	150	40	331	11640	6.5	1.038	0.037	0.06
OM104	G1	054895	257942	15	51	110	35	321	14943	5.2	1.031	0.030	0.04
OM105	G1	056584	259040	15	32	205	51	346	15395	7.8	1.049	0.048	0.33
OM106	G3	052218	257726	15	35	93	35	335	5083	6.7	1.041	0.040	0.27
OM107	G3	052344	257784	15	39	86	46	298	3348	6.3	1.040	0.040	0.43
OM108	G2	052571	257776	15	39	97	34	335	10161	4.4	1.026	0.026	-0.18
OM109	G1	054106	255307	13	21	39	7	132	14555	7.1	1.048	0.046	0.53
OM11	KIA	KIA	KIA	KIA	KIA	KIA	KIA	KIA	KIA	KIA	KIA	KIA	KIA
OM110	G3	053013	255162	12	18	42	7	134	1408	6.5	1.042	0.041	0.41
OM111	G3	053260	255103	12	17	57	72	221	1090	5.0	1.030	0.029	0.22
OM112	G2	053584	254934	10	1	44	46	136	2454	3.8	1.025	0.024	0.45
OM113	G1	053426	257108	13	47	87	34	312	14337	5.4	1.033	0.032	-0.24
OM114	G1	054217	259871	13	54	183	35	347	12628	6.5	1.040	0.039	0.26
OM115	G1	054777	259004	9	35	163	55	344	12638	4.9	1.032	0.031	-0.44
OM116	G1	055231	259304	8	6	213	79	336	5058	5.7	1.044	0.043	0.82
OM117	G1	056417	259694	13	39	223	6	317	12019	6.7	1.049	0.047	0.67
OM12	G1	058061	255442	21	14	218	51	111	4183	3.5	1.023	0.023	-0.60
OM13	G1	057445	259756	17	41	210	48	17	11598	8.2	1.050	0.049	0.28
OM14	G1	057275	258980	8	14	245	33	11	10579	9.3	1.066	0.064	0.61
OM15	G1	058041	259001	19	40	241	9	339	12307	5.1	1.035	0.035	0.59
OM16	G1	057372	258237	10	34	227	40	351	10110	4.2	1.027	0.026	0.41
OM17	G2	056523	257658	18	40	225	39	358	11727	7.6	1.060	0.058	0.84
OM18	G2	056637	257698	14	52	45	20	288	13224	5.5	1.036	0.036	0.49
OM19	G3	056253	257916	20	28	213	41	331	1318	6.5	1.043	0.042	0.50
OM1A	G1	057842	256311	9	48	60	35	279	11211	2.7	1.017	0.017	0.42
OM2	G1	057817	256045	18	39	254	17	358	12904	4.7	1.031	0.031	0.48
OM20	G2	056470	258109	15	27	217	31	325	13975	7.0	1.046	0.045	0.46
OM21	G1	056023	258863	19	42	238	47	43	5438	8.3	1.049	0.048	-0.01
OM21B	G1	056023	258863	10	40	233	50	47	5393	10.1	1.061	0.059	-0.13
OM22	G1	055407	258669	17	40	191	50	4	1089	6.2	1.038	0.038	0.30
OM23	G3	055379	257629	14	37	101	36	338	4112	5.8	1.034	0.034	0.06
OM24	KIA	KIA	KIA	KIA	KIA	KIA	KIA	KIA	KIA	KIA	KIA	KIA	KIA
OM25	G1	055396	256790	20	19	32	64	257	4011	6.3	1.042	0.041	0.51
OM26	G1	055941	255044	4	51	9	39	175	17420	2.5	1.015	0.015	-0.17
OM27	G1	055352	256014	19	24	43	5	135	15400	4.5	1.029	0.028	0.38
OM28	KIA	KIA	KIA	KIA	KIA	KIA	KIA	KIA	KIA	KIA	KIA	KIA	KIA
OM29	G1	057505	255339	19	24	260	55	131	13144	3.1	1.021	0.021	0.63
OM3	G1	059309	256393	13	22	244	68	61	11007	4.7	1.039	0.038	0.95
OM30	G1	057061	256183	11	66	271	18	135	8887	1.3	1.007	0.007	-0.11
OM31	G1	056986	256800	20	11	219	69	98	11344	3.9	1.028	0.027	0.70
OM32	G1	056189	256870	17	18	237	56	117	3548	2.7	1.017	0.017	-0.39
OM33	KIA	KIA	KIA	KIA	KIA	KIA	KIA	KIA	KIA	KIA	KIA	KIA	KIA
OM34	G1	059332	256377	18	35	281	16	179	14443	6.7	1.045	0.044	0.52
OM35	G1	059226	256366	13	31	243	59	65	10226	4.6	1.028	0.028	0.31
OM36	G1	059376	256001	13	38	257	17	154	13131	5.0	1.033	0.033	0.53

AMS Data from the Omey Pluton

Site ID	Facies	East	North	N	K3 Plunge	K3 Trend	K1 Plunge	K1 Trend	Km x10^{-6}(SI)	H (%)	Pj	lnPj	Tj
OM37	G1	059308	255900	15	24	240	51	116	16679	4.5	1.030	0.029	0.48
OM38	KIA	KIA	KIA	KIA	KIA	KIA	KIA	KIA	KIA	KIA	KIA	KIA	KIA
OM39	G1	059158	255814	20	42	238	43	91	4963	8.0	1.056	0.054	0.59
OM4	G1	059224	256423	18	56	242	10	347	14416	4.8	1.037	0.036	0.82
OM40	G1	059175	255761	12	29	239	51	104	10412	4.0	1.023	0.023	0.03
OM41	G1	059131	255399	18	9	91	51	192	6983	6.7	1.040	0.039	0.14
OM42	G1	057170	259324	20	18	216	52	331	17820	8.5	1.062	0.060	0.68
OM43	G1	057017	259930	21	27	211	48	335	7833	7.6	1.050	0.049	0.46
OM44	G1	058063	258990	20	60	240	16	359	12554	9.0	1.054	0.053	-0.19
OM45	G1	058060	258991	19	67	8	23	185	14180	8.5	1.051	0.050	0.17
OM46	KIA	KIA	KIA	KIA	KIA	KIA	KIA	KIA	KIA	KIA	KIA	KIA	KIA
OM47	G1	056862	257780	4	55	225	29	6	3694	8.4	1.064	0.062	0.78
OM48	G1	056864	257786	12	35	220	36	340	13254	6.9	1.047	0.046	0.56
OM49	G1	056804	258409	18	30	44	36	160	15624	6.3	1.045	0.044	0.67
OM5	G1	058772	256267	21	22	251	63	109	14771	6.5	1.048	0.046	0.72
OM50	G1	056804	258410	20	42	69	3	162	1922	4.3	1.026	0.026	0.27
OM51	G3	056232	257697	18	24	228	37	119	383	4.0	1.026	0.026	0.44
OM52 A	G3	056235	257471	8	41	221	28	338	1526	4.0	1.029	0.029	0.75
OM52 B	G3	056235	257471	18	40	225	21	116	549	4.5	1.034	0.034	0.84
OM53	G3	056233	257489	17	28	230	55	10	1129	5.4	1.037	0.036	0.55
OM54	G1	055302	258508	14	36	159	54	339	12095	6.1	1.036	0.036	0.20
OM55	G1	054813	257622	20	28	94	45	332	15037	6.4	1.038	0.037	-0.01
OM56	G1	054315	257065	18	33	81	36	322	14249	6.8	1.043	0.042	-0.36
OM57	G1	058069	256291	16	12	207	77	51	5721	5.4	1.033	0.033	-0.33
OM58 A	G1	057277	255740	11	25	230	24	128	14334	2.8	1.017	0.016	0.07
OM58 B	G1	057277	255740	14	15	223	39	120	13821	2.7	1.016	0.016	0.26
OM59	G1	056786	254806	10	29	30	35	142	10186	3.9	1.025	0.025	-0.49
OM6	G1	059309	255946	22	7	217	47	315	13219	5.9	1.040	0.039	0.55
OM60	G1	055938	255055	12	55	36	21	159	12745	5.1	1.030	0.030	0.03
OM61	G1	056407	256295	12	18	205	68	25	9872	4.9	1.029	0.029	-0.05
OM62	KIA	KIA	KIA	KIA	KIA	KIA	KIA	KIA	KIA	KIA	KIA	KIA	KIA
OM63	G1	055855	255689	12	43	32	17	138	14866	3.6	1.023	0.023	-0.49
OM64	G1	056341	255788	19	60	346	25	131	14034	4.8	1.028	0.028	-0.01
OM65	G1	058285	255286	12	54	21	34	177	3506	6.9	1.047	0.046	-0.57
OM66	G1	058273	255287	12	13	260	55	151	10422	3.9	1.026	0.026	-0.55
OM67	KIA	KIA	KIA	KIA	KIA	KIA	KIA	KIA	KIA	KIA	KIA	KIA	KIA
OM68	G1	054527	257286	13	41	75	25	322	17690	5.2	1.032	0.032	-0.35
OM69	G1	059034	255887	12	44	325	46	131	15134	5.0	1.031	0.030	-0.36
OM7	G1	058533	255703	7	29	296	3	28	11932	2.1	1.012	0.012	0.07
OM70	G2	056308	258227	18	46	201	35	336	12772	7.5	1.046	0.045	0.26
OM71	G2	056027	258109	15	11	236	69	356	6683	5.8	1.035	0.035	-0.29
OM72	G3	055980	257990	12	14	205	21	110	244	1.6	1.011	0.011	0.62
OM73	G3	055955	257974	14	18	202	50	314	3114	8.8	1.063	0.061	0.66
OM74	G3	055634	257957	13	13	186	40	287	3155	5.8	1.036	0.036	0.35
OM75	G3	055931	257854	15	22	216	5	308	727	7.2	1.048	0.047	0.52
OM76	G2	055343	257884	16	3	205	73	306	167	1.2	1.007	0.007	0.27
OM77	G2	055274	258097	14	27	188	18	287	12409	5.1	1.035	0.034	0.61
OM78	G1	058049	257822	12	43	223	19	332	14355	6.1	1.045	0.044	0.76
OM79	G1	059249	256505	21	37	51	27	163	9501	3.3	1.024	0.023	0.70
OM8	G1	059018	255290	13	39	220	51	41	10587	4.9	1.034	0.033	-0.61
OM80	G1	059275	256446	19	33	239	7	145	12462	5.0	1.039	0.039	0.89
OM81	G1	056025	256126	15	8	23	24	116	11624	2.2	1.014	0.014	-0.49

AMS Data from the Omey Pluton

Site ID	Facies	East	North	N	K3 Plunge	K3 Trend	K1 Plunge	K1 Trend	Km x10^{-6}(SI)	H (%)	Pj	lnPj	Tj
OM82	G1	055631	256018	15	39	41	3	308	14771	4.5	1.028	0.028	-0.35
OM83	G1	055861	255682	15	54	16	34	173	14506	4.6	1.034	0.033	0.74
OM84	G1	055875	255696	14	35	255	31	141	12310	3.9	1.028	0.027	-0.71
OM85	G1	056126	255507	15	13	59	75	210	6340	8.9	1.053	0.051	-0.10
OM86	G1	056347	255210	11	31	215	15	315	1741	5.8	1.041	0.040	0.64
OM87	G1	056552	254747	15	42	44	1	135	12149	4.2	1.025	0.024	-0.66
OM88	G1	056145	254757	15	41	38	33	163	15304	5.2	1.031	0.030	-0.15
OM89	G1	057075	254939	14	35	88	12	186	155	1.6	1.010	0.009	0.34
OM9	G1	058393	256620	15	25	248	31	354	10676	4.7	1.032	0.031	0.55
OM90	G1	056846	255128	15	5	209	77	98	4705	2.8	1.016	0.016	-0.14
OM91	G1	057034	255931	14	15	29	45	134	12641	2.7	1.016	0.016	-0.27
OM92	G1	058003	255762	7	59	267	27	121	13813	3.7	1.022	0.021	-0.04
OM93	G1	058380	255581	15	50	355	34	192	9755	4.6	1.027	0.027	0.08
OM94	G1	058769	255584	15	52	267	22	145	11502	3.9	1.023	0.023	-0.06
OM95	G1	054447	257178	15	32	53	35	298	6049	5.7	1.034	0.033	-0.14
OM96	G1	054445	257111	14	20	74	40	327	9636	6.4	1.041	0.040	-0.44
OM97	G1	054917	257080	15	11	53	25	318	10559	7.0	1.041	0.040	-0.04
OM98	G1	054607	257151	11	1	0	29	270	9723	5.6	1.033	0.033	-0.17
OM99	G1	054397	257388	11	12	49	48	306	10020	3.6	1.021	0.021	0.07

AMS Data from the Roundstone Pluton

Site ID	Facies	East	North	N	K3 Plunge	K3 Trend	K1 Plunge	K1 Trend	Km x10^{-6}(SI)	H (%)	Pj	lnPj	Tj
RD1	RD1	072653	239317	17	48	63	32	198	21038	29.8	1.254	0.226	0.76
RD10	RD1	073396	241769	17	10	101	42	2	16178	17.1	1.147	0.137	0.91
RD100	RD1	074511	241400	11	15	85	73	239	17543	9.1	1.066	0.064	0.66
RD101	RD1	074637	241841	15	14	89	60	333	17072	7.2	1.052	0.050	0.67
RD102	RD1	075025	242126	11	13	97	73	232	13206	8.6	1.055	0.053	0.39
RD103	RD2	075510	242125	15	4	125	83	2	10406	4.0	1.023	0.023	0.17
RD104 A	RD1	075247	242120	18	12	90	74	310	16954	8.9	1.058	0.057	0.45
RD104 B	RD1	075247	242120	16	7	281	81	69	16051	9.4	1.061	0.059	0.41
RD105 A	RD2	075484	242437	20	10	135	72	258	9970	5.6	1.033	0.032	-0.10
RD105 B	RD2	075484	242437	14	11	131	75	265	9443	5.8	1.035	0.034	-0.21
RD106	RD2	075926	242433	18	3	219	75	320	14165	8.0	1.048	0.047	-0.18
RD107	RD2	076564	241935	18	19	209	70	6	15890	9.0	1.061	0.059	0.52
RD108	RD2	075973	241745	17	36	193	54	7	19817	10.0	1.060	0.059	0.16
RD109	RD2	076004	242061	13	2	30	85	272	12148	10.7	1.067	0.064	0.27
RD11	RD1	073234	241381	16	10	97	12	190	15735	17.8	1.146	0.136	0.82
RD110	RD1	077543	242473	13	0	235	24	325	17343	6.1	1.048	0.047	0.87
RD111	RD1	078768	242388	16	1	258	77	353	15445	20.8	1.153	0.143	0.58
RD112	RD1	078427	242547	15	2	246	82	353	20478	15.8	1.122	0.115	0.72
RD113	RD1	078111	242431	17	4	75	82	318	16159	13.5	1.113	0.107	0.89
RD114	RD1	078422	242080	16	9	76	18	343	19745	16.5	1.140	0.131	0.89
RD115	RD1	078108	241700	16	4	241	25	333	13945	8.1	1.053	0.052	0.43
RD116	RD1	078034	241300	17	16	254	38	357	20323	9.4	1.072	0.070	0.77
RD117	RD1	077558	240933	15	1	261	63	353	8881	7.6	1.048	0.047	0.34
RD118	RD1	076928	241836	15	15	233	69	4	22480	8.2	1.055	0.054	0.51
RD119	RD1	077336	242043	15	4	232	86	28	18055	11.2	1.076	0.073	0.50
RD12	RD1	073159	241029	17	19	81	43	190	16614	21.7	1.171	0.158	0.71
RD120	RD1	077618	241834	15	1	232	79	139	19079	10.7	1.072	0.070	0.49
RD121	RD1	077360	241556	14	39	338	50	144	16549	7.0	1.046	0.045	0.48
RD122	RD2	076551	241729	14	21	235	69	62	11603	6.6	1.041	0.040	0.30
RD123	RD2	076845	241389	15	20	240	70	54	13287	9.1	1.054	0.053	0.15
RD124	RD2	076504	241428	15	54	274	12	21	13932	10.3	1.072	0.070	0.57
RD125	RD1	075020	240434	15	82	105	5	233	14695	9.6	1.069	0.066	0.64
RD126	RD1	074925	240762	15	29	63	17	163	11001	8.5	1.054	0.053	0.39
RD127	RD2	075752	241197	15	52	70	37	265	19103	10.2	1.063	0.061	-0.29
RD128	RD1	075706	240919	15	62	54	25	204	19144	16.8	1.105	0.099	0.18
RD129	RD2	076024	240881	15	28	55	42	173	16902	12.8	1.081	0.078	-0.35
RD13	RD1	073458	240872	17	14	88	38	190	14646	19.1	1.154	0.144	0.77
RD130	RD1	076290	240694	15	38	278	35	154	10332	7.5	1.044	0.043	0.08
RD131	RD1	075469	240354	11	26	65	61	216	24084	13.7	1.085	0.081	0.20
RD132	RD2	075807	240250	15	20	35	57	160	15003	11.1	1.072	0.070	0.39
RD133	RD2	076164	240308	15	23	257	20	158	13952	4.7	1.029	0.028	0.29
RD134	RD2	076261	239837	15	2	63	47	155	17428	6.3	1.040	0.039	-0.43
RD135	RD2	076717	240781	14	15	281	5	13	10138	8.6	1.052	0.050	0.17
RD136	RD1	077106	240726	15	62	270	13	153	14948	8.6	1.051	0.050	-0.11
RD137	RD2	077300	240482	15	8	67	44	166	14848	6.0	1.043	0.042	-0.71
RD138	RD2	077339	240220	15	49	355	26	119	19267	4.0	1.025	0.025	0.42
RD139	RD1	077293	239969	15	54	267	35	102	20718	8.4	1.050	0.049	0.15
RD14	RD1	074052	241703	11	29	101	60	295	17775	10.3	1.072	0.069	0.59
RD140	RD2	076728	239869	15	9	176	62	283	13773	4.7	1.032	0.031	-0.57
RD141	RD1	076745	240175	15	44	346	46	173	13974	9.7	1.058	0.056	-0.08
RD142	RD2	076859	240560	13	5	67	48	162	11400	7.1	1.049	0.048	-0.60
RD143	RD2	077029	240364	15	38	47	35	170	13909	4.4	1.029	0.028	-0.47

AMS Data from the Roundstone Pluton

Site ID	Facies	East	North	N	K3 Plunge	K3 Trend	K1 Plunge	K1 Trend	Km x10^{-6}(SI)	H (%)	Pj	lnPj	Tj
RD144	RD1	076039	239516	15	33	47	35	164	18005	6.3	1.042	0.042	0.55
RD145	RD2	075166	239681	14	11	58	68	177	11493	9.3	1.058	0.056	0.26
RD146	RD1	074952	240014	12	25	41	65	210	6067	5.9	1.035	0.034	0.14
RD147	RD1	075501	239517	15	22	56	58	186	17909	7.7	1.045	0.044	0.02
RD148	RD1	075904	239123	13	39	33	40	165	19065	10.3	1.061	0.060	0.10
RD149	RD1	076234	239558	15	13	19	73	157	22440	9.0	1.055	0.054	-0.29
RD15	RD1	073956	241228	14	24	88	65	289	15434	10.0	1.073	0.070	0.67
RD150	RD1	075719	239821	15	10	50	60	157	21254	10.3	1.062	0.060	0.08
RD151	RD1	075447	237060	15	31	21	58	217	16201	26.5	1.180	0.165	0.35
RD152	RD1	075047	237105	14	43	18	47	192	15145	28.9	1.194	0.177	0.30
RD153	RD1	074769	237106	14	48	11	40	212	9662	12.0	1.072	0.069	-0.09
RD155	RD1	075945	237029	13	24	356	65	192	9204	19.8	1.130	0.122	0.34
RD156	RD1	076210	237334	15	30	20	57	173	14889	12.0	1.077	0.074	0.36
RD157	RD1	076573	237491	14	38	34	52	227	17832	24.3	1.152	0.141	0.05
RD158	RD1	076969	237505	19	44	21	46	204	17755	33.0	1.218	0.197	0.20
RD159	RD1	077501	237632	19	34	341	56	160	19268	17.5	1.107	0.102	0.11
RD16	RD1	073783	242098	16	15	99	50	351	12888	8.7	1.068	0.066	0.82
RD160	RD1	077848	238144	19	39	318	50	155	10860	10.7	1.064	0.062	0.04
RD161	RD1	077720	237780	20	46	345	42	187	7023	14.7	1.110	0.105	0.69
RD162	RD1	078164	238097	19	42	316	45	162	5822	10.8	1.065	0.063	-0.05
RD163	RD1	079493	241079	20	13	271	74	126	18541	19.0	1.132	0.124	0.48
RD164	KIA	078251	239690	KIA	KIA	KIA	KIA	KIA	KIA	KIA	KIA	KIA	KIA
RD165	RD1	078867	239224	20	13	272	56	162	20941	14.5	1.116	0.110	0.82
RD166 A	RD1	079010	239632	18	12	266	75	52	16346	21.9	1.156	0.145	0.50
RD166 B	RD1	079010	239632	19	15	267	70	44	13815	20.5	1.153	0.142	0.61
RD167	RD1	078832	239995	16	16	269	72	56	20016	21.0	1.138	0.130	0.34
RD168	RD1	079582	240542	0	37	270	43	136	12722	13.3	1.086	0.083	0.37
RD169	RD1	079170	240665	0	21	277	62	43	12173	19.6	1.150	0.140	0.67
RD17	RD1	073488	242364	16	17	95	36	353	14229	13.1	1.090	0.086	0.52
RD170	RD1	078875	241151	0	3	274	57	9	14847	21.3	1.164	0.152	0.67
RD171	KIA	078936	241625	KIA	KIA	KIA	KIA	KIA	KIA	KIA	KIA	KIA	KIA
RD172	KIA	079499	241805	KIA	KIA	KIA	KIA	KIA	KIA	KIA	KIA	KIA	KIA
RD173	KIA	080000	241899	KIA	KIA	KIA	KIA	KIA	KIA	KIA	KIA	KIA	KIA
RD18	RD1	073109	240538	17	13	83	20	179	14288	23.4	1.187	0.171	0.71
RD19	RD1	073218	240020	16	17	73	64	204	9869	21.8	1.134	0.126	0.04
RD2	RD1	072643	239714	17	32	57	56	214	11726	24.9	1.197	0.180	0.68
RD20	RD1	074179	239577	16	15	227	50	336	11408	9.4	1.073	0.070	0.81
RD21	RD1	074003	240756	16	30	83	5	176	12870	7.6	1.059	0.057	0.81
RD22	RD1	074312	240307	17	11	65	37	163	14785	8.6	1.068	0.066	0.85
RD23 A	RD1	073363	239381	12	31	239	44	5	19904	28.4	1.218	0.197	0.59
RD23 B	RD1	073363	239381	16	28	236	41	354	20773	29.2	1.227	0.205	0.61
RD24	RD1	073833	238745	17	30	47	58	204	6186	21.1	1.148	0.138	0.48
RD25	RD1	073407	237922	17	24	250	55	20	1207	7.5	1.045	0.044	0.20
RD26	RD1	073127	238368	16	54	56	36	232	17520	29.7	1.230	0.207	0.59
RD27	RD1	073379	238768	15	37	53	53	223	15386	24.6	1.162	0.150	0.28
RD28	RD1	074314	238211	17	53	56	24	183	14770	23.8	1.186	0.171	0.67
RD29	RD1	074148	238845	16	21	54	42	164	19257	28.2	1.222	0.201	0.65
RD3	RD1	072497	240003	17	21	79	51	197	2734	11.5	1.081	0.078	0.58
RD30	RD1	073805	239126	14	17	64	45	172	15199	23.9	1.177	0.163	0.56
RD31	RD1	073757	238103	17	55	48	34	210	18303	33.8	1.231	0.208	0.29
RD32	RD1	072773	242824	16	21	126	69	319	12267	17.0	1.127	0.120	0.65
RD33	RD1	073205	242722	17	26	122	16	23	12914	18.8	1.154	0.143	0.81

AMS Data from the Roundstone Pluton

Site ID	Facies	East	North	N	K3 Plunge	K3 Trend	K1 Plunge	K1 Trend	Km x10^{-6}(SI)	H (%)	Pj	lnPj	Tj
RD34	RD1	073590	242806	15	13	118	56	228	12432	13.9	1.104	0.099	0.68
RD35	RD1	073113	243247	17	31	324	49	190	12084	16.1	1.129	0.121	0.79
RD36	RD1	073800	243877	17	20	125	31	227	8887	14.9	1.113	0.107	0.71
RD37	RD1	073574	243552	17	20	137	68	343	16542	16.9	1.128	0.120	0.67
RD38	RD1	074229	244155	15	22	141	68	333	15292	14.0	1.095	0.091	0.49
RD39	RD1	074156	243662	15	18	128	65	261	14663	15.0	1.106	0.101	0.56
RD4	RD1	072447	240491	18	54	98	10	202	10355	22.3	1.172	0.159	0.66
RD40	RD1	073732	243187	15	10	133	40	231	14120	12.0	1.092	0.088	0.76
RD41	RD1	074005	243372	15	9	138	52	239	11899	13.4	1.092	0.088	0.50
RD42	RD1	074379	243881	15	23	125	67	294	16421	17.0	1.117	0.111	0.49
RD43	RD1	074152	242506	17	19	120	14	25	13582	8.8	1.061	0.059	0.60
RD44	RD1	073983	242809	17	3	118	21	27	10512	10.5	1.088	0.084	0.93
RD45	RD1	074185	242996	17	1	314	83	214	19388	11.1	1.090	0.086	0.85
RD46	RD1	074535	243432	14	6	137	46	233	15714	9.1	1.062	0.060	0.53
RD47	RD1	074441	242270	11	20	108	66	323	15797	6.8	1.048	0.047	0.66
RD48	RD1	074988	242377	17	5	125	77	12	12449	5.0	1.031	0.031	0.35
RD49	RD1	076403	243458	15	11	47	70	286	16255	5.6	1.034	0.033	0.23
RD5	RD1	072452	240978	13	41	90	23	202	13624	28.5	1.221	0.200	0.62
RD50	RD1	076248	243084	17	0	45	71	315	7986	7.3	1.045	0.044	0.32
RD51	RD1	075683	242931	14	16	163	58	279	16061	6.6	1.039	0.038	-0.09
RD52	RD1	075242	242673	14	15	102	74	268	17545	8.5	1.051	0.049	0.07
RD53	RD1	074871	242879	16	0	294	40	204	9844	4.7	1.029	0.028	-0.32
RD54	RD1	075728	243327	7	10	12	80	18	15850	4.5	1.027	0.027	-0.33
RD55	RD1	075292	243537	15	2	351	81	247	18591	7.6	1.045	0.044	0.05
RD56	RD1	075071	243313	12	16	338	67	206	5651	6.3	1.043	0.042	0.57
RD57	RD1	074658	244058	14	10	132	71	252	11617	12.4	1.094	0.090	0.74
RD58	RD1	075014	243522	15	7	318	12	226	14213	4.6	1.036	0.036	0.87
RD59	RD1	074839	244360	16	23	144	58	277	17650	14.8	1.092	0.088	0.22
RD6	RD1	072585	241500	17	26	84	28	188	11912	22.3	1.169	0.157	0.63
RD60	RD1	074835	244363	15	19	145	61	273	15659	16.6	1.112	0.107	0.45
RD61	RD1	075276	244357	13	12	150	63	263	18118	14.3	1.090	0.086	0.26
RD62	RD1	075475	244691	15	8	167	74	284	7949	12.2	1.073	0.070	-0.09
RD63	RD1	076558	243627	17	1	23	84	281	11721	10.2	1.067	0.065	0.46
RD64	RD1	076290	243964	17	13	10	76	79	11931	8.2	1.049	0.047	0.05
RD65	RD1	076058	244171	17	0	188	80	281	14857	6.0	1.035	0.035	0.00
RD66	RD1	075854	244188	16	8	351	63	246	11159	6.7	1.040	0.040	0.19
RD67	RD1	075956	244455	17	6	9	67	264	16302	12.8	1.091	0.087	0.60
RD68	RD1	076608	244218	17	7	24	69	275	14711	7.9	1.051	0.050	0.40
RD69	RD1	077578	243713	17	7	216	82	66	16968	15.9	1.110	0.104	0.51
RD7 A	KIA	072831	242308	KIA	KIA	KIA	KIA	KIA	KIA	KIA	KIA	KIA	KIA
RD7 B	KIA	072831	242308	KIA	KIA	KIA	KIA	KIA	KIA	KIA	KIA	KIA	KIA
RD70	RD1	076998	244140	17	1	46	74	140	13392	10.3	1.071	0.068	0.54
RD71	RD1	077814	243733	9	0	234	79	324	16032	18.1	1.126	0.119	0.51
RD72	RD1	078365	243325	13	2	232	84	121	19728	25.7	1.209	0.189	0.72
RD73	RD1	078618	243092	13	5	248	63	147	7531	17.9	1.130	0.122	0.59
RD74	RD1	079565	242390	16	19	277	12	183	13374	12.0	1.087	0.083	0.64
RD75	RD1	079265	242372	15	2	77	47	344	18730	23.2	1.190	0.174	0.76
RD76	RD1	079430	242629	14	2	239	79	338	12985	18.0	1.129	0.121	0.56
RD77	RD1	079115	242800	17	3	49	76	149	16322	18.6	1.168	0.155	0.97
RD78	RD1	078936	243017	14	6	59	75	308	17474	20.9	1.171	0.158	0.79
RD79	RD1	078861	243292	17	1	32	83	298	4134	13.3	1.093	0.089	0.56
RD8	RD1	073152	242093	17	8	104	73	221	17957	21.4	1.191	0.175	0.92

AMS Data from the Roundstone Pluton

Site ID	Facies	East	North	N	K3 Plunge	K3 Trend	K1 Plunge	K1 Trend	Km x10^{-6}(SI)	H (%)	Pj	lnPj	Tj
RD80	RD1	078059	243752	19	6	278	67	21	15397	21.7	1.154	0.143	0.51
RD81	RD1	076639	244571	19	1	213	81	309	13282	14.5	1.094	0.090	0.36
RD82	RD1	076259	244688	20	2	210	69	305	9576	17.0	1.105	0.100	0.13
RD83	RD1	078326	242794	15	1	246	13	156	3889	11.5	1.083	0.079	0.63
RD84	RD1	077044	243458	2	11	43	38	141	15578	10.7	1.085	0.081	0.82
RD85	RD1	076835	243039	18	14	64	75	265	19332	8.3	1.052	0.051	0.34
RD86	RD1	077050	242942	20	7	59	82	271	6291	21.1	1.131	0.123	0.09
RD87	RD1	077175	242787	20	6	64	67	168	10736	7.6	1.054	0.053	0.66
RD88	RD1	077373	243241	19	18	61	69	209	22083	11.7	1.087	0.083	0.69
RD89	RD1	077639	243069	18	8	57	48	318	10729	9.5	1.069	0.067	0.67
RD9	RD1	073169	242122	17	12	284	70	49	17426	21.1	1.186	0.170	0.90
RD90	RD1	077923	242831	11	10	62	79	221	10105	11.7	1.097	0.093	0.90
RD91	RD2	076342	242403	18	5	54	84	212	11299	6.3	1.042	0.041	0.49
RD92	RD1	076785	242592	16	22	43	67	247	8503	5.0	1.030	0.030	0.20
RD93	RD1	076343	242775	16	10	40	73	165	17555	9.2	1.060	0.058	0.42
RD94	RD1	076636	242554	17	12	61	67	181	17158	8.9	1.060	0.058	0.48
RD95	RD1	076636	242553	19	19	63	71	244	15099	7.6	1.053	0.052	0.62
RD96	RD1	076791	242376	14	6	56	80	179	11918	9.5	1.058	0.056	-0.22
RD97	RD1	076843	242219	17	8	58	77	187	16839	10.3	1.079	0.076	0.77
RD98	RD2	075453	241361	19	36	136	54	310	12679	11.2	1.072	0.070	0.39
RD99	RD1	074998	241017	16	31	79	54	226	11381	4.2	1.025	0.025	0.22

AMS Data from the Carna Pluton

Site ID	East	North	N	K3 Plunge	K3 Trend	K1 Plunge	K1 Trend	Km x10^{-6}(SI)	H (%)	Pj	lnPj	Tj
G1.1	066547	239406	15	7	263	55	3	2871	5.3	1.03	0.03	-0.50
G1.10	066615	238850	15	34	98	39	335	4764	8.1	1.05	0.05	-0.05
G1.11	066907	238815	12	9	178	59	283	3915	5.3	1.03	0.03	0.35
G1.12	067925	238846	12	5	93	47	358	4777	10.0	1.06	0.06	-0.03
G1.13	067312	239218	15	3	267	43	0	3169	9.6	1.06	0.06	0.51
G1.14	067365	239500	8	25	270	11	5	94	2.7	1.02	0.02	0.09
G1.15	067157	239901	15	79	337	11	145	27	4.8	1.03	0.03	-0.03
G1.16	067528	239925	15	65	66	25	254	38	2.6	1.02	0.02	0.47
G1.17	067745	239681	15	2	266	40	174	1484	7.6	1.05	0.05	0.56
G1.18	067858	239903	15	67	156	10	272	39	2.2	1.01	0.01	-0.02
G1.19	068241	239754	15	78	11	3	115	29	3.9	1.02	0.02	0.21
G1.2	067832	239265	11	24	258	58	34	3443	8.5	1.05	0.05	-0.06
G1.20	068297	239281	15	18	274	31	15	895	15.9	1.12	0.11	0.63
G1.3	067832	239265	10	19	272	54	30	2063	12.2	1.07	0.07	0.05
G1.4	066820	239633	15	9	266	37	3	305	9.6	1.06	0.06	0.44
G1.5	068281	238873	15	39	246	42	24	8360	3.3	1.03	0.03	0.88
G1.6	068319	238967	13	3	261	84	144	292	4.4	1.03	0.03	0.13
G1.7	066362	239442	15	12	254	58	5	37	1.3	1.01	0.01	0.59
G1.8	066201	239153	9	2	62	62	328	2772	2.3	1.02	0.02	0.62
G1.9	066201	239153	15	27	103	50	336	3370	3.0	1.02	0.02	0.03
G2.1	071155	238254	13	18	217	71	54	13107	6.2	1.04	0.04	-0.11
G2.10	071493	238817	15	14	236	76	61	16537	5.9	1.04	0.04	0.42
G2.11	071953	238771	15	3	70	30	339	206	2.9	1.02	0.02	0.22
G2.12	067263	238564	15	25	163	64	323	7809	6.7	1.05	0.05	-0.63
G2.13	067263	238564	15	0	71	25	341	12648	9.8	1.06	0.06	0.44
G2.14	067263	238564	15	28	228	49	355	13450	6.3	1.04	0.04	-0.55
G2.15	067263	238564	15	7	111	24	18	14762	6.5	1.04	0.04	0.05
G2.16	072139	238594	14	69	253	11	134	15977	3.1	1.02	0.02	-0.39
G2.17	070588	239340	11	11	236	0	326	14584	3.5	1.02	0.02	0.17
G2.18	070161	239390	15	26	240	23	342	11669	4.5	1.03	0.03	0.42
G2.19	069631	239515	13	20	259	70	78	14732	4.3	1.03	0.03	0.42
G2.2	070655	238308	15	28	238	57	22	18045	6.4	1.04	0.04	0.19
G2.20	069096	239586	10	15	255	29	354	8077	5.4	1.03	0.03	-0.28
G2.21	068837	239548	4	29	47	61	219	2881	7.6	1.04	0.04	0.08
G2.22	068837	239548	4	20	240	47	354	10857	5.8	1.04	0.04	0.28
G2.23	068736	239107	15	14	81	47	187	16227	4.7	1.03	0.03	-0.10
G2.24	069416	239052	13	0	285	21	15	621	1.5	1.01	0.01	0.01
G2.25	069727	239040	10	59	236	29	30	18068	4.6	1.03	0.03	-0.11
G2.26	070694	239123	22	43	326	40	7	13478	2.7	1.02	0.02	-0.27
G2.27	067946	238467	15	8	79	31	344	8413	6.1	1.04	0.04	0.18
G2.28	068188	238791	12	9	267	80	111	10418	4.2	1.02	0.02	-0.16
G2.29	069141	238140	8	9	82	27	176	116	1.4	1.01	0.01	0.49
G2.3	070157	238544	15	12	237	70	111	10030	6.0	1.04	0.04	0.33
G2.30	069054	237730	11	36	171	48	28	13694	6.3	1.04	0.04	-0.55
G2.31	068749	237421	12	8	264	36	0	15553	5.7	1.03	0.03	0.21
G2.32	068749	237421	9	74	216	14	62	7239	12.7	1.08	0.08	-0.28
G2.33	068467	237770	12	1	85	54	354	16205	5.0	1.03	0.03	-0.33
G2.34	068622	238052	16	34	132	39	10	12479	5.4	1.04	0.04	-0.60
G2.35	068819	238146	11	3	100	26	9	5917	7.3	1.04	0.04	0.24
G2.36	068967	238239	13	2	258	36	349	10758	5.9	1.04	0.03	0.12
G2.37	069479	237732	12	11	208	65	322	20081	4.1	1.02	0.02	0.20
G2.38	069728	238280	15	17	273	37	17	17968	4.7	1.03	0.03	-0.55

AMS Data from the Carna Pluton

Site ID	East	North	N	K3 Plunge	K3 Trend	K1 Plunge	K1 Trend	Km x10^{-6}(SI)	H (%)	Pj	lnPj	Tj
G2.39	068855	238839	13	14	100	25	3	14334	2.9	1.02	0.02	-0.39
G2.4	070188	238822	13	23	274	33	20	7010	4.7	1.03	0.03	0.08
G2.40	069203	238722	15	9	92	65	203	10158	7.4	1.05	0.05	0.35
G2.41	069415	238465	13	17	269	61	32	13847	3.4	1.02	0.02	0.19
G2.42	069283	238612	9	4	217	31	309	3482	3.2	1.02	0.02	0.45
G2.43	069283	238642	12	9	242	60	348	12694	7.5	1.04	0.04	0.13
G2.44	069283	238652	13	38	249	42	23	18434	9.9	1.06	0.06	0.27
G2.45	074093	236666	13	1	53	55	145	15115	9.5	1.07	0.07	0.72
G2.46	074105	236670	9	23	278	54	153	21764	4.5	1.04	0.04	0.94
G2.47	074875	236194	13	17	231	39	126	17855	10.2	1.07	0.06	0.38
G2.48	076581	234937	11	41	254	28	137	5752	20.8	1.13	0.12	-0.01
G2.49	071624	237844	12	8	203	82	39	5470	6.6	1.04	0.04	-0.18
G2.5	070786	238449	4	27	110	57	251	9091	5.4	1.04	0.04	0.55
G2.50	072129	237780	10	25	241	56	14	17268	4.8	1.03	0.03	0.58
G2.51	073681	237213	10	18	190	69	336	5654	7.5	1.04	0.04	-0.02
G2.6	070786	238449	8	13	267	59	19	8572	6.9	1.04	0.04	0.03
G2.7	071137	238696	6	20	243	67	31	13702	3.4	1.02	0.02	0.31
G2.8	071555	238559	11	28	255	56	112	190	1.8	1.01	0.01	-0.47
G2.9	071555	238559	8	14	288	64	169	2885	4.9	1.03	0.03	0.32
G3.1	069654	237020	14	11	211	75	73	22241	5.4	1.04	0.03	0.47
G3.10	076968	230377	10	56	287	33	94	13800	4.4	1.03	0.03	0.23
G3.11	077661	230378	12	9	76	79	221	22601	5.9	1.04	0.04	0.28
G3.12	077643	231241	12	6	253	8	162	24971	6.9	1.04	0.04	0.46
G3.13	077193	231965	12	7	258	68	151	2368	10.8	1.07	0.06	-0.18
G3.14	077274	232749	10	11	239	19	145	22965	22.6	1.15	0.14	0.39
G3.15	077054	234093	12	18	236	23	138	13366	18.8	1.12	0.12	0.35
G3.16	076789	233924	11	7	233	22	141	13422	21.0	1.13	0.13	0.20
G3.17	076419	233420	11	17	232	1	142	15450	16.6	1.11	0.10	0.31
G3.18	076482	232079	12	13	234	22	139	11628	10.6	1.06	0.06	0.03
G3.19	076133	232506	10	7	220	57	119	16352	7.2	1.04	0.04	0.31
G3.2	070069	237162	8	15	221	75	27	20212	5.1	1.03	0.03	-0.52
G3.20	074521	235227	12	24	254	53	128	16433	5.1	1.04	0.04	0.76
G3.21	074521	235227	11	6	226	58	326	21267	10.3	1.06	0.06	0.17
G3.22	075180	235634	9	10	228	5	319	14828	8.6	1.06	0.05	0.38
G3.23	075022	234903	10	4	225	17	134	22033	15.0	1.09	0.09	0.23
G3.24	074767	234317	13	7	49	5	318	13974	10.3	1.07	0.07	0.55
G3.25	075319	234005	10	11	238	18	144	19680	16.3	1.11	0.11	0.49
G3.26	075670	233665	12	17	233	2	142	302	9.5	1.06	0.06	0.27
G3.27	076387	234422	10	17	231	24	133	17896	15.2	1.10	0.09	0.35
G3.28	074843	233322	12	15	219	69	353	16727	9.5	1.08	0.07	0.86
G3.29	073591	233218	13	26	194	13	290	21819	7.9	1.05	0.05	0.51
G3.3	070082	237426	15	18	167	67	26	17908	7.1	1.04	0.04	-0.28
G3.30	074250	233670	11	9	204	46	303	15213	6.1	1.04	0.04	0.59
G3.31	073936	234055	14	29	360	7	266	24602	13.3	1.10	0.10	0.73
G3.32	073424	235323	13	8	54	29	319	22946	8.3	1.05	0.05	0.43
G3.33	074095	234853	11	4	33	16	302	21128	8.6	1.05	0.05	0.36
G3.34	074417	229278	11	32	19	3	287	5783	9.6	1.06	0.06	0.03
G3.35	073037	234892	13	21	225	3	134	25385	4.5	1.03	0.03	0.36
G3.36	071455	236934	11	26	212	62	55	6297	5.1	1.04	0.04	0.71
G3.37	072027	236987	10	11	211	62	100	19910	7.8	1.05	0.05	0.54
G3.38	075794	234632	10	13	206	8	114	13033	13.7	1.09	0.09	0.45
G3.39	069388	237323	12	31	168	59	351	20843	7.0	1.04	0.04	-0.15

AMS Data from the Carna Pluton

Site ID	East	North	N	K3 Plunge	K3 Trend	K1 Plunge	K1 Trend	Km x10^{-6}(SI)	H (%)	Pj	lnPj	Tj
G3.4	075674	232795	15	22	238	32	133	14092	12.3	1.08	0.07	0.29
G3.40	069737	237544	11	30	152	60	345	17786	6.4	1.04	0.04	0.41
G3.5	076910	228348	10	10	319	13	227	20078	5.9	1.04	0.04	0.62
G3.6	076940	229656	12	23	292	67	105	15184	3.2	1.02	0.02	-0.07
G3.7	076391	229319	11	31	307	47	76	14895	4.5	1.04	0.04	0.90
G3.8	075453	229738	10	60	309	23	87	10730	5.0	1.03	0.03	0.39
G3.9	076080	230552	10	13	271	71	138	17948	5.6	1.04	0.03	-0.44
G4.1	073333	232209	15	8	284	23	17	9194	6.7	1.04	0.04	0.00
G4.10	074497	231116	15	16	298	44	44	7634	16.9	1.12	0.12	0.62
G4.11	074796	231038	15	53	262	37	76	8926	5.6	1.04	0.04	0.42
G4.12	074909	231930	15	44	244	19	135	17773	7.4	1.05	0.05	0.60
G4.13	075752	231159	15	46	256	40	107	18613	8.9	1.05	0.05	0.12
G4.14	075837	231723	11	10	225	13	133	4942	4.9	1.03	0.03	0.20
G4.15	074144	233038	11	4	187	62	286	54	1.2	1.01	0.01	-0.37
G4.16	073178	230171	12	48	66	40	270	8311	6.7	1.04	0.04	0.51
G4.17	071802	230259	12	18	53	36	309	20753	9.0	1.07	0.07	0.77
G4.18	072148	229743	11	24	68	64	228	12017	7.2	1.05	0.05	0.55
G4.19	073824	229573	12	38	31	7	296	10842	9.2	1.07	0.07	0.85
G4.2	073816	232297	29	68	167	5	270	20955	5.5	1.03	0.03	0.37
G4.20	074588	229699	11	45	356	5	91	10122	7.9	1.05	0.05	0.51
G4.3	073700	232634	15	25	185	7	92	8429	8.6	1.06	0.06	0.54
G4.4	074314	232851	15	7	269	78	145	2306	6.8	1.04	0.04	-0.40
G4.5	073541	231573	13	73	52	16	213	111	1.1	1.01	0.01	0.56
G4.6	073543	231580	15	55	104	21	341	6247	15.6	1.09	0.09	-0.08
G4.7	074710	232411	15	45	197	17	305	5533	3.7	1.02	0.02	0.45
G4.8	075155	232505	15	13	252	7	344	6761	6.3	1.04	0.04	0.56
G4.9	074386	231507	15	33	247	33	3	4192	3.9	1.03	0.03	0.66
G5.1	073684	231435	12	15	268	41	165	4089	5.6	1.03	0.03	-0.01
G5.2	073693	231426	15	6	81	55	343	2252	5.3	1.04	0.04	0.84
G5.3	074128	231552	15	37	96	31	339	801	1.9	1.01	0.01	0.19

Appendix D:

Rock Magnetic Principles and Practices

D.1 History and Topics Covered

Between 1819 and 1850, Hans C. Oersted, Andre-Marie Ampere, Jean-Baptiste Biot, Felix Savart, Michael Faraday and Lord Kelvin established the foundational concepts upon which our understanding of current and magnetism are based (see Whittaker (1951)). Later *Maxwells' Equations* (Maxwell 1865) capitalised upon the efforts of the above workers and gave a primitive synopsis on the relationship between electricity and magnetism. These equations show that a fundamental relationship exists between magnetic fields and current. By 1905 Einstein had demonstrated, through quantum physics and his theory of special relativity, that electric and magnetic fields are essentially the same phenomena simply viewed from contrasting reference frames (original paper Einstein (1905), see English translation in Einstein (1923)).

The basic electromagnetic principals developed by the above authors are exploited in order to understand the magnetic properties of geological samples (Stacey and Banerjee 1974; Collinson 1983; Tarling 1983; O'Reilly 1984; Tarling and Hrouda 1993; Hunt and Moskowitz 1995; Dunlop and Ozdemir 1997). Such data may be used at a outcrop or grain scale to identify a sample's constituent minerals by bulk susceptibility and remanence measurements (Lowrie and Fuller 1971; Lowrie 1990; Tarling and Hrouda 1993; Dunlop and Ozdemir 1997), to indirectly measure the crystal preferred orientation of a rock via Anisotropy of Magnetic Susceptibility analysis (Borradaile 1987; Tarling and Hrouda 1993; Bouchez 1997; Borradaile and Jackson 2010), to study the continental drift cycle of tectonic plates via magnetic remanence and palaeomagnetic studies (Tarling 1983; Tauxe 2002) or identify large scale structures and composition differences through, for example, airborne or ground based total magnetic intensity and vertical magnetic radiometry surveys (Nettleton 1971; Lowrie 2007).

At a fundamental level, rock magnetic experiments quantify the magnetic properties of a sample based on the influence that sample has on a controlled electromagnetic field. Section I establishes the electromagnetic principals from which the rock magnetic properties are calculated (summarised in Moskowitz (Unpublished)). Section II is a full account of factors which need to be taken into account during AMS analysis including measurement, statistical parameters, magnetic properties of minerals, grain scale anisotropy and the interpretation of AMS of rock samples. Section III details the principals behind techniques used to characterise the magnetic assemblage in material specimens. This has implications of both AMS and paleomagnetic interpretations as well as applications in secondary mineralisation processes and metamorphic geology. Section IV summaries key points which impact upon the interpretation of AMS analysis.

Section I Fundamental Equations

I.1 Fundamental equations

Any electrical current will have an associated magnetic field. In a loop with current (I) and radius (r) the *magnetic field* (H) at the centre of the loop is given by the equation;

$$H\ (A/m) = I / 2r$$

A *magnetic moment* (m), is associated with the magnetic field and determines the force that the magnet can exert, it is given by;

$$m\ (Am^2) = i \times \pi\ r^2$$

The *magnetisation* (M) is the intensity of the magnetic force per unit volume (v) and is calculated by;

$$M\ (A/m) = i \times \pi\ r^2 / v$$

Magnetic induction (B) is related to the magnetic field and magnetisation by;

$$B\ (T) = \mu_0\ (H + M)$$

where μ_0 is a constant, the permeability of free space.

The *magnetic moment per unit mass* (σ) is given by;

$$\sigma\ (Am^2/kg) = \frac{i \times \pi\ r^2 / v}{m}$$

Susceptibility (K) is an important property in rock magnetism. It is a measure of the ratio between magnetisation (M) and magnetic field (H) and is thus a dimensionless unit. It is given by;

$$K = M/H$$

The mass susceptibility of a material (χ) is given by;

$$\chi\ (m^3/Kg) = \sigma / H$$

Section II Measurement of low field magnetic susceptibility

II.1 Introduction

If any material is exposed to an electromagnetic field it will, at that time, become magnetised and interact with the applied field. Magnetic susceptibility (K) quantifies this interaction by measuring the ratio between the induced magnetisation and the applied field, as both M and H are measured in A/m, K is a unit-less quantity of measure. Several methods have been devised in order to measure magnetic susceptibility in the laboratory (see Tarling and Hrouda (1993) and Borradaile and Jackson (2010)) and in the field (e.g. Fugro instruments RT-1 magnetic susceptibility meter). In this study, all susceptibility measurements were carried out using AC currents on the Agico KLY-3 or MFK1-A Kappabridge and so only the measurement of low field susceptibility is discussed.

A low field magnetic susceptibility may be induced by lowering a sample (cube or cylinder) into a coil through which a weak AC current is passed. The applied current acts to temporally magnetise the sample and a neighbouring sensory coil measures the change in ambient magnetic field in the presence and absence of the subject sample, thus the influence of the specimen on the applied controlled fields is measured. By this means the induced magnetisation or magnetic susceptibility generated by the interaction between the samples mineral assemblage and the applied AC field is quantified. This gives the susceptibility of that sample along the axis parallel to the applied field only.

As individual minerals of the assemblage, as well as the sample itself, are texturally and magnetically anisotropic (e.g. Owens and Bamford (1976); Tarling and Hrouda (1993); Bouchez (1997)) the magnetic susceptibility will differ if measured along contrasting axes. In order to measure the *Anisotropy of Magnetic Susceptibility* (AMS) of the same sample it is necessary to repeat the above process on at least two more axes orthogonal to the first.

As with any statistical work, the more measurements made the better (assuming a systematic approach is taken). Generally speaking, as equipment has improved (e.g. Agico have manufactured the KLY1 and KLY2 that require manual sample rotation, the KLY3 is automated allowing more rapid measurement of multiple axes and the MFK 1 has the ability to vary the inducing field as well as automatically rotate a specimen) a larger number of axes are routinely measured (n=7, 9, 12, 15, 18, 24, 192 see Girdler (1961); Jelinek (1977); Borradaile and Stupavsky

(1995); Jelínek and Pokorný (1997); Tauxe (1998); Trindade *et al.* (2001); Kelso *et al.* (2002)). The convention of Jelinek (1977) has been applied by many authors in examining the structural evolution of igneous bodies (e.g. O'Driscoll *et al.* (2008); Stevenson (2009); Stevenson and Bennett (2011); Magee *et al.* (2012)) and has been deemed acceptable for this project.

Once recorded, susceptibility data can then be applied to a choice of matrix equations (see Girdler (1961); Jelinek (1977); Owens (2000a); Borradaile (2003)) all designed to solve the 6 independent elements of the second-rank tensor that defines the anisotropy of magnetic susceptibility (AMS) of a given sample. The second-rank tensor may be projected as a magnitude ellipsoid (Nye 1957) defined by the magnitude and orientation of the K_1, K_2 and K_3 axes which reflect the maximum, intermediate and minimum magnetic susceptibility axes of the sample under the specified induced magnetic field.

The shape and intensity of a specimen's magnetic susceptibly ellipsoid reflects the preferred orientation of the minerals within a sample, thus it can be related in orientation, but not directly in terms of magnitude, to the principal axes of the finite strain ellipsoid (e.g. Borradaile (1987); Tarling and Hrouda (1993); Borradaile and Henry (1997); Bouchez (1997); Borradaile and Jackson (2004, 2010)). It is important to note at this stage that the principal axes of the AMS ellipsoid may not always coincide with crystallographic long, short and intermediate axes (e.g. Potter and Stephenson (1988); Rochette (1988)) and further scrutiny of data is essential in order to correctly attribute AMS to the shape preferred orientation of silicate minerals, this is discussed further below.

So, AMS is an indirect means of measuring the material tensor. Just as measurement of quartz c-axes, reduction spots, enclaves, pebbles or fossils may be used to partially quantify finite strain but not finite stress, so too can AMS. However, the critical difference between the AMS ellipsoid and the finite strain ellipsoid is that the AMS ellipsoid varies in both shape and magnitude while the strain ellipsoid may only vary in shape. Therefore, data derived from traditional methods of strain quantification may be directly compared from outcrop to outcrop while AMS data may not and the relative magnitude of each ellipsoid must also be considered as this is controlled partially by crystalline anisotropy but also by the susceptibility properties of constituent minerals.

The means through which the AMS ellipsoid may be evaluated (data manipulation), the factors that control it (magnetic properties of minerals), the methods used to investigate these controls

(rock magnetic experiments), and the interpretation of AMS data (grain scale and composite rock samples) are discussed here.

II.2 AMS parameters and data manipulation

AMS analysis will yield three principal susceptibility vectors, K_1, K_2 and K_3. Regardless of the approach taken all subsequent interpretations are derived from these data and so it is important to capitalise upon this information without over interpreting it.

An averaged mean susceptibility value, (K_{mean}), is always calculated;

$$K_{mean} = \frac{K_1 + K_2 + K_3}{3}$$

this provides the mean value for the integral of the susceptibly value of the entire specimen (Nagata 1961). It may be used to indicate the quantity and species of the dominant magnetic mineralogy within the specimen (Tarling and Hrouda 1993) and also to normalise the susceptibility tensor to aid in distinguishing composite fabrics (Owens 2000b; Borradaile 2003).

The geometrical mean of the principal susceptibly axes (K_{geom}) may also be calculated;

$$K_{geom} = \sqrt[3]{(K_1 \times K_2 \times K_3)}$$

if it is desirable to represent the radius of the initial isotropic magnetic ellipsoid from one sample (as the undeformed strain ellipsoid) and compare it to the radius of neighbouring samples. This may be applied in attempts to correlate the magnitude of anisotropy with strain (Hirt *et al.* 1988).

Quite a broad variety of equations have been derived which attempt to characterise the shape and magnitude of the susceptibility ellipsoid (Nagata 1961) derived from K_1, K_2 and K_3 (see Tarling and Hrouda (1993) pp.18). The parameters;

$$L = K_1/K_2 \qquad F = K_2/K_3 \qquad P = K_1/K_3$$

where L = lineation (Balsley and Buddington 1960), F = foliation (Stacey 1960) and P = the anisotropy degree (Nagata 1961) are generally accepted as the most important. A sample may be strongly prolate or oblate or have both a L and F component. The relationship between these values may be determined by plotting L vs. F on a simple Cartesian graph.

This is an attractive system as it allows for very rapid "first glance" data evaluation. However, it is agreed that these parameters alone are insufficient for dealing with particularly low degrees of anisotropy, as is typically the case in AMS studies (e.g. Khan (1962); Hrouda *et al.* (1971); Owens (1974); Jelínek (1981)). L and F are merely ratios between the principal strain axes and do not take into account all available information, similarly the anisotropy degree is designed to describe the "*scatter*" of data points but fails to account for the K_2 value. Furthermore the P parameter does not really facilitate the scenario where a broad spectrum of susceptibly is measured within the same lithology; i.e. the anisotropy degree may appear to increase or decrease relative to a neighbouring sample when in fact no difference exists outside of a fluctuation in susceptibility brought on by composition variation (e.g. magnetite) rather than anisotropy.

Shape Factor and Corrected Anisotropy Degree

Recognising that the ratios between the principal susceptibility axes are of interest and not necessarily their absolute value (when determining AMS as opposed to mineralogy), Jelinek (1981) proposed a suite of new parameters which are calculated using the natural logarithms of K_1, K_2 & K_3;

$$n_1 = \text{Loge } K_1 \qquad n_2 = \text{Loge } K_2 \qquad n_3 = \text{Loge } K_3$$

and

$$n = n_1 + n_2 + n_3$$

Through this adaption, Jelinek (1981) calculated a new parameter, the *corrected anisotropy degree*;

$$P' = \exp \sqrt{\{ 2 [(n_1 - n)^2 + (n_2 - n)^2 + (n_3 - n)^2]}$$

to describe the scatter of the natural logarithms of the principal susceptibilities. Evaluating the natural logarithm values n_1, n_2, & n_3 relative to the principal quadratic elongations axes of Ramsay (1967), Jelinek (1981) also calculated the *shape factor* (T);

$$T = \frac{2n_2 - n_1 - n_3}{n_1 - n_3}$$

to describe the overall shape of the ellipsoid. T will always return a value between -1 and 1. When $-1 < T < 0$ the shape anisotropy is dominantly prolate and when $0 < T < 1$ the shape anisotropy is oblate, if T=0 the magnetic susceptibility is isotropic. As a quick means of testing the validity of data the *difference shape factor* U;

$$U = \frac{2K_2 - K_1 - K_3}{K_1 - K_3}$$

may be compared to T. As U is based only on the difference between the K_1, K_2 & K_3, in cases where anisotropy degree is low, a negligible difference between T and U is noted.

If P' and T are plotted on a simple Cartesian graph a poor representation of the actual fabric shape and degree of anisotropy is returned. As such, Borradaile and Jackson (2004) conclude that in order to obtain an unbiased distribution a polar plot is the preferred method of data projection, particularly when dealing with small P' values.

The advantage of this system over others is that in just two parameters one may concisely describe any ellipsoid based on an interpretation derived from all available data on a scale that suits the nature of the raw data (i.e. subtle degrees of anisotropy). Parameter P' allows one to efficiently determine the intensity or quantity of anisotropy, a neutral ellipsoid will return P' = P. The shape of two ellipsoids may be readily compared completely autonomously of P'. In this way one may compare and contrast neighbouring data points in terms of fabric quality and shape

independently. This is a valuable parameter for evaluating strain distribution as, for example, it provides a single parameter for each data point which may be contoured for the visual representation of large data sets (e.g. Esmaeily *et al.* (2007); Petronis *et al.* (2012)).

Another useful set of parameters are the Lineation (L_1) and Foliation (F_1) of Khan (1962) and the percent of total anisotropy (H) and the anisotropy shape (μ) of Owens (1974), these are defined as;

$$L_1 = \frac{K_1 - K_2}{K_{mean}} \qquad F_1 = \frac{K_2 - K_3}{K_{mean}} \qquad H = \frac{K_1 - K_3}{K_{mean}} \qquad \mu = \tan\text{-}1\ L_1/F_1$$

These parameters normalise all product values to K_{mean} and so the problems relating to susceptibility contrasts with L, F and P are avoided. H represents the total anisotropy degree and is often quoted as a percentage (O'Driscoll *et al.* 2008; Stevenson *et al.* 2008b; Magee 2011; Stevenson and Bennett 2011), which requires the product of this parameter to be multiplied by 100. The anisotropy shape μ ranges from 0-90°, if $0 < \mu < 45$ the fabric sits in the oblate field while if $45 < \mu < 90$ a prolate fabric is present, in the same fashion as the symmetry for the deformation ellipsoid is determinable using the Flinn (1965) nomenclature.

Stereographic projection of Normalised vs. Un-normalised tensor data

In order to obtain a high quality representative AMS ellipsoid, it is good practice to analyse between 10-20 sub-samples per site where possible (depending on grain size see Tarling and Hrouda (1993)). This data is incorporated into the statistics above in order to determine the magnitude and shape of the ellipsoid. It is also useful to project the orientation of K_1, K_2 & K_3 onto a stereonet.

On a stereonet, the pole of a foliation is defined by K_1 while the best fit great circle between K_2 & K_3 denotes the foliation plane. A prolate fabric is defined by the orientation of K_1. Depending on the distribution of data points one may determine whether an L, S or L-S fabric is present. Generally speaking, if K_3 has a tight confidence ellipse and K_1 & K_2 overlap an oblate fabric will be interpreted, a prolate fabric is determined in the reverse case where K_2 & K_3 overlap

and K_1 is well constrained. In the instance where K_1, K_2 & K_3 are well constrained a L-S fabric may be interpreted.

Data is typically projected stereographically in one of three formats, individual point data with a K_1, K_2 & K_3 for each sub-sample from a single block, un-normalised (six-fold tensor) point data represented by a 95% confidence ellipse for each K_1, K_2 or K_3 axis or as data normalised by the mean of its trace elements (five-fold tensor) and represented by a 95% confidence ellipse for each K_1, K_2 and K_3 axis. Projecting data in this manner allows one to inspect the relative orientation of each individual sub-sample analysis and thus further evaluate interpretations made on the parameters discussed above.

Hext (1963) formulated a basis for evaluating error during the measurement of physical vector quantities described by 3x3 symmetrical matrices (applicable to the AMS tensor) and Jelinek (1977) devised a six fold multivariate statistical model for the analysis of the six independent elements of the AMS tensor. As this analysis is based on un-normalised data, the authors assume a normal distribution between independent elements of the susceptibility tensor. When dealing with geological samples, it is quite resonable to consider the possiblity that this is not the case (e.g. Constable and Tauxe (1990)). Owens (2000b) highlights that the statistical analysis of Jelinek (1977) was designed to deal with un-normalised data sets (six-fold), thus this author deemed the methodology unsuitable for dealing with normalised data (five-fold) and developed a new analysis method more suited to the evaluation of normalised data.

The importance of inspecting both normalised and non-normalised data in order to avoid incorrect interpretation of AMS data is now well documented. More often than not, the actual orientation of the principal susceptibiltiy axes will not be significantly repositioned after normalisation but confidence ellispse fluctuations can occur and may suggest that a unimodal interpretation is too simplistic.

Using two contrasting samples Owens (2000b) demonstrated the benefits of inspecting both normalised and unnormalised data. In his example, the stereographic projection from one sample exhibits almost identical normalised and un-normalised distributions while data from a second sample shows a significant discrepencey between the size and shape of normalised and unnormalised confidence ellipses. If inconsistencies are observed between the normalised and un-normalised stereographic projections it is not advisable to represent the principal susceptability data by a single mean as it is likely that more than one fabric is present that has

produced a composite AMS. In such cases further investigation using more sophisticated magnetic analysis methods is advised (e.g. Hrouda (1992); Housen *et al.* (1993); (Martin-Hernandez and Ferre 2006)).

Summary

A broad variety of parameters are available to statistically evalute AMS second order tensor data. Two of the more commonly applied methods are discussed above and both are applied in the course of this work, the parameters of Jelinek (1981) are favoured.

The P' parameter incorporates K_2, as well as K_1 and K_3 and thus takes advantage of a broader data field than some other statistical options. Furthermore, this parameter is based on logarithmic values and thus is best suited to describe the lognormal distribution of the anisotropy degree parameter (Tarling and Hrouda 1993). The T parameter is chosen as, again, it incorporates all available data and is symmetrical in its distribution of values across all ellipsoid shapes (Jelinek 1981). In addition the U offers an immediate means through which one may directly compare T, if a low degree of anisotropy is present U and T will be very close.

The parameters L_1, F_1, H_1 and μ are also applied in this study and used primarily as a means to cross examine interpretations from the primary set of calculations discussed above. These cannot be considered more appropriate for measuring low degrees of anisotropy (*c.f.* O'Driscoll *et al.* (2008)). Only very rarely is any contrast of potential consequence noted, it seems that either set of statistics may be used with crudely equal merit for the structural investigation of intrusive bodies. However given the broader user base of Jelineks' parameters and the added robustness of the log based system, L_1, F_1, H_1 and μ are only used as a means to double check the validity of manipulated data. Since these calculations can be made in such an efficient manner (automated in Microsoft Excel) and plotted instantaneously (ArcMap 10.1 and Golden Software Surfer8) it seems sensible to quickly compare these two sets of statistics.

In the case where small variations in distribution exist between sub-specimen vectors, un-normalised and normalised data return similar stereographic projections, thus un-normalised data is preferable in this case (Lienert 1991). If a broad distribution is detected or suspected, further investigation of normalised data may aid invesitagion of polyphase fabric development and final intepretation (Owens 2000b; Borradaile 2003).

The software used to generate AMS stereographic projections and numerical data (see Appendix F) facilitate the rapid generation of RS6 and RS5 data files (un-normalised and normalised respecively). From these a variety of styles of stereographic projection can be generated with little effort. As such, normalised and un-normalised stereographic projects have been used in interpreting AMS data from all sites examined in this work. In addition, both data sets are plotted against each other in map view (plotted as foliations and lineations) to scrutinise the product data for any inconsistencies which may uncover hidden information.

Finally, it is important to reitterate that AMS data provide the end user with three orthogonal best fit susceptability vectors, K_1, K_2 & K_3 and a stereographic projection of the distribution of sub-samples from each studied site. Correct handling of these data may facilitate the isolation of AMS contributions from specific mineral species and hence identify distinct fabrics within a single sample (Borradaile 2003; Borradaile and Jackson 2010). At the same time, data can easily be over interpreted and valuable information lost through lack of proper data analysis and scrutiny. AMS is a tool best complimented by solid field mapping, microstructural evaluation, petrographic analysis and, critically, a sound understanding of the magnetic behaviour of the host's mineral assemblage (e.g. Steenken *et al.* (2000); López de Luchi *et al.* (2004); Petronis *et al.* (2004); Mamtani and Greiling (2005); Esmaeily *et al.* (2007); Petronis *et al.* (2011); Petronis *et al.* (2012)).

II.3 Magnetic classification of materials

All materials will become magnetised to some degree when placed inside a magnetic field. At room temperature all rock forming minerals can be classified as either *ordered* or *disordered*.

At the atomic level and in the absence of an inducing magnetic field, disordered minerals have a random, uncooperative electron spin, as such no net magnetic moment is present. By applying a progressively intense magnetic field, electron spin moments begin to become ordered and the mineral will become magnetised. Once the magnetic field is removed magnetic ordering will be lost and no magnetic remanence will remain. So, disordered materials exhibit a linear and reversible relationship between the applied field and induced magnetisation under "normal" (see below) magnetic fields. Most rock forming minerals are disordered and fall into one of two material categories, *diamagnetic* or *paramagnetic*.

Ordered minerals exhibit magnetic ordering at room temperature and so can (but don't have to) posses a net magnetic moment outside of an induced magnetic field. Such minerals exhibit a non-linear relationship between an applied field, induced magnetisation will plateau once a critical field intensity is reached, at this point the material reaches its *saturation magnetisation* (M_S). After M_S is reached, M will not increase regardless of an increase in the inducing H. Ordered minerals are also capable of retaining some of the magnetisation gained during exposure to a magnetic field, this is referred to the *remanant magnetisation* (M_r). Magnetically ordered minerals all fall under the umbrella term ferromagnetic *senso lato*.

II.3.1 Diamagnetism

Diamagnetic minerals characteristically exhibit a very weak inverse linear relationship with induced magnetic fields. Random electron spin moments in full orbital shells prevent magnetic ordering outside of a magnetic field. When exposed to a magnetic field, due to the absence of unpaired electrons, intrinsic electron magnetic moments cannot generate any overall influence and instead magnetisation is driven solely by the orbital motion of paired electrons. This results in the development of a weak magnetic moment generated in the opposite direction to that imposed by the inducing field.

As all materials have paired electrons, all exhibit diamagnetic behaviour but only matter with fully paired outer shells will exhibit purely diamagnetic behaviour. As such only very few common rock forming minerals are exclusively diamagnetic (quartz, orthoclase feldspar, calcite, fosterite) and exhibit weakly negative magnetic susceptibilities in the order of $\chi \sim 8 \times 10^{-9}$ m^3/kg (Tarling and Hrouda 1993). Under most conditions the presence of paramagnetic or ferromagnetic minerals will dominate any diamagnetic influence; however diamagnetism is not temperature dependent and ferromagnetism (*senso lato*) is. Therefore, where a sample contains very small proportions of ferromagnetic minerals, or at elevated or reduced temperatures, paramagnetic minerals may dominate. Where ferromagnetic minerals are absent and only a small proportion of paramagnetic minerals are present, diamagnetic minerals may dominate. A table of some diamagnetic minerals and their generalised properties may be found in Tarling and Hrouda (1993) pp. 32.

II.3.2 Paramagnetism

Paramagnetic minerals do not retain any magnetisation outside of an applied magnetic field but do exhibit a net magnetic moment in the direction of an applied field. These minerals have some proportion of atoms or ions (most commonly Fe) which have only partially filled orbital's and so carry a net magnetic moment. In the context of magnetic behaviour of the crystal as a whole unit, magnetic moments between atoms with electron vacancies are assumed not to interact (Dunlop and Ozdemir 1997) and thus outside of a magnetic field these moments are randomly ordered. When a magnetic field is applied, atoms with electron vacancies become ordered and a magnetic moment in the direction of the induced field is produced. A positive linear relationship between the applied field and induced magnetisation is observed at room temperature under "normal" magnetic field conditions. Paramagnets can reach saturation magnetisation (Ms) but extremely large magnetic fields are required in order to align the maximum amount of permanent moments (*c.* 100T). Thus paramagnetism is the partial alignment of atomic magnetic moments in the direction of an applied field (Dunlop and Ozdemir 1997), once the field is removed the sample loses any magnetic ordering and no magnetic remanence is preserved. A diamagnetic component from paired electrons is always generated but it is outweighed by the paramagnetic component.

Paramagnetic minerals are temperature dependent and subject to Curie's Law where;

$$M = C (B / T)$$

This shows that at a fixed temperature a linear relationship between M and H is expected but as temperature increases susceptibility decreases, i.e. susceptibility is inversely proportional to temperature (see Dunlop and Ozdemir (1997) pp. 24). At room temperature, most paramagnetic minerals exhibit susceptibilities of $\chi \sim 1\text{-}13 \times 10^{-7}$ m^3/kg (will fluctuate positively with increasing iron content in the crystal lattice). So, paramagnetic minerals are several orders of magnitude more susceptible than diamagnetic species and so only a small amount of paramagnetic material (*c.* 5 wt %) is required in order to overshadow a diamagnetic influence (Rochette 1987; Tarling and Hrouda 1993). Most iron bearing silicates, carbonates and sulphides are paramagnetic at ambient temperatures (e.g. biotite, chlorite, muscovite, tourmaline, amphiboles, ilmenite, and pyrite) (see table in Tarling and Hrouda (1993) pp. 32).

II.3.3 Ferromagnetism

The term ferromagnetic *senso lato* refers to a group of materials which exhibit spontaneous magnetisation. Three sub-groups of materials are included by this definition; ferromagnetism, anti-ferromagnetism and ferrimagnetism, these are distinguished based on the means through which electron exchange forces interact. Thus ferromagnetism is used in reference to all "magnetic" materials but also in a more precise sense to describe a specific style of spontaneous magnetic coupling which is not observed in anti-ferromagnetic or ferrimagnetic materials (see Getzlaff (2007)).

II.3.3.1 The Ferromagnetic Group

In the broadest sense, ferromagnetism describes a material which has a spontaneous magnetisation, i.e. possesses magnetic ordering outside of a magnetic field, such material is sometimes referred to as being *magnetic* (Dunlop and Ozdemir 1997; Getzlaff 2007). This is a property of the first transition series of elements and compounds of them. In geology and rock magnetism the oxides, hydroxides and sulphides, particularly those containing iron, are of particular importance.

Spontaneous magnetisation is associated with the spontaneous coupling of electron spins, this generates a net magnetic moment at the crystal lattice scale. Characteristically, ferromagnetic minerals exhibit a non-linear relationship between an applied field and magnetic susceptibility. Magnetic saturation (M_s) is reached in lower magnetic fields relative to paramagnets and partial magnetic ordering may be retained after a strong magnetic field is removed, giving a remanant magnetisation (M_r). These properties may be exploited in order to identify the type of ferromagnetic minerals in a sample, their relative quantities, grain size and so grain scale magnetic properties (e.g. Strangway *et al.* (1967); Lowrie and Fuller (1971); Dunlop (1986); Potter and Stephenson (1988); Borradaile and Puumala (1989); Kletetschka *et al.* (2000); Aubourg and Robion (2002); Lui *et al.* (2004)), this is discussed below.

Ferromagnetism is temperature dependent, once a critical temperature is exceeded no spontaneous magnetic ordering will remain and the material will behave paramagnetically (see below). Thus, ferromagnetism is always superimposed over paramagnetic and diamagnetic components. At room temperature, due to very large susceptibly contrasts between diamagnetic and ferromagnetic minerals, a minute quantity of the latter (*c.* 0.1-1 wt%) is generally sufficient

to cloak a diamagnetic contribution (Rochette 1987; Tarling and Hrouda 1993). Similarly, but not in such an extreme manner, a smaller quantity of ferromagnetic material can drown out a paramagnetic susceptibly component. As a very rough guide, if $K_{mean} \sim 5 \times 10^{-3}$ and the host is *c.*10% paramagnetic AMS is likely controlled by a ferromagnetic fraction, if K_{mean} is $\sim 5 \times 10^{-4}$ and the host is ≥ 10% paramagnetic AMS is dictated by the paramagnetic component (Tarling and Hrouda 1993). AMS is more often controlled by a combination of both ferromagnetic and paramagnetic components, the predominance of one over another is dictated by the magnetic properties of the particular mineral species, their relative concentration and the ambient temperature (see Lowrie (1990); Tarling and Hrouda (1993); Borradaile and Stupavsky (1995); Dunlop and Ozdemir (1997); Edgardo (2001); Borradaile and Jackson (2004); Gaillot *et al.* (2006); Borradaile and Jackson (2010)).

II.3.3.2 Types of Ferromagnetic Materials

If electron spins are coupled between two adjacent cations without the use of an intermediate anion the *exchange force* between electrons causes all magnetic moments to align in the same direction, this behaviour is known as *ferromagnetism senso stricto* (Tarling and Hrouda 1993). Direct exchange of electrons occurs in simple compounds of the first transition series elements and in some alloys of these.

When electron coupling is facilitated by an intermediate ion, a *super exchange force* acts to couple electron spin moments. This leads to adjacent cations having reverse electron spins, and so equal magnetic moments align in an anti-parallel fashion across the crystal lattice. Ultimately these magnetic forces cancel each other out and no net moment is generated, this is *anti-ferromagnetic* behaviour (Tarling and Hrouda 1993). Anti-ferromagnetism is observed in more complex compounds of the first transition series.

In the case where opposing magnetic moments are aligned in anti-parallel fashion but magnetisation is greater in one direction, a net spontaneous magnetic moment will be generated, this is *ferrimagnetic* behaviour (e.g. magnetite, titanomagnetite).

A final sub-group, which is very similar to anti-ferromagnetic ordering, is *canted* or *parasitic* magnetism. This occurs when neighbouring spin moments are very slightly oblique (*c.*1°) and thus the magnetic moments from anti-parallel lattices do not cancel each other out perfectly. Hematite is a well studied example of canted anti-ferromagnetism.

For a more comprehensive account of properties of ferromagnetic minerals (*senso lato*) the reader is referred to Dunlop and Ozdemir (1997) and Getzlaff (2007). A generalised table of ferromagnetic minerals and their properties may be found in Tarling and Hrouda (1993) pp 30.

So, a ferromagnetic material (senso stricto) is one in which the spontaneous magnetic moments are ordered in the same direction, anti-ferromagnetic materials have adjacent spontaneous sub lattice moments ordered in exactly equal but opposite directions and have no net moment and ferrimagnetism occurs when sub-lattice moments are in non-equal opposing directions giving a net moment in one direction.

II.3.3.3 Temperature dependence

All ferromagnetic materials (*senso lato*) exhibit temperature dependent magnetism. Above a critical temperature, known as the Curie Temperature (T_C) for ferromagnetic and ferrimagnetic materials and Neel Temperature (T_N) for anti-ferromagnetic materials, thermal energy will overcome electron exchange and super exchange forces and destroy magnetic coupling. As a result, the material will behave paramagnetically. Disturbance of the ordering of electron spin moments is caused by a 2nd order phase transition, i.e. the change of specific energy and density is continuous and no release or absorption of latent heat occurs (see Brokate and Sprekels (1996) pp. 155).

As ferromagnetic materials behave paramagnetically above T_C/T_N, they will acquire a relatively small net magnetisation when exposed to a magnetic field. The magnetism gained by the re-ordering of thermally disordered electron spin moments is given by the Curie-Weiss Law;

$$K = C / (T - T_C)$$

where C is Curies constant of a material, T is the absolute temperature in Kelvin and T_C is the Curie temperature of the subject material. This equation accounts for the fact that moments are now coupled by a magnetic field and not by mutually independent electron exchange forces and shows that above T_C susceptibility approaches infinity (see Dunlop and Ozdemir (1997) pp.27).

T_C/T_N will vary within a characteristic temperature bracket according to mineral species and precise elemental composition. A stepwise heating and cooling T *vs.* K profile between room and *c.*700°C is commonly used to identify particular minerals and properties present in a composite material, such a geological sample (e.g. Petrovský *et al.* (2006)). T_C/T_N may be estimated using the inflection point method (Tauxe 1998) or the Hopkinson peak method (Moskowitz 1981), hence ferromagnetic mineral species can be identified (e.g. Lattard *et al.* (2006)).

Due to the dependence of these T_C on mineral composition, Curie point estimations can also used as a proxy for Ti content in titanomagnetite (Akimoto (1962); Lattard *et al.* (2006), but see Petrovský *et al.* (2006)). The grain size of ferromagnetic minerals may also be estimated based on the shape of the Hopkins Peak, a narrow abrupt peak is more typical of single domain grains while a smoother curve indicates either a mixed or multidomain grain size (Dunlop and Ozdemir 1997). The precedence of SD over MD grains in a specimen may generate inversion of the AMS fabric (see below). Thus, inspection of the shape of the Hopkins Peak can be used as an aid to determine the relationship between magnetic and visually observed fabrics. The shape of a continuous T vs. K profile may indicate the presence of more than one ferromagnetic mineral, and interpreting the shape of the heating *vs.* cooling curve, one may interpret weather the heating process generated new mineral growth, this can carry inferences regarding, for example, the hydrothermal alteration history of a granite (e.g. Petronis *et al.* (2011)).

II.3.3.4 Domain theory

Spontaneous magnetisation is uniform in magnitude but may not be in direction across a sample. Areas within a single crystal that have different spontaneous magnetisation directions are called *domains*. Magnetic domains vary between 1-100's microns in size, two neighbouring domains are separated by a *bloch* or *domain wall* which mark the reversal of the direction of spontaneous magnetisation between domains (for example see O'Reilly (1984); Hunt and Moskowitz (1995); Getzlaff (2007)). In the absence of an inducing magnetic field, neighbouring magnetic domains serve to counteract each other and reduce magnetostatic energy (Landau and Lifschitz 1935). Thus, the domain architecture of a crystal is controlled by the availability of magnetostatic energy, ultimately this is dependent on grain size of a particular composition at a constant temperature.

Positive and negative charges will segregate to opposite ends of a single domain grain to create a simple loop system. The *surface charge* or *demagnetising field* formed by this concentration of charge is termed the *magnetostatic energy*, it is energetically favourable to have this value low. Magnetostatic energy can be continually reduced by dividing a grain into increasing numbers of domains each separated by a domain wall. Domain walls are transitional zones along which magnetic moments are progressively rotated into parallelism with adjacent domains. Large numbers of broad domain walls greatly reduces exchange energy by comparison to fewer more abrupt walls (Dunlop and Ozdemir 1997). Thus competition exists between magnetostatic energy and exchange energy and this dictates the domain architecture of ferromagnetic grains. For a comprehensive treatment of magnetic domains the reader is referred to (Dunlop and Ozdemir 1997).

Smaller grains have fewer domains due to lower abundance of magnetostatic energy. Generally speaking, in smaller grains (e.g. magnetite or hematite *c.*1µm) it is not energetically favourable to build domains walls, hence *single domain* (SD) grains are common (Tarling and Hrouda 1993). For larger grains (*c.*100µm) magnetostatic energy is elevated if only a SD exists, in order to obtain an energetically favourable scenario two or more magnetic domains form, this is called a *multidomain* (MD) grain (Tarling and Hrouda 1993).

Pseudo single domain behaviour has also been documented (Stacey 1963) whereby larger grains exhibit SD behaviourisms (see below). The most important of these is that SD and PSD grains have high coercivity of remanence and so are magnetically *hard* while MD grains have lower coercivity of remanence and are magnetically *soft*. Tarling and Hrouda (1993) attribute such characteristics to lattice imperfections which pin domain walls and thus impede the "easy" reorientation of domain walls.

II.4 Grain Scale Magnetic Anisotropy

The magnetic anisotropy of individual grains is controlled by three phenomenon, magnetocrystalline, shape and magnetostriction anisotropy, the relative importance of these varies according to mineralogy and grain size. Magnetic anisotropy controls the remanence and coercivity of minerals, and thus has implications for the interpretation of rock magnetic experiments.

II.4.1 Magnetocrystalline Anisotropy

Magnetocrystalline anisotropy is a measurement of the energy required to deflect the magnetic moment in a crystal from one crystallographic direction to another. This intrinsic property is dependent on crystalline structure as this determines "easy" and "hard" directions of magnetisation. A perfect sphere of magnetite exhibits six easy axes of magnetisation that correspond to three [111] axes while chain and sheet silicates may exhibit just one easy axis approximately parallel to the longest axis of the crystal and a hard axis at a high angle to the basal c-plane (Dunlop and Ozdemir 1997).

Self demagnetising fields are negligible in paramagnetic and antiferromagnetic grains and so crystallographic controls over these minerals magnetic anisotropies are extremely prevalent (Borradaile and Jackson 2004). Hence for most of these minerals a strong relationship prevails between the AMS ellipsoid and crystal orientation, as K1 and K3 are typically close to parallel to respective long and short axes of a subject mineral (Tarling and Hrouda 1993). More information on the magnetic properties of paramagnetic minerals can be found in (Beausoleil *et al.* 1983; Tarling and Hrouda 1993; Borradaile and Werner 1994; Dunlop and Ozdemir 1997; Martin-Hernandez and Hirt 2003b)

Most rock forming minerals exhibit paramagnetic magnetisation, the anisotropy of which is controlled by crystal structure (e.g. phyllosilicates, olivine, pyroxenes, amphiboles, see Borradaile and Jackson (2004)). Tourmaline exhibits an inverse magnetic anisotropy in an inducing field due to K3 being parallel to the long axis (c-axis), cordierite also sometimes returns an inverse AMS fabric (Rochette *et al.* 1992). This is a rare feature of paramagnetic minerals and can lead to gross misinterpretation, in such cases careful data and analytical analysis is required (see below).

II.4.2 Shape Anisotropy

The formation of poles at the surface of magnetised grains generates a surface charge distribution that acts in opposition to the magnetisation that produces this charge, this is known as the *demagnetising field*. The intensity of the demagnetising field (H_d) is given by;

$$H_d = -NM$$

where N is the demagnetising factor. It follows that the internal field of a grain (H_i) that is subjected to a magnetic field H_o may be given by;

$$H_i = H_o + H_d$$

and that measured susceptibility (K_o) is determined by the sample's intrinsic susceptibility (K_i) (both of which are ratios of magnetisation against measured and induced magnetic field respectively) by the equation;

$$K_o = \frac{K_i}{1 + NK_i}$$

as the demagnetisation factor must be taken into account (see Borradaile and Jackson (2010) and references there in).

Shape anisotropy is a product of the net interaction between a grain's magnetostatic self-demagnetisation and its intrinsic magnetisation which is accentuated by grain shape (Borradaile and Jackson 2010). As expected from the above equations, self demagnetisation is increasingly prevalent in smaller grains which exhibit higher spontaneous magnetisations, fewer domains and larger aspect ratios as such characteristics serve to further increase surface charge and the demagnetising field. Thus, in cases where SD needle shaped grains are present magnetocrystalline and magnetoelastic anisotropies are usually completely cloaked by the overwhelming effects of shape anisotropy while for spherical grains no shape anisotropy will be present (Dunlop and Ozdemir 1997). Relatively speaking however, ferromagnetic minerals are always affected to some extent by shape anisotropy as spontaneous magnetisation will always generate a demagnetising field. A relationship exists between M_S and the precedence of shape anisotropy over magnetocrystalline anisotropy in that when M_S is reached at lower fields anisotropy tends to be dictated more so by the latter (Dunlop and Ozdemir 1997). On the other hand, in paramagnetic minerals magnetic susceptibility is always dictated by the structure of the crystal lattice, as do some exceptional ferromagnetic minerals such as hematite and pyrrhotite i.e. magnetocrystalline anisotropy (Rochette *et al.* 1992; Tarling and Hrouda 1993).

II.4.3 Magnetostriction

Modification in the dimensions of a ferromagnetic crystal as a direct product of magnetisation is known as *magnetostriction* (Dunlop and Ozdemir 1997). This phenomenon is caused by small spontaneous strains on the crystal lattice associated with magnetisation, strain causes either positive or negative magnetostriction depending on whether it operates in opposition or parallel to the magnetisation direction (Moskowitz 1993). *Magnetoelastic anisotropy* acts to counter magnetostriction and causes magnetisation energy to fluctuate positively with tensile stress and negatively with compressive stress (Moskowitz 1993). The product of stress associated with magnetisation is that remanent magnetisation rotates away from the principal axis of compressive stress thus magnetisation is reduced along this axis, a permanent or passive affect is dependent on material properties and intensity of an applied inducing field (Nagata and Kinoshita 1967; Revol *et al.* 1978). In terms of implications for AMS analysis magnetostriction is negligible as the spontaneous strain associated with spin-orbit coupling is extremely small (order of 10^{-5}) and thus shape anisotropy and magnetocrystalline anisotropy are much more influential (Dunlop and Ozdemir 1997; Borradaile and Jackson 2010).

II.5 AMS of some minerals

The relationship between the orientation of the AMS ellipsoid, and bulk susceptibility, of individual minerals vary according to stoichiometry, impurity and inclusion content, thus no standard values relating AMS to mineral structure exist (Borradaile and Jackson 2010). Published values (e.g. Rochette *et al.* (1992); Tarling and Hrouda (1993); Dunlop and Ozdemir (1997)) act as guides but not absolute values which characterise susceptibility in any particular mineral. For a detailed account of AMS associated with particular minerals the reader is referred to Nagata (1961); O'Reilly (1984); Thompson and Oldfield (1986); Tarling and Hrouda (1993) and Dunlop and Ozdemir (1997).

II.5.1 Common Diamagnetic Minerals

In rocks which are composed almost exclusively of diamagnetic minerals, such as quartz, calcite, and dolomite, only weak negative susceptibility values are detected which is controlled by

the predominant diamagnetic mineral, in such circumstances these are important magnetic carriers (Friedman and Higgs 1981). However, due to extremely low susceptibility values exhibited by these minerals, a presence of only 0.001% of ferromagnetic or less than 10% of paramagnetic minerals is sufficient to generate bulk positive susceptibility values and dictate the low field AMS of a sample (Tarling and Hrouda 1993).

Quartz and calcite have been reported to return inverse AMS fabrics (e.g. Owens and Rutter (1978); Rochette (1988)). Such instances occur in deformed specimens as a product of crystal plastic deformation which promotes recrystallisation and c-axes growth perpendicular to the principal stress direction (Lagroix and Borradaile 2000b; Almqvist *et al.* 2010). Thus the most negative susceptibility axes, equivalent to K1, is orientated perpendicular to the new foliation (Hamilton *et al.* 2004).

II.5.2 Common Paramagnetic Minerals

Iron bearing paramagnetic silicate minerals are important contributors to the AMS ellipsoid especially in samples with low ferromagnetic abundances (*c.* <1-2% (Tarling and Hrouda 1993)). Crystalline structure dictates the magnetic anisotropy of these minerals as demagnetising fields and magnetisation values are extremely low (Dunlop and Ozdemir 1997). Amphibole, pyroxene and olivine all return principal susceptibility axes approximately parallel with attributing crystal dimensions and thus conveniently relate petrofabrics to the AMS ellipsoids (Borradaile and Jackson 2004). As discussed above, tourmaline and cordierite may return inverse fabrics (e.g. (Bouchez *et al.* 2006)).

Due to the high shape parameter and anisotropy degree values exhibited by phyllosilicates (Martin-Hernandez and Hirt 2003a) and their vulnerability to recrystallisation during deformation (Vernon 2004; Passchier and Trouw 2005), this group of minerals are important contributors to petrofabric AMS analysis in deformed rocks, particularly those which lack ferromagnetic minerals (Borradaile and Werner 1994; Bouchez 1997; Borradaile and Jackson 2004). Biotite is often a key mineral in the study of granitic rocks (e.g. Mintsa Mi Nguema *et al.* (2002); Ono *et al.* (2010)). This sheet silicate generates a nearly perfect oblate ellipsoid, the symmetry of which is parallel to that of crystal's cleavage (Martin-Hernandez and Hirt 2003b; Borradaile and Jackson 2004). Hence, magnetic lineations are determined by the alignment of this plane (Tarling and Hrouda 1993). The mica group, and particularly biotite, are susceptible to kinking, folding and cleavage parallel slip deformation at low temperature and reasonably low stress rates (Kanaori *et al.* 1991; Vernon

2004; Passchier and Trouw 2005). Therefore, crystallographically controlled magnetic anisotropy closely associated with the cleavage plane can be easily distorted and may need to be allowed for during interpretation.

It is often the case that ferromagnetic inclusions within the crystal lattice, especially along cleavage planes, of paramagnetic minerals cause elevated susceptibly values and that shape anisotropy of such ferromagnetic grains can mask the magnetocrystalline influence of host minerals (Rochette *et al.* 1992; Hunt and Moskowitz 1995). The influence and properties of such inclusions can be quantified by remanence experiments (Borradaile and Werner 1994; Borradaile and Lagroix 2001). The misalignment of the AMS ellipsoid with the crystallographic axes, which is typically a few degrees, can be attributed to the interaction between inclusion and host crystal magnetic fields (Borradaile and Jackson 2010). However Archanjo *et al.* (1995); Borradaile and Jackson (2004) and Ono *et al.* (2010) show that the crystallographic axes of ferromagnetic and silicate grains share shape preferred orientations and thus the interpreted AMS ellipsoid does, in the bulk of cases, relate in a simple way to petrofabric symmetry once a sufficient number of samples are analysed (Borradaile and Jackson 2010).

Iron bearing paramagnetic minerals can breakdown to form secondary ferromagnetic grains who's symmetry may pseudomorph the mineral being replaced (Tarling and Hrouda 1993). Magnetite, hematite, goethite and maghemite commonly strongly influence the AMS of a specimen in by this means (Lowrie and Heller 1982; Rozenson *et al.* 1982; Ellwood *et al.* 1989). In such cases the resulting susceptibility parameters are accentuated and do not reflect the primary rock forming processes. Similarly, oxidation of ferromagnetic minerals may cause growth of secondary ferromagnetic grains which may exhibit differing anisotropic properties potentially causing inversion of the original magnetic fabric symmetry (Tarling and Hrouda 1993). Such a process is commonly observed during experiments involving elevated temperatures. For example, in T *vs.* K experiments, for estimation of T_C, the cooling curve often deviates from the path of the heating curve indicating that oxidation or other new mineral growth has occurred due to elevated temperature conditions (Hrouda 2003). Such alterations may have profound effects on the direction and magnitude of the principal susceptibility axes as demonstrated by the breakdown of iron carbonates to form maghemite (Ellwood *et al.* 1986) and iron rich clays to hematite (Perarnau and Tarling 1985). Thus, evaluating the genesis of dominant magnetic minerals is just as important when interpreting AMS data as is understanding their magnetic properties.

II.5.3 Common Ferromagnetic Minerals

The iron oxide titanomagnetite (ulvospinel - magnetite) and ilmenohematite (ilmenite - hematite) solid solutions are major contributors to AMS if present, even in very small quantities. Minerals on this spectrum generally contain compositionally segregated zones, at room temperature only magnetite and hematite are ferromagnetic and thus they generally dictate AMS (O'Reilly 1984). Cooling magma from 1200-800°C titanomagnetite preferentially crystallises and tends to segregate into ulvospinel and magnetite (60:40%), by 750°C all iron oxide phases have crystallised but existing grains continue to adjust to temperature and chemical conditions as cooling progresses (Tarling and Hrouda 1993). Cooling below 800°C promotes oxidisation and any new crystals formed have a titanomaghemite (spinel) structure but compositionally tend toward ilmenohematite, this is characteristic of intermediate and more evolved magmas (Tarling and Hrouda 1993). During the later stages of cooling, the average composition of the iron oxide solution series is compositionally stable but the internal crystalline structure will modify to segregate the crystal lattice into zones which tend toward end members of either the titanomagnetite or ilmenohematite solid solution series. Members of the titanomagnetite series may generate ilmenohematite end-members through, for example, the oxidation of ulvospinel to form ilmenite and magnetite (Tarling and Hrouda 1993). Thus such grains are generally composed of relatively pure inter-grown lamellae of ilmenite and hematite or ulvospinel and magnetite (unless rapid cooling preserved the primary iron-oxide phases). The presence of sulphur and lattice impurities will complicate this simple model.

Magnetite, titanomagnetite and titanomaghemite have cubic crystal structures and are ferrimagnetic at room temperature. T_C will decrease from 578°C (pure magnetite) to -153°C (pure Ulvospinel) as Ti increases (Tarling and Hrouda 1993). In the solution series equation $Fe_{3-x}Ti_xO_4$, as x increases T_C is reduced, when x=0.6 T_C = 150°C and M_S is halved (Dunlop and Ozdemir 1997). Pure magnetite will morph from a cubic to orthorhombic structure at low temperature (-155°C), this is the *Verwey Transition* (Verwey and Haayman 1941). The Verwey Transition will also vary with composition and may be combined with the T_C value in order to obtain a stoichiometric proxy (Verwey 1939; Verwey and Haayman 1941; Akimoto 1962). Thompson and Oldfield (1986) highlight the dependence of M_S on magnetite content and grain size. They illustrate that when ilmenite is > 70% paramagnetic properties are exhibited while if magnetite is > 30% ferromagnetism is dominant. They also show that MD susceptibility is increased by lower grain

magnetite content and the opposite is true for SD grains, however MD grains always exhibit higher susceptibility values than SD grains of the same mineral species.

Titanomaghemite ($xFeTiO_3.(1-x)Fe_2O_3$) and maghemite (Fe_2O_3) have a structure very similar to magnetite but have compositions tending toward ilmenohematite and hematite respectively. As magnetism is controlled by their crystal structure and not composition, these minerals are ferrimagnetic as oppose to antiferromagnetic as could be inferred from the attributed chemistry. Maghemite is unstable and will convert to hematite at *c.*350°C (Dunlop and Ozdemir 1997), thus its presence may be indicated, for example, from the T *vs.* K heating curve.

The role of grain size in determining AMS in magnetite titanomagnetite and titanomaghemite is critical. Taking pure magnetite as an example, equi-dimensional grains typically form 0.06 - 0.08µm domains, as grain aspect ratios increase so too does domain size (axial ratios of 2:1 and 8:1 are associated with domain diameters of *c.*0.03 - 0.3 µm and *c.*1µm respectively) (Tarling and Hrouda 1993). Small grains (>1µ) which exhibit high aspect ratios commonly only possess a single domain which serve to concentrate surface charge and the demagnetising field (Dunlop and Ozdemir 1997). In such cases AMS is controlled by shape anisotropy as magnetocrystalline and magnetostriction effects are relatively minute. In this case the orientation of the principal susceptibility axes will be inverse relative to crystal dimensions (Potter and Stephenson 1988; Borradaile and Puumala 1989) due to the strength of the magnetostatic interaction driving shape anisotropy. Larger grains, up to *c.*10µm exhibit PSD behaviour while grains 10's - 100's µm contain multiple domains (Thompson and Oldfield 1986). Due to the formation of multiple domains in larger grains, the effects of self demagnetisation are reduced and anisotropy is dictated more so by crystallography which ultimately aligns K1, K2 & K3 to the respective maximum, intermediate and minimum axes of the ferromagnetic grain i.e. normal fabrics are generated. Thus depending on grain size the AMS of this group of ferrimagnetic minerals may be inverse or normal (see Thompson and Oldfield (1986); Tarling and Hrouda (1993); Dunlop and Ozdemir (1997)).

The ilmenohematite solution series possess a rhombohedral crystal structure with two anti-parallel lattices which are of equal strength. However due to *canted* or *parasitic* magnetisation, at room temperature, respective magnetic moments do not perfectly cancel out and a net magnetic moment does persist (anti-ferromagnetic). For pure hematite T_C is 680°C but this can vary up to 720°C depending on precise stoichiometry (Dunlop and Ozdemir 1997). Similarly the *Morin Transition* (Morin 1950) is susceptible to chemical change but is generally observed at *c.*15°C ± 5°C (Tarling and Hrouda 1993). Due to the delicate balance between anti-parallel magnetic

moments, impurities within the crystal lattice can play a significant role in determining the AMS of this group of minerals. Furthermore, Dunlop (1971) argue that finer grained hematite is more susceptible to magnetostriction. For reasons such as these the precise properties minerals in the ilmenohematite series are generally less precise.

The magnetic properties of ilmenohematite ($Fe_{2-x}TixO_3$) predictably varies with Ti content. T_N fluctuates from 680°C (pure hematite) to -213°C (pure ilmenite) (Dunlop and Ozdemir 1997). Furthermore, as hematite content increases from 70% to 100%, M_S decreases and H_C increases if Ti content increases but if Ti remains constant, M_S in MD grains will increase while that associated with SD grains decreases (O'Reilly 1984).

The domain structure of hematite is again dependent on grain size. Domains within equi-dimensional grains are usually *c.*1-1.5µm while elongate grains generally exhibit domains *c.*10-20µm is diameter (O'Reilly 1984). As observed in titanomagnetites, PSD behaviour is exhibited under the influence of lattice impurities and imperfections (Tarling and Hrouda 1993). The ilmenohematite series exhibit very weak M_S and very high H_C, even when compared to SD magnetite (Dunlop and Ozdemir 1997). This is dictated by a strong magnetocrystalline anisotropy controlled by the basal c-plane. This is much more influential than shape anisotropy even in small grains, hence, converse to the titanomagnetite series, no inversion of AMS is observed between SD, PSD or MD grains as AMS is dictated by magnetocrystalline anisotropy (Tarling and Hrouda 1993).

II.6 Interpreting AMS of rocks

Ising (1942) first used AMS as an investigative technique in a geological context to examine stratified sediments, later Graham (1954) emphasised the usefulness of this technique in geological investigations on a much broader sense. AMS is now a widely accepted method of indirect non-destructive petrofabric and strain analysis and has a broad variety of applications in structural geology (Jackson and Tauxe 1991; Tarling and Hrouda 1993; Borradaile and Henry 1997; Borradaile and Jackson 2004, 2010).

Rocks are composed of polyphase mineral assemblages and the AMS of a rock is determined by the net statistical alignment of the long axes or easy direction of magnetisation of individual crystals depending on whether shape or magnetocrystalline anisotropy is dominant (O'Reilly 1984; Tarling and Hrouda 1993).

An elementary application of AMS in the investigation of granitic bodies relates the magnetic susceptibility ellipsoid to a petrofabric, hence providing information on the rock's strain history. Bouchez (1997) highlighted that fact that the crystalline matrix of granite is never isotropic, which makes sense as granite flows during ascent and emplacement and may then undergo further plastic or brittle deformation and so an anisotropic texture is expected. Prior to the point at which crystallising granite reaches the RCMP (of Arzi (1978), comparable to the CMP of Van der Molen and Paterson (1979) or the MCT and SLT of Rosenberg and Handy (2005)) strain will be recorded as a magmatic state fabric. Such a crystalline anisotropy may be easily overprinted by subsequent deformation which occurs under the same rheological conditions and no sign of internal plastic strain and differential strain will be recorded (Paterson *et al.* 1989; Blenkinsop 2000; T.G. 2000; Vernon 2004). Hence, due to constantly evolving rheological parameters crystallising magma records strain in a complex manner and magmatic state fabrics, in particular, often return extremely low degrees of anisotropy (Bouchez 1997).

If any degree of anisotropy is present and quantifiable, certain information on the finite strain ellipsoid may be inferred. Generally, the principal anisotropy axes are used as a proxy for finite strain i.e. a long, intermediate and short axes can be identified. In the context of rock fabrics, the long axes of the ellipsoid is typically associated with the linear component of a rock fabric while the position of the short axes defines the pole of the foliation plane. Identification of the local and regional principal strain axes is essential when structurally assessing a plutonic body (e.g. Hutton (1988); Paterson *et al.* (1998); Vigneresse *et al.* (1999); Paterson *et al.* (2004)). The methods for evaluating strain in granites is discussed in Chapter 6. The long axis is typically associated with magma flow direction (Callot and Guichet 2003; Archanjo and Launeau 2004) or that of least compressive stress which facilitates the intrusion process (Grocott *et al.* 2009; Benn 2010). In the simplest cases, sheet intrusions or lava flows exhibit foliations parallel to the bounding structures of the igneous body while lineations, the long axis is of the strain ellipsoid, reflects direction of flow (e.g. Waters (1960); Varga *et al.* (1998)) while in some circumstances imbrication features may be used to determine flow direction (e.g. Hippertt (1993); Philpotts and Asher (1994)).

In plutonic rocks with subtle anisotropy values the foliation plane can often be partially quantified by direct observation in the field, however the long axis of the strain ellipsoid is often much more difficult to constrain and typically requires detailed and time consuming analytical examination (e.g. Shelley (1993); Schulmann *et al.* (1997); Mees *et al.* (2003); Launeau and Robin (2005)). As well as being a less tedious analytical method, the AMS technique does not rely on qualitative observation by the human eye and, unlike most other fabric analysis methods, measures the contribution made by every constituent mineral of a 3D sample finally combining

these to produce a bulk susceptibility ellipsoid. This accurately, although indirectly, reflects the shape preferred orientation of macroscopic fabric axes (Ising 1942; Graham 1954; Granar 1958; Graham 1966) and is thus a very rapid and sensitive method of identifying anisotropy in samples which otherwise appear isotropic (Bouchez 1997).

In the same manner as traditional fabrics, AMS fabrics may be used to identify planar and linear petrofabric components (e.g. King (1966); Callot *et al.* (2004); Fanjat *et al.* (2012)) and distinguish their relative significance (e.g. K1 does not automatically reflect a flow direction). More dynamic AMS fabrics have been interpreted to determine flow direction and shear sense indicators (e.g. Callot and Guichet (2003); Stevenson *et al.* (2007); Stevenson and Bennett (2011); Magee *et al.* (2012)). Such interpretations are extremely convincing when coupled with supporting evidence from traditional flow and shear sense indicators (e.g. Femenias *et al.* (2004); O'Driscoll *et al.* (2008); Ono *et al.* (2010); Valley *et al.* (2011)). In addition, it is now almost common practice to use microstructural investigation to determine the rheological state of a host rock during fabric development (e.g. Bouchez *et al.* (1990); Cruden *et al.* (1999); Archanjo and Launeau (2004); Mamtani and Greiling (2005); Esmaeily *et al.* (2007)). So it is clear that in a great many cases the internal architecture of plutonic rocks may be described in intricate detail using a combination of AMS, meso, micro and map scale structural analysis.

Due to the sensitivity of the AMS technique, materials which appear to be isotropic by some quantitative methods often return anisotropic AMS fabrics. The interpretation of AMS data under such circumstances should be carried out in a scrupulous manner, particularly in the scenario where no silicate fabric is clearly identifiable. This is due the simple fact that the relationship between a sample's AMS ellipsoid and petrofabric cannot be assumed to relate in a simple way (e.g. Rochette (1988); Rochette and Fillion (1988); Borradaile and Puumala (1989); Ferré (2002); Debacker *et al.* (2004); Fanjat *et al.* (2012)), much less the possibility of a measured fabric representing a tectonic or magmatic flow fabric. To evaluate the relationship between the AMS tensor and any possible petrofabric (or petrofabrics) one must consider the following potential caveats;

1. Possibility of inverse, normal or intermediate fabrics
2. The mineralogy and dominant magnetic minerals in an assemblage
3. Magnetic interaction between ferromagnetic grains
4. Relationship between silicate lattice and ferromagnetic grains
5. Presence of multiple petrofabrics

Any one of these factors may cause the misalignment of the AMS ellipsoid with that of the targeted silicate petrofabric. In addition, the validity of an interpretation based on rock magnetic analysis may be determined by its compatibility with data from other sources such as field, petrographical, geophysical and regional tectonic evidence; a new interpretation need not fit a current hypothesis but it must not ignore conflicting evidence. These topics are discussed below.

II.6.1 Normal, Inverse and Intermediate fabrics

The terms normal inverse and intermediate fabric are used in AMS studies to describe the directional relationship between the orientation of the long, intermediate and short dimensions of a grain (X, Y, Z) to the principal susceptibility axes of the AMS tensor (K1, K2, K3). In the straightforward case, a *normal* AMS ellipsoid has K1, K2, and K3 orientated respectively parallel to the X, Y & Z. If the magnetic fabric is inverted relative to the dimensional axes of a grain, positioning K1 parallel to the Z axis and K3 parallel to the X axis, the AMS fabric is said to be inverse while if a mixture of both normal and inverse components are detected the AMS fabric is said to be intermediate (Ferré 2002).

Quartz and calcite are both diamagnetic minerals which may generate inverse AMS ellipsoids (Owens and Rutter 1978; Rochette 1988) as under strain both re-crystallise with c-axes (most negative and so equivalent to K1) perpendicular to the developing cleavage or foliation (Hamilton *et al.* 2004). The crystallographic long axis of tourmaline is parallel to the magnetocrystalline difficult axis of magnetisation, hence it is an example of an inverse paramagnetic mineral, cordierite is sometimes also inverse (Rochette *et al.* 1992). Single domain ferromagnetic minerals are the most problematic, SD magnetite, titanomagnetite and maghemite can all generate inverse AMS ellipsoids (Potter and Stephenson 1988; Borradaile and Puumala 1989), MD grains of these minerals or SD or MD grains of hematite do not (Dunlop and Ozdemir 1997).

As the AMS of a specimen is a measurement of the net susceptibility of all constituent grains, the presence of the above minerals will generate a bulk normal, inverse or intermediate magnetic fabrics for that specimen, leading to paradoxical interpretations if not correctly identified. Several examples of such properties in natural and synthetic samples have been documented (e.g. Rochette (1988); Rochette and Fillion (1988); Rochette *et al.* (1999); Chadima *et al.* (2009)). It is now well established that such behaviourisms are associated with primary SD ferromagnetic

bearing rocks as well as those with ferromagnetic grains which are derived from alteration of paramagnetic minerals (Ellwood *et al.* 1986; Ellwood *et al.* 1989). Ferré (2002) developed theoretical models for investigating the behaviour of specimens with both normal and inverse contributors that generate intermediate fabrics. They found that samples with both normal and inverse components yielded lower anisotropy values and that a minimum of 20% inverse component is required before an intermediate fabric may form. So, in specimens returning intermediate fabrics it is important to determine the relative mineralogical contributions as the fabric yielded will be dependent on this and do not necessarily relate to strain in a straightforward manner (Ferré 2002).

Deformation processes or flow dynamics are also cited as explanations for unexpected AMS results, these are sometimes termed inverse and intermediate fabrics but are not necessarily caused by inverse susceptibilities associated with the host rock's mineralogy. The rolling affects of simple shear flow or the cross cutting of flow fabric by some shear structure can lead to the formation of an intersection lineation between two planes, this can be detected by AMS (e.g. Parés and van der Pluijm (2002a); Callot and Guichet (2003)). Also cited are emplacement and cooling related stresses and hydrothermal alteration processes (e.g. Rochette *et al.* (1992); Raposo *et al.* (2004)), although the latter is likely to involve at least some contribution from mineralogical modification. The influence of magnetic interaction between ferromagnetic grains can also cause the AMS ellipsoid to reflect distribution of magnetic particles in the rock (Hargraves *et al.* 1991; Femenias *et al.* 2004; Fanjat *et al.* 2012) i.e. textural anisotropy (Fuller 1963; Wolff *et al.* 1989). This can generate fabrics which appear to be intermediate but in truth are attributed to completely different phenomenon than those described above and do not reflect the preferred orientation of a host mineral assemblage.

II.6.2 Mineralogy and dominant magnetic minerals

The presence and relative abundance of ferromagnetic and paramagnetic minerals is a major factor in determining the AMS of granitic rocks. The influence of diamagnetic components can be ignored due to their relative negligible susceptibility (although inclusions of ferromagnetic grains in the crystal lattice may be an influential factor).

For convenience in AMS studies, granitic rocks may be classified as either *magnetic* and *non-magnetic* (Ellwood and Wenner 1981; Tarling and Hrouda 1993). Predictably, the former refers to

facies which return higher susceptibility values (*c.*10^{-3} - 10^{-2}) reflecting the presence of a significant proportion of ferromagnetic minerals, most often titanomagnetite or ilmenite. The latter is used in reference to specimens which return lower bulk susceptibility values (*c.*10^{-5} - 10^{-4}) which reflects a lack of high susceptibility minerals and is indicative that AMS is controlled by paramagnetic, typically biotite and possibly hornblende, or by some ilmenohematite phase. Broadly speaking, bulk susceptibility values may be used as a approximation for granite type (Takahashi *et al.* 1980). In keeping with the classification schemes of Chappell and White (1974) and Pitcher (1982), magnetic granites are generally associated with I-type or A-type biotite-hornblende tonalites and alkaline granites while non-magnetic granites are most commonly of S-type two-mica granites.

As already discussed if a small proportion of ferromagnetic minerals are present (>1% volume) they will significantly influence the AMS ellipsoid and in rocks with < 10% paramagnetic components, the ferromagnetic assemblage is likely to be dominant (Tarling and Hrouda 1993). In specimens with a very low ferromagnetic component, typical of S-type granites, AMS is likely to be controlled by micas and the product ellipsoid is easy to relate to any observed fabric (e.g. Ono *et al.* (2010)) as the AMS characteristics of the mica group are well known (discussed above).

In instances where ferromagnetic minerals dominate susceptibility it becomes important to establish whether those minerals are primary and related to, and therefore reflective of, the emplacement process. Ferromagnetic grains can form by alteration of iron bearing paramagnetic minerals, in granite these will be amphiboles and micas (Bouchez 1997). Although alteration to ferromagnetic grains tend to pseudomorph earlier mineral phases (Tarling and Hrouda 1993), and thus relate to the original petrofabric in similar fashion to the original mineral in terms of shape, size and distribution, primary magnetite, micas and amphiboles exhibit different rheological responses to differential stress during fabric development (Vernon 2004; Passchier and Trouw 2005). Hence the amplified AMS contribution given by ferromagnetic grains which replace silicate minerals will contribute to the bulk ellipsoid in a different way when compared to that expected from the original unaltered assemblage. Similarly, alteration of titanomagnetites during cooling and hydrothermal alteration may generate new ferromagnetic minerals with differing susceptibility properties as in Petronis *et al.* (2011). While such alteration processes may have an undesirable affect on the relationship between petrofabric and AMS ellipsoid (i.e. inversion) this is not the default case. Alteration of the silicate assemblage may cause segregations along cleavage planes, micro-fracture infilling, chloritisation of biotite, the breakdown of plagioclase, hornblende, and biotite to form epidote, calcite and sericite and the leucoxenization of sphene while pyrite

will exhibit oxidised rims, primary magnetite may show signs of maritization and secondary magnetite will exhibit hematite inclusions and infilling fractures which cross cut the primary rock texture (e.g. Bolle *et al.* (2003); Just *et al.* (2003); Just *et al.* (2004); Valley *et al.* (2011)). Careful examination of such characteristics coupled with AMS and remanence studies can successfully strip back the post emplacement history and positively identify distinct contributions to the bulk AMS tensor be they from primary crystallisation processes, hydrothermal or brittle/ductile deformation (e.g. Just *et al.* (2004)).

Regarding mineralogy, another crucial consideration is based around the intrinsic magnetic anisotropy of individual ferromagnetic grains. K_1, K_2 & K_3 of MD grains relate normally to the max, intermediate and minimum dimensional axes respectively, the inverse case is true for some SD grains. Hence, the simple, and more common case when dealing with granitic rocks, is where MD grains dominate the AMS ellipsoid and it relates in a simple way to magmatic flow or tectonic deformation which may be observed in the silicate matrix (e.g. Stevenson *et al.* (2007); Grocott *et al.* (2009); Žák *et al.* (2010)). Cases are reported where SD magnetite grains preside over other mineral phases (Ellwood *et al.* 1986; Potter and Stephenson 1988; Ellwood *et al.* 1989). In any case where unusual or suspect AMS results are returned it is desirable to investigate the precise contribution of different magnetic carriers to make an informed interpretation. Preferably, the presence, relative abundance and contribution of ferromagnetic phases should be evaluated using a suite of standardised rock magnetic experiments (e.g. Bolle *et al.* (2003); Petronis *et al.* (2011)) in conjunction with the statistical and analytical cross checks suggested by Borradaile and Jackson (2010).

II.6.3 Magnetic Interaction

Hargraves *et al.* (1991) argued that AMS may be controlled in igneous rocks by anisotropic magnetic interaction between constituent ferromagnetic grains. Using magnetite grains ordered and embedded in epoxy mixtures, they showed that despite the fact that magnetite grains used were magnetically isotropic, anisotropic AMS data were returned with K1 parallel to aligned ferromagnetic partials. The same paper published data from ferromagnetically isotropic rock samples which exhibited a textural anisotropy (Fuller 1963; Wolff *et al.* 1989) when sub-specimens were placed within critical proximity. This work was later supported by analytical models devised by Stephenson (1994) on magnetic interactions between independently isotropic

but co-operatively anisotropic neighbouring ferromagnetic partials. Grégoire *et al.* (1995) argued that magnetic fabrics returned from AMS analysis of granitic samples was a product of both shape preferred orientation of magnetite grains and the net magnetic interaction of neighbouring grains. This paper claimed that once the distance between grain centres is double that of the typical grain size or less, K and AMS will be enhanced. This clarified that the interaction of ferromagnetic grains was dependent on distribution and grain density and that grain-grain interaction could become more influential to a samples AMS than the actual orientation of the ferromagnetic grains. Contrary to Grégoire *et al.* (1995), Cañón-Tapia (1996) argued that whenever magnetic interaction takes place AMS is dominated by the distribution of grains (textural anisotropy) and not by the preferential orientation of those grains and further stipulated that the combined effects of these two factors may produce a hybrid magnetic fabric which does not simply relate to petrofabric nor textural anisotropy.

Contrasting this school of thought, Archanjo *et al.* (1995) demonstrated a strong relationship between petrofabric (biotite, feldspar, enclave), MD magnetite shape fabrics and AMS using examples from the Gameleiras pluton, Brazil. Through comparison with thin-section image analysis, this work concluded that AMS was controlled by the statistical alignment of the long axes of inequant magnetite grains and that magnetic interactions between grains only accounted for observed scattering or abnormal anisotropy values and did not detrimentally affect magnetic data despite grains typically occurring in clusters. In a similar example from Madagascar, Grégoire *et al.* (1998) illustrated, through the use of 3D fabric analysis and AMS, that bulk-AMS was derived from the shape preferred orientation of ferromagnetic grains in granitic rocks and a close correlation exists between magnetic and petrographic fabric anisotropy.

Numerous other authors also report a positive relationship between AMS and silicate fabric (e.g. Borradaile and Henry (1997); Bouchez (1997); Neves *et al.* (2003); López de Luchi *et al.* (2004); Esmaeily *et al.* (2007); Ono *et al.* (2010); Petronis *et al.* (2011)) suggesting cases which exhibit no relationship, or a weak relationship, are anomalous rather than typical cases (e.g. Fanjat *et al.* (2012)). In reported cases where AMS is controlled by magnetic interaction, (natural, analytical and numerically modelled examples) identical coaxial ferromagnetic particles are used which are not typical of natural examples but do facilitate controlled modelling (Hargraves *et al.* 1991; Stephenson 1994; Cañón-Tapia 1996). Recognising this Gaillot *et al.* (2006) proposed a new model based on a two-grain macroscopic numerical model. This facilitated the examination of the role played by magnetic interaction between grains of different sizes and axial ratios and hypothesised that a critical ratio between grain axis length and distance between grain centres

(d/r) was a primary factor in determining whether grain interaction would be sufficiently intense to detrimentally impact on bulk AMS. This hypothesis was experimentally validated by mounting two magnetite grains on paramagnetic discs of known susceptibility and progressively reducing the distance between the grains by removing glass lamellae spacers. In summary, this test found that interaction intensity was reduced if a heterogeneous grain size was used and that interaction was rapidly reduced from a d/r value = 1 (grains in contact) to d/r value = 0.8 and become insignificant by d/r = 0.5. So magnetic interaction is negligible in natural samples once grains are spaced by a distance larger than the mean grain size and quite small until grain centres are separated by < *c.*0.5 of the mean grain size (Gaillot *et al.* 2006). It is worth noting that such an analysis is compatible with findings of Hargraves *et al.* (1991) and Stephenson (1994) and the concept of the generalised total AMS tensor (T) of Cañón-Tapia (2001). Furthermore, an earlier experiment by Grégoire *et al.* (1998) showed that in samples with up to 3% volume magnetite, magnetic interaction only affected a few percent of the total number of magnetite grains and thus this factor had a negligible effect on the overall AMS ellipsoid. Hence, the work of Gaillot *et al.* (2006) is deemed an acceptable resolution to the debate and validates the interpretation that AMS does, in most cases, reflect the preferred orientation of ferromagnetic grains, which typically coincide with the orientation of larger silicate minerals and thus AMS is a valid petrofabric indicator.

II.6.4 Relationship between ferromagnetic and silicate minerals

The orientation of ferromagnetic grains relative to silicate minerals in a rock specimen is critical to the interpretation to AMS. We have already seen that minerals exhibit either normal or inverse fabrics. If AMS as a petrofabric analysis method is valid, the expectation is that, for a composite specimen, the observed averaged preferred orientation of crystallographic long axes should coincide with that of a samples bulk AMS (assuming a normal fabric). This hypothesis has been tested using numerical modelling and x-ray goniometry on natural rock samples where results show that as magnetic anisotropy increases so too does crystallographic preferred orientation and that AMS can be used to quantify the degree of preferred alignment of a specimen's minerals (Richter *et al.* 1993a; Richter *et al.* 1993b; Cifelli *et al.* 2009).

Samples which contain a combination of ferromagnetic minerals and paramagnetic/diamagnetic constituents are more complex as AMS is not simply measuring the

bulk preferred orientation of partials which contribute to the bulk ellipsoid in a more or less similar way. In an example from a granite pluton in northwest Brazil, Archanjo *et al.* (1995) demonstrated that the overall AMS ellipsoid was dictated by MD magnetite and was always approximately parallel (few degrees) to the magmatic state fabric measured in the field, defined by K-feldspar phenocrysts and elongate magic enclaves. Using automated software, Archanjo *et al.* (1995) compared 2D shape fabrics of biotite and magnetite from a large sample group (*c.*500) of orientated polished thin sections. Results show that biotite grains correlated to within 7° and magnetite to within 12° of the AMS ellipsoid. Thus, this work strongly supports the hypothesis that the shape preferred orientation of magnetite grains is consistent to that of silicate minerals and thus AMS is a valid proxy for the preferred orientation of silicate minerals in the studied samples.

In contrast to the previous example, Archanjo and Launeau (2004) showed that AMS ellipsoids, derived from titanomagnetite exhibiting signs of pervasive alteration to ilmenite, returned magnetic fabrics which were typically highly oblique to magmatic fabric, defined by the shape preferred orientation of plagioclase laths. The authors attributed the observed discrepancies to modification to the shape of titanomagnetite after exsolution of ilmenite lamellae which lead to an inconsistent grain shape and shape anisotropy.

When present, it is common for ferromagnetic grains to become included in the lattice of silicate minerals. In such cases the symmetry between AMS and silicate crystal symmetry will be adversely affected (Owens and Bamford 1976; Lagroix and Borradaile 2000a; Martin-Hernandez and Hirt 2003b). Usui *et al.* (2006) documents a case where the orientation of magnetite needles are controlled by crystallographic planes within plagioclase and clinopyroxene causing a misfit between AMS and crystal preferred orientations. In this circumstance, included grains are stripped from the bulk ellipsoid by application of anisotropy of partial anhysteretic remanant magnetisation techniques, a discriminatory technique targeting differing grain size (Dunlop and Ozdemir 1997).

The influence of ferromagnetic grains included in silicate minerals is generally most severe in pyroxene and olivine crystals and less so in the mica group (Lagroix and Borradaile 2000a). This is attributed to a lower number of inclusions present in minerals such as biotite and muscovite and the common alignment of these along to the cleavage of the monoclinic crystal structure. Due to the typical mineralogy of granitoids, there is no common issue of major disruption of AMS by ferromagnetic inclusions within pyroxenes and olivines while the influence of such a features in minerals such as biotite are seldom a major problem, although never entirely insignificant (Tarling

and Hrouda 1993; Lagroix and Borradaile 2000a). In fact, in some instances, it has been shown that a weak anisotropy in paramagnetic granite may be accentuated by stimulating the growth of secondary mimetic magnetite (Hrouda *et al.* 1997; Mintsa Mi Nguema *et al.* 2002), but this is not always the case (Henry *et al.* 2003).

In any case, the above examples highlight the requirement for independent evaluation methods to be coupled with AMS analysis (e.g. Olivier *et al.* (1999); Pignotta and Benn (1999); Bolle *et al.* (2003)), particularly in cases where only weak degrees of anisotropy are found (Archanjo and Launeau 2004).

II.6.5 Evaluating multiple sub-fabrics

Rocks are made up of multiple crystals which all contribute to AMS but will act to collectively reduce the overall shape anisotropy due to competing indepent tensors, as such, as a general rule the Pj of a sample is always under-estimated (Borradaile and Jackson 2010). In the case of a specimen with one or more sub-fabrics this rule of thumb is more important as sub-fabrics are usually defined by different mineral phases which act to reduce overall anisotropy values. Hrouda (2010) has shown that if 80% or more of a samples bulk susceptibility is dependent on a single ferromagnetic or paramagnetic material the resultant AMS will essentially only reflect the preferred orientation of the dominant mineral phase.

A sub-fabric may be generated in two ways, either by successive tectonic overprints e.g. bedding-cleavage (Parés and van der Pluijm 2002a; Parés 2004) or by episodic mineral growth, e.g. secondary magnetite due to hydrothermal alteration (Usui *et al.* 2006; Petronis *et al.* 2011). In addition, the AMS ellipsoid may be affected by contributions from minerals which are driven by magnetic interaction, mineral abundance, or burial and alteration processes (summarised in (Martin-Hernandez and Ferre 2006)). As such the role of different components can be fundamental to understanding the bulk AMS ellipsoid, these may be evaluated by either statistical or analytical means.

II.6.5.1 Statistical evaluation of magnetic sub-fabrics

A simple, time efficient and free means of determining the presence and influence of multiple sub-fabrics in a specimen is by statistical analysis. The obvious attraction of such an approach is

that anyone can do it and no sophisticated equipment (outside of a brain) is required. However, it is important to always consider that results are a product of statistical manipulation rather than direct physical evidence, a fact that is true for most rock magnetic parameters.

Standard statistical bootstrapping methods applied to AMS unit vectors are used in order to statistically separate magnetic sub-fabrics (Constable and Tauxe 1990). Pointing out that the linearization method used to estimate confidence ellipse for AMS parameters often returned inappropriately reduced error margins, Constable and Tauxe (1990) proposed a bootstrap re-sampling scheme to determine the distribution of uncertainties in AMS data. Effectively, a broader degree of uncertainty suggests the presence of a sub-fabric and such an approach is affective as long as contrasting sub-fabrics are punctuated by differences in orientation and ferromagnetic and paramagnetic mineralogy. The methodology and logic behind comparing normalised and un-normalised AMS tensors to detect sub-fabrics has been discussed above. Such an approach is now applied across a broad spectrum of problems relating to both simple and more complex tectonic problems (Borradaile 2003; Borradaile and Jackson 2004, 2010).

If the bulk susceptibility of both the ferromagnetic and silicate components of a rock can be independently determined, the contribution of these components to the bulk AMS ellipsoid may be calculated (Henry and Daly 1983). This is achieved by physical or chemical separation of the targeted minerals and measurement of the susceptibly of mineral separates from different but related samples (i.e. neighbouring samples from the same block). Although this method has been validated by AIRM analysis (Henry 1985, 1988), due to the tedious and time consuming nature of this process, and the poor level of consistency more often reported (Jackson 1991), it is not viewed as a preferable technique.

II.6.5.2 Analytical analysis of magnetic sub-fabrics

Some image analysis methods can distinguish between sub-fabrics (Launeau and Robin 1996; Robin 2002; Launeau and Robin 2005) but these can only take a number of 2D images into account and thus a much smaller sample size. Magnetic analysis exploits the magnetic properties of individual mineral phases in order to target minerals which are suspected to be dominant carriers of distinct fabrics. Many different techniques have been devised for stripping back the bulk AMS tensor and identifying fabrics defined by minerals of different composition and or grain size (review in Martin-Hernandez and Ferre (2006)). Analytical methods essentially use one the following;

1. Dependency of susceptibility on temperature
2. Dependence of susceptibly on the frequency of the inducing field
3. Measurement of induced remanence anisotropy
4. Measurement of magnetic properties at high inducing field above M_S

According to the Curie-Weiss Law, magnetic susceptibility in paramagnetic materials increases at low temperature, diamagnetic susceptibility will not change and ferromagnetic materials will modify once below the Verwey or Morin transition (Dunlop and Ozdemir 1997). Thus the contribution made to the AMS ellipsoid by paramagnetic minerals will be accentuated at lower temperature. Such a characteristic has been used to compare the preferred orientation of paramagnetic minerals to that of others or the bulk AMS ellipsoid by measuring AMS of a composite specimen while submersed in liquid nitrogen (77K) (Lüneburg *et al.* 1999; Parés and van der Pluijm 2002b).

Conversely, by increasing a sample's temperature, paramagnetism is reduced while ferromagnetism increases, due to the Hopkinson effect (Nagata 1961) until, T_C is reached, at which point ferromagnetism is completely removed. The point at which specific ferromagnetic materials reach T_C will vary with mineral composition (discussed above), heating can also cause new mineral growth which may serve to accentuate or reduce a specimen's AMS ellipsoid (discussed above). Such techniques have their uses but do not directly measure the AMS tensor. Attempts have been made to measure AMS at temperatures above the T_C of constituent minerals but elevated background noise, caused by the affects of thermal expansion on apparatus, returned an unsatisfactory level of precision (Martin-Hernandez and Ferre 2006). Such an experiment could facilitate the identification of the components from minerals of contrasting T_C and that from diamagnetic minerals once an allowance is made for the remaining paramagnetic component of ferromagnetic partials.

The susceptibility of minerals fluctuate with varying inducing field frequency, this is known as electromagnetic susceptibility (Ellwood *et al.* 1993). Early experiments show that at lower frequencies ferromagnetic minerals, including magnetite and maghemite, exhibit frequency dependent susceptibility (Vincenz 1965; Bathal 1971). In a series of experiments, conducted at room temperature, Ellwood *et al.* (1993) demonstrated that at frequencies between 1 - 50kHz some paramagnetic and diamagnetic materials exhibited predictable dependency on frequency. This paper demonstrated that by measuring susceptibility at two frequencies and subtracting the

high frequency tensor from the standard low field AMS tensor one may successfully determine the contribution made to bulk susceptibility made by targeted minerals.

Anisotropy of magnetic remanence is used as a means to evaluate the anisotropy of ferromagnetic minerals (as only these may carry magnetic remanence). Anisotropy of Anhysteretic remanent magnetisation (AARM) involves exposing a sample to an AF field and a weak steady field which causes any mineral with a coercivity lower than that applied AF field to become magnetised. The anisotropy of the magnetised field is measured and plotted onto an ellipsoid in a similar fashion to the manner in which AMS data is collected (Girdler 1961). The AMS and AARM data may then be compared to evaluate the preferred orientation of ferromagnetic minerals relative to the orientation of the full composite AMS ellipsoid (e.g. Lagroix and Borradaile (2000a)). Partial anisotropy of anhysteretic remanent magnetisation (pAARM) (Edwards 1984) applies a decaying AC field upon a sample and a DC field for a set period between two AF peak values, this magnetises partials with coercivity between the AC field intensities over which the DC field was imposed. This method is often used in order to discriminate between anisotropy magnitude and orientation in ferromagnetic grains of differing sizes based on coercivity values (e.g. Aubourg and Robion (2002); Usui *et al.* (2006)).

Remanence of isothermal remanent magnetisation (Daly and Zinsser 1973) is used to evaluate whether ferromagnetic minerals have a preferred orientation of remanence. This technique requires a sample to have an IRM imposed, measured, removed by AF cleaning and, imposed again in the opposite direction along the same axis and re-measured (e.g. Cagnoli and Tarling (1997); Robion *et al.* (1999)). By measuring IRM in opposite directions along the same axis, the recorded difference between remanence is quantified, this reflects the preferred direction of remanence, and so may be used to determine grain orientation. Hrouda (2002) demonstrated the correlation between AMS and isothermal remanent magnetisation tensors in different samples containing MD or SD magnetite. This work illustrated that the AMS tensor may be resolved into ferromagnetic and paramagnetic components by the use of magnetic remanence techniques and also that issues regarding SD magnetite and AMS (already discussed) may be overcome in this way.

For more examples of the application of magnetic remanence to overcome problems surrounding AMS and composite fabrics the reader may refer to Borradaile and Tarling (1981); Rochette and Fillion (1988); Hrouda (1992); Housen *et al.* (1993); Trindade *et al.* (2001); Callot and Guichet (2003).

Varying the applied magnetic field may also uncover the contribution made by different mineral species to the bulk AMS ellipsoid. As magnetisation is proportional to the applied magnetic field for paramagnetic and diamagnetic materials, the torque associated with magnetisation is proportional to the square of the applied field (Dunlop and Ozdemir 1997). Thus as the inducing field increases ferromagnetism will eventually reach M_S while other constituents will continue to become increasingly magnetised (within intermediate fields, torque is proportional to the applied field for minerals exhibiting strong crystalline anisotropy (Porath and Chamalaun 1966)). Torque measurements were first used as a means to investigate the mineralogy of a specimen (e.g. Williams (1937); Tarasov (1939)) and later applied to separate individual components of a magnetic fabric (Hrouda and Jelínek 1990). Hrouda and Jelínek (1990) suggested that components of a fabric could be individually identified once the constituent ferromagnetic minerals reached M_S. They argued that if two torque measurements were made in two different high magnetic fields the difference between these values was determined by the paramagnetic (dominant) and diamagnetic component (almost negligible) constituents. So, low field susceptibility is most often controlled by ferromagnetic minerals if present, high field torque measurements are carried out above M_S and so the summarised method above measures the anisotropy of non-ferromagnetic minerals, thus combining these two methods the relative contribution of both mineral species can be accurately determined.

A yet more complicated (but more accurate and sensitive) method of determining the relative contribution of different mineral phases, and thus identify distinct fabrics, is through the exploitation of the dependence of magnetisation on both temperature and intensity of the inducing field. As discussed, in high fields ferromagnetic materials are saturated and by measuring the susceptibility of a sample as it rotates one may define a high field susceptibility ellipsoid determined by the paramagnetic component of the sample. By greatly reducing ambient temperature, the relative contributions to AMS made by diamagnetic and paramagnetic minerals may be determined at various fields. This is known as cryogenic magnetometry. Such a method is quite an efficient means of accurately determining the contribution made to composite magnetic fabrics by different mineral phases (Rochette and Fillion 1988; Aubourg and Robion 2002), however the process requires very specialised and expensive equipment and thus is not widely available (as is the case for this project).

II.6.6 Summary and Practicalities of AMS interpretation

Hutton (1988) emphasised the importance of identification of fabrics in granitic bodies and summarised the means by which such fabrics may be interpreted to determine principal stress directions during emplacement and subsequent deformation. Such an evaluation is critical if the tectonic regime at the time of emplacement is to be understood. Bouchez (1997) points out that even though such important strain markers may not be determinable in the field, AMS analysis can always return principal susceptibility axes, even if anisotropy degrees are extremely small. In most cases, magnetic fabrics share a normal relationship with the orientation of principal axes of the local strain ellipsoid (magnitude is not proportional as it is controlled by mineralogy as well as strain, see discussion in Borradaile and Jackson (2010)). Thus these are viable strain markers, just as silicate fabrics, mafic enclaves, country rock deformation features, and are invaluable in the absence of such obvious structures (Tarling and Hrouda 1993).

In cases where AMS data are used to interpret flow or strain it must be supported by independent data as in all cases the feasibility of any hypothesis drawn will be subject to its compatibility with direct field and petrographic evidence as such observations cannot be ignored. Such support should be sought by methods independent of rock magnetic analysis where possible in order to form a robust hypothesis. To this end many authors have supported AMS interpretations with shape or crystal preferred orientation analysis (e.g. Archanjo *et al.* (1995); O'Driscoll *et al.* (2008)), x-ray analysis (e.g. Takahashi and Noguchi (2003); Cifelli *et al.* (2009)) and fabric analysis in the field (e.g. Esmaeily *et al.* (2007); Stevenson *et al.* (2008b)), the latter almost always accompany, and must compliment, AMS interpretations. Microstructural analysis coupled with detail analysis of meso and macro scale features in the field are used to determine the rheological state of fabric development (e.g. Cruden *et al.* (1999); Mamtani and Greiling (2005)), thus a distinction between primary emplacement related and secondary tectonic related fabrics may be discernible. On a larger plutonic scale the pattern of fabrics may also reveal the relationship between rheology and fabric development without the need for such detailed analysis. As a general rule emplacement related fabrics (directly observed and magnetic) will be related to the shape of the intrusion and will cross cut pre-existing country rock structure, however the natural grain of the country rock will play an active role in controlling ascent and emplacement paths and so magmatic fabrics are often parallel to local or regional scale structures. The application of airborne and ground based geophysics are also applied, the co-incidence of steep lineation's with gravity or magnetic anomalies may indicate ascent sites while

consistent lineation patterns may infer magma emplacement directions (Vigneresse 1990; Ameglio *et al.* 1997; Améglio and Vigneresse 1999; Vigneresse *et al.* 1999; Vegas *et al.* 2008).

Finally, one of the major justifications for the academic pursuit of plutonic development is that this research plays a major role in understanding regional scale plate tectonics over protracted periods of time. In terms of the Caledonian Orogeny, large scale plate tectonic models (Gee 1975; Lambert and McKerrow 1977; Soper and Hutton 1984; Soper *et al.* 1987; Scotese and McKerrow 1990; Soper *et al.* 1992; Trench and Torsvik 1992; Pharaoh *et al.* 1993; Torsvik *et al.* 1996; Dewey 1997; van Staal *et al.* 1998; Pharaoh 1999; McKerrow *et al.* 2000; Hartz and Torsvik 2002; Dewey 2005; Cawood and Pisarevsky 2006) are based on and supported by evidence from a multitude of sources including palaeomagnetism, geochronology, geochemistry and structural data derived from granitoid bodies. So large scale regional models are determined by evidence derived from the study of relatively small scale projects. As such, when synthesising emplacement models, based on magnetic or other fabric data, it is important to consider the currently accepted regional scale kinematic setting into which emplacement was achieved. In essence each study should seek to critique and progress existing regional scale models, not be bound by them, and ultimately determine the evolution of the studied intrusion in the context of regional scale kinematics (as in Goodenough *et al.* (2006); Stevenson (2008); Stevenson *et al.* (2008a); Neilson *et al.* (2009); Feely *et al.* (2010)).

Section III Characterising the magnetic properties of a specimen

III.1 Introduction

A specimen's mineral composition, abundance and grain size are critical contributors that determine a samples AMS ellipsoid. As such it is vital to constrain these parameters in order to validate any interpretation of AMS data.

Reflective and transmitted light petrographic examination, isothermal susceptibility data and stepwise heating *vs.* susceptibility experiments can effectively identify and isolate the contribution of certain minerals to the overall AMS tensor (Borradaile and Jackson 2010). These are effective and fast means by which one may gain an idea of a sample's dominant magnetic minerals. As discussed, any interpretation of AMS data is extrapolated from just three principal susceptibly data points which are the bulk product of a the net interaction between a sample's constituent minerals. The relative contribution of ferromagnetic minerals of differing grain size and species can be difficult to determine from susceptibility data alone and is always open to an increased error potential as such interpretation is based on statistical manipulation rather than direct measurement (e.g. Owens (1974); Rochette *et al.* (1999); Owens (2000b); Ferré (2002)). Reflective microscopy can be used to determine grain size and mineralogy but cannot be reliably used to identify smaller grain sizes or subtle compositional differences in a mineral species. Of the three examples discussed, stepwise heating in a constant magnetic field is probably the best way to identify the most influential magnetic minerals in a sample. However, no inference of mineral abundances may be obtained and while the domain state may be estimated (discussed above) this is considered a crude estimate rather than a robust means to determination.

In order to fully characterise the magnetic properties of a sample's mineral assemblage, and thus interpret the crystallisation, deformation and alteration history of a sample from magnetic analysis, a suite of experiments are devised designed to identify and quantify the abundance of particular magnetic carriers. A comprehensive account of such methodologies is provided in Dunlop and Ozdemir (1997), those which are applicable to this work are discussed below.

III.2 Hysteresis and Remanence

Ferromagnetic materials (*senso lato*) are capable of retaining an element of magnetisation after exposure to a sufficiently large inducing field, this behaviour is called *hysteresis*. Natural

defects in a crystal lattice act as obstructions to the realignment of domain walls into parallelism with an imposed field; excess energy, only available if the imposed field is strong enough, is required in order for walls to realign. After the magnetic field is removed domain walls may remain *pinned* by the grain scale imperfections that initially impeded alignments, thus pinning features prevent the domain structure from relaxing back to its original symmetry. In this way part of the imposed magnetic field is preserved by *wall pinning* which maintains some degree of magnetic ordering outside of an imposing field. *Nucleation* of new domains formed, for example, about grain scale defects in very intense magnetic fields can also cause a magnetic moment to remain aligned once the inducing field is removed. A comprehensive treatment of hysteresis and its causes is detailed in Dunlop and Ozdemir (1997) and Brokate and Sprekels (1996).

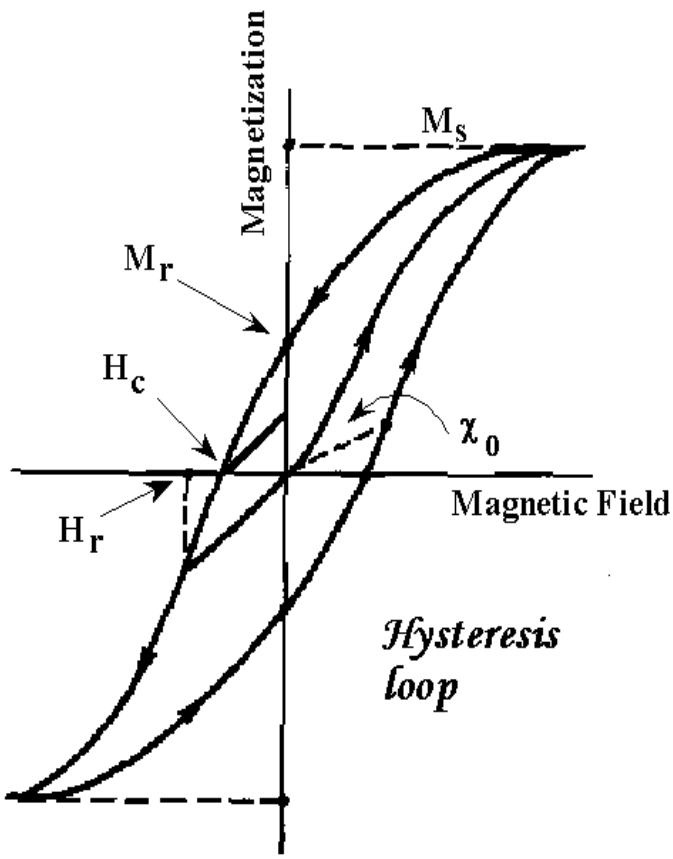

Fig. D.1 The Hysteresis Loop. Exposing a ferromagnetic material to a adequately strong magnetic field (usually *c.* 2T) along one axes causes it to reach saturation magnetisation (M_s), no further increase in H will cause M in the sample to increase. Upon removing the inducing field a remanant magnetisation (Mr), which is greater than the initial susceptibility (χ_o), remains. Imposing a magnetic field in the opposite direction along the same axes reduces the magnetisation of the sample. When magnetisation of a sample is reduced to zero in the relatively reversed field the *coercivity* (H_c) is reached, if the induced field is removed some magnetic remanence will still remain. Further increasing the reverse field results in Mr reaching zero when the field is removed, this point is known as the *coercivity of remanence* (H_r or H_{CR}).

Manipulation of a samples M_r is brought about by either realigning domain walls (energetically easy) or by rotating the magnetization of an entire grain (energetically very difficult). Thus grains which have multiple domains are energetically easier to magnetise (and demagnetise) and are

considered magnetically *soft* while single domain grains require much higher inducing fields and are considered magnetically *hard*. Magnetic "*hardness*" may be determined from the shape of the hysteresis loop. Generally speaking materials magnetically dominated by SD grains return broader loops while those with larger proportion of MD grains have slender abrupt loops as lower coercivity facilitates rapid acquisition of magnetisation. Higher coercivity and remanence values are indicative of smaller SD or PSD grains.

Magnetic stability may be quantified by measuring the ratios H_r/H_C and M_r/M_S. As hardness is a proxy for grain size, these ratios can be used to indicate the grain size as well as domain state (e.g. Dunlop (1990)). Larger magnetic fields are required to alter the M_r of SD grains, once induced magnetic remanence will also be much more stable. Thus higher M_r/M_S and lower H_r/H_C ratios suggest a MD grain size while the opposite is indicative of SD grains. For magnetite, M_r/M_S values >0.5 suggest *c.*0.06µm SD grains, pseudo single domain grains an inferred between *c.*0.1-0.5 and multidomain grains measuring *c.*10-20µm are indicated by ratios <0.1 (Day *et al.* 1977; Dunlop 1986). H_r/H_C ratios of 1-2, 2-4 and >4 are suggestive of SD, PSD and MD grains respectively, and H_C is generally reached by *c.*10mT for MD grains, SD and PSD grains require more, typically *c.*15mT (Day *et al.* 1977; Dunlop 1986).

III.2.1 Natural Sources of Remanence

Geological samples that contain ferromagnetic minerals carry a *natural remanent magnetisation* (NRM), this is the vector sum of all contributors to that samples remanent magnetisation. Remagnetisation during the rock's history may alter the direction and/or intensity of contributions from grains with contrasting coercivity values, obviously this is a feature of materials containing two or more distinguishable ferromagnetic grain sizes. Thus as a remagnetisation force becomes progressively intense a primary remanent magnetisation will be overprinted in increasingly harder (higher coercivity) magnetic grains. For this reason, SD grains are considered ideal for palaeomagnetic analysis due to increased magnetic stability relative to MD grains, however for AMS analysis a MD grain size is preferable as complexities arising from inverse magnetic fabrics in SD grains are less of a concern (Tarling and Hrouda 1993).

Thermoremanent magnetisation (TRM) is remanence acquired as a sample is cooled through T_C. Heating a sample above T_C removes M_r, a point is reached upon cooling through T_C where the energy barrier preventing net magnetic alignment to an external field is very low, this is the

blocking temperature (T_B). Under such conditions a relatively weak magnetic field can induce a M_r and once the sample is cooled progressively greater field intensities are required to over print the TRM. This is an important type of remanence for all rock samples subjected to elevated temperatures, particularly igneous rocks, and is of vital importance to paleomagnetic studies.

Other means through which a sample may become magnetised include chemical remanent magnetisation (ChRM), depositional remanent magnetisation (DRM), post depositional remanent magnetisation (pDRM) and viscous remanent magnetisation (VRM). ChRM results from chemical modification of a mineral (e.g. mineral growth during diagenesis or oxidation) in an external field. DRM is produced when suspended sediments are deposited in the presence of an external field and post depositional remanent magnetisation (pDRM) modifies magnetic remanence due to mechanical interaction between wet sediment and magnetic grains. VRM is acquired over an extended period of time and in lower magnetic fields, thus it serves to overprint all types of remanence even in high coercivity grains but at a very slow rate. Due to the dependence of ferromagnetism on temperature, at room temperature and under normal magnetic fields (similar to earth's magnetic field) samples are essentially stable over geological time periods. For a full account of sources of natural remanence the reader is referred to Dunlop and Ozdemir (1997).

III.2.2 Isothermal Magnetisation and Demagnetisation Techniques

Appling a suitable magnetic field to generate a magnetic remanence within a sample under isothermal conditions (most often room temperature) results in isothermal magnetisation. In nature only electromagnetic fields generated by lightning strikes are sufficient to generate a stable isothermal magnetisation. Magnetisation gained from less intense sources are easily countered by fields of similar weak intensities, thus such magnetisation is not directly useful to palaeomagnetic or anisotropy studies.

Stable isothermal remanence can be generated and removed from a sample in the laboratory. *Isothermal remanent magnetisation* (IRM) is remanence gained by a sample after an adequate stable field has been applied for a short time period (seconds to a couple of minutes). For magnetite *c.*50mT will generate an IRM in MD grains via domain wall translation while fields greater than this are required to force domain rotation in MD grains or cause moment rotation in SD grains (Dunlop and Ozdemir 1997). If a sufficiently large field is applied, a sample will reach saturation magnetisation, this is sometimes called *saturation isothermal remanent magnetisation*

(SIRM). *Anhysteretic remanent magnetisation* (ARM) is generated by applying a large, progressively decaying alternating field (AF) and a second smaller constant DC field across a sample.

Thermal demagnetisation involves heating and cooling a sample in a zero field over a series of temperatures. After each heating cycle magnetic remanence is measured, any loss in magnetisation is related to the temperature of the previous heating cycle and thus the unblocking temperature of constituent minerals can be constrained and the remanence carriers identified. Temperatures of 700°C are usually sufficient to unblock most ferromagnetic minerals unless particularly high coercivity phases such as very fine grained hematite are present.

AF demagnetisation applies a peak alternating field value across a sample which is progressively reduced to zero. Magnetic remanence is measured at intervals as progressively larger peek values (from zero to c. 120mT) are applied to demagnetise the sample. The AF value required to half the original magnetic remanence is referred to the *median destructive field* (MDF). The MDF is indicative of domain state, a higher value reflects higher coercivity. Through demagnetisation profiles the ferromagnetic constituents of a sample can be examined as magnetically soft grains will decay first while harder grains (e.g. hematite) will not demagnetise and require thermal demagnetisation.

The shape of NRM, IRM and ARM acquisition curves and associated demagnetisation behaviour, during thermal or AF demagnetisation or by applying a reverse IRM field, are used to characterise ferromagnetic minerals in a sample (Dunlop and Ozdemir 1997). The field intensity required for acquisition and demagnetisation for isothermal magnetisation are dependent on the coercivity of constituent ferromagnetic minerals. Thus, from the above discussion, it is clear that the behaviour of a sample during stepwise acquisition and removal of remanence is useful in determining the composition, domain structure, grain size and proportions of ferromagnetic minerals in a sample (e.g. Fuller (1963); Lowrie and Fuller (1971); Day *et al.* (1977)). The intensity and symmetry of the AMS ellipsoid is not simply controlled by the average grain shape preferred orientation of particular dominant mineral species alone. Domain state (Potter and Stephenson 1988; Rochette and Fillion 1988) and textural anisotropy (Fuller 1963; Gaillot *et al.* 2006) are highly influential. Therefore, it is important to gain an understanding of the above parameters, particularly where AMS data return information seemingly contrary to direct field observations.

III.3 Characterisation techniques

Detailed below is a brief account of some principal rock magnetic experiments which are often used in evaluating magnetic properties of geological samples, for a comprehensive review of these and more the reader is referred to Dunlop and Ozdemir (1997). These have been utilised in the course of this study to characterise the magnetic mineralogy of subject specimens and thus achieve a more comprehensive understanding of the AMS data.

III.3.1 Variable frequency vs. low field susceptibility (AF vs. K)

Ferromagnetic minerals commonly found in granitic rocks, including magnetite, maghemite, and titanomagnetites exhibit frequency dependent susceptibility (Vincenz 1965; Bathal 1971). Some paramagnetic material, including biotite also exhibit this trait (Ellwood *et al.* 1993). A completely non destructive method to evaluate a mineral assemblage exploits this by varying the frequency of the inducing field while susceptibility is simultaneously measured. While not conclusive, this method provides a rapid means to evaluate part of the basic mineralogy of a specimen using relatively basic equipment (e.g. the Agico MFK-1A) without damaging the sample in anyway.

III.3.2 Temperature vs. low field susceptibility (T vs. K)

Following AMS analysis, the most straight forward means by which one can evaluate a mineral assemblage from a magnetic point of view is by measuring susceptibility variation with temperature under a constant inducing field. This experiment involves exposing a sample to a constant weak magnetic field as ambient temperature is progressively increased. The fluctuation in susceptibility as temperature increases (following the Curie-Weiss Law and Curies Law) is measured at short regular intervals.

Monitoring susceptibility fluctuation with temperature from room temperature to *c.*700°C allows one to evaluate the magnetic composition of a given sample. The Curie Point, the temperature at which super exchange and exchange forces are no longer effective and ferromagnetic materials behave paramagnetically (Getzlaff 2007), may be estimated based on the

Hopkinson peak method (Moskowitz 1981) or the inflection point method (Tauxe 1998). From this the Ti content of titanomagnetites can be inferred (Akimoto 1962; Lattard *et al.* 2006). The shape of the Hopkinson peak, if present, may be used as a crude proxy for grain size and domain state as SD grains are more likely to exhibit an abrupt peek over a shorter temperature range relative to MD grains (Dunlop and Ozdemir 1997).

Inspection of the shape of the progressive heating and cooling curve vs. susceptibility can reveal other less obvious magnetic contributors which have T_C/T_N at lower temperatures and contribute less to the bulk susceptibility (e.g. Hrouda *et al.* (2006)). Fluctuation in susceptibly prior to the arrival at T_C may be investigated by repeating the T *vs.* K experiment at progressively higher temperatures using fresh samples each time (Hrouda 2003). Examination of the heating and cooling curves may be used to determine whether susceptibility fluctuation was driven by the presence of a primary or secondary mineral phase, an incomplete oxidation of ferromagnetic minerals or simply due to contamination of the sample with air at elevated temperature during the experiment (e.g. Petronis *et al.* (2011) Just and Kontny (2012)).

In summary, low field K vs. T can be used to evaluate the minerals present in a sample. Minerals with similar H_C may exhibit large differences between their respective Curie temperatures (e.g. T_C ~ 575 for magnetite and ~ 350 for maghemite yet both have H_C ~ 0.3 (O'Reilly 1984)), thus this test can easily identify the dominance of either of these two mineral phases. This test is a convenient and automated means of determining magnetic constituents but does not definitively determine domain state, grain size or relative or absolute mineral abundance (Tarling and Hrouda 1993; Dunlop and Ozdemir 1997). Thus it is desirable to further investigate a sample's magnetic properties where possible.

III.3.3 IRM, ARM, NRM AF demagnetisation

Experimental results show that normalised data returned from two cycles of AF demagnetisation on the same sample, first targeting an imposed ARM and the second a subsequently imposed SIRM, will return different relationships depending on weather SD or MD grain size dominate (Lowrie and Fuller 1971). The Lowrie-Fuller test (Lowrie and Fuller 1971) was devised to exploit this characteristic and aid in evaluating domain state of a sample's ferromagnetic carriers. This work proposes that for larger grains ARM is removed by weaker AF demagnetising fields than that which is required for demagnetisation of SIRM (note ARM and

SIRM are used here in place of natural weak-field TRM and strong field TRM respectively). Most notably, in MD grains the MDF of ARM is less than that observed during demagnetisation of SIRM. When SD grains are analysed the opposite relationship was found. Thus by carrying out two progressive demagnetisation tests Lowrie and Fuller (1971) were able to propose a means through which one may evaluate grain size.

This test is not totally reliable. While adhering to this methodology, smaller MD grains have been reported to return SD traits, this attributed to PSD behaviourisms (Dunlop *et al.* 1973; Bailey and Dunlop 1983). Much larger magnetites over 100µm may also return SD characteristics (Heider *et al.* 1992), this is attributed to hydrothermal affects which are believed to have played a pivotal role in the generation of the subject MD magnetite grains (Xu and Dunlop 1995).

Ultimately the Lowrie-Fuller test is considered useful in evaluating magnetic properties of a sample. Comparing the shape of ARM and SIRM demagnetising curves reflects the coercivity spectrum oppose to domain state and grain size directly (Dunlop and Ozdemir 1997). Thus, this test can be used as an indirect means through which one may evaluate the former parameters but best practice will seek to compliment this technique with further work.

III.3.4 IRM acquisition curves

IRM acquisition is achieved by inducing a progressively larger magnetic field along a single axis of a previously AC demagnetised sample. Remanent magnetisation is measured after each exposure and field intensity is gradually increased until SIRM is reached. The magnetic field is then reversed along the same axes and back-field IRM (BIRM) records the reverse field required to return M_r to a value of zero from M_S.

This is a non-destructive method (not magnetically but in terms of sample integrity) for investigating the coercivity spectrum of a sample (Dunlop and Ozdemir 1997) and results are comparable to those generated from full hysteresis measurements. Although the current method is much more time consuming it may be carried out using standard palaeomagnetic equipment, equipment required to carry out hysteresis experiments are not always available (as was the case in this study).

Resulting data characteristically shows rapid acquisition in MD grains relative to SD grains of the same mineral species. It follows that for progressively smaller grain sizes and simpler domain

structures M_S is reach in progressively elevated fields (e.g. Day *et al.* (1977); Argyle and Dunlop (1990)). Furthermore, as coercivity contrasts between distinct ferromagnetic minerals exist, and M_S is reached under differing fields, analysis of both SIRM and BIRM curves can be used to aid in evaluating the presence of mineral species as well as domain state. Magnetite generally reaches M_S by *c.*300mT while hematite requires fields in excess of 2.5T (Lowrie and Heller 1982; O'Reilly 1984). Thus the presence of these two carriers, for example, may be identified by stepwise increases in the inducing IRM field from 0 to *c.*3T (Butler 1982) and grain size/domain state may be indicated by the relationship between the increasing IRM curve and BIRM curve in a similar fashion to that is used for evaluating data from a full hysteresis loop (Dunlop and Ozdemir 1997).

III.3.5 Thermomagnetic Analysis of Three-Component IRM

As minerals of the same species and similar grain size exhibit characteristic coercivity spectra and demagnetisation properties, these features may be used to evaluate the type of magnetic minerals present by combining IRM acquisition with thermal demagnetisation (Dunlop 1972). However, many ferromagnetic minerals have coercivity characteristics that overlap. Below .3T M_r in MD magnetite, maghemite and pyrrhotite will all rapidly increase while goethite may exhibit coercivity values similar to that of hematite (Dunlop and Ozdemir 1997). This makes identification of dominant carriers difficult if only single IRM acquisition curves are used.

Thermomagnetic analysis of three-component IRM (Lowrie 1990) is executed by applying predetermined magnetic fields of contrasting intensity along three orthogonal axes (X, Y, Z) of a previously AF-demagnetised sample. The three inducing fields are selected based on prior knowledge of suspected magnetic contributors established from IRM acquisition data. In the original experiment (Lowrie 1990) fields of 1.2T, 0.4T and 0.12T were applied to test for the presence of goethite, pyrrhotite hematite, maghemite and magnetite. Magnetic remanence is then measured before, and episodically during, stepwise thermal demagnetisation, usually from 0°C to 700°C as the unblocking temperature of hematite is *c.*675°C (O'Reilly 1984). The magnitude of M_r along each axes during each demagnetisation interval, and the temperature required to fully remove M_r is used to interpret the mineral species present and their relative proportions.

Section IV Summary

IV.1 Summary

Owing to the high degree of accuracy, sensitivity and efficiency, rock magnetic analysis, and AMS in particular, is invaluable to the investigation of plutonic rocks. In the past two decades progress in equipment development has improved functionality, accuracy and efficiency (Bouchez 1997; Borradaile and Jackson 2010) and a more detailed understanding of the controls over AMS have been quite thoroughly investigated (Tarling and Hrouda 1993; Dunlop and Ozdemir 1997; Borradaile 2001, 2003; Borradaile and Jackson 2004; Martin-Hernandez and Ferre 2006; Borradaile and Jackson 2010). As a product of this work, even complex composite or inverse to intermediate fabrics may be evaluated and valuable information drawn if the correct methodology is applied.

Low field AMS in granite is controlled by either ferromagnetic minerals, typically some titanomagnetite composition, in the absence or very low concentrations of such minerals, paramagnetic minerals will dictate the AMS ellipsoid, this is typically some form of mica or amphibole. The diamagnetic component is negligible due to extremely weak susceptibility values associated with diamagnetic minerals. It has been proven in a multitude of cases that the relationship between the AMS tensor and petrofabric is normal and K1, K2 & K3 equate to within a few degrees of the maximum, intermediate and minimum axes of the finite strain ellipsoid in orientation but not in magnitude as anisotropy is dependent on both composition and particle spatial anisotropy, i.e. a higher ferromagnetic content may reflect a higher anisotropy degree and not necessarily a higher strain rate (Rochette *et al.* 1992). Hence AMS is a useful indirect method of determining petrofabric symmetry but may not be directly equated to the finite strain ellipsoid (Borradaile and Jackson 2010). In the case where inverse or intermediate fabrics are suspected one may identify these through a variety of statistical, magnetic or optical methods and valuable information regarding strain, alteration history and mineralogy may still be determined.

There is no question about the validity of AMS as a viable tool in structural analysis (Tarling and Hrouda 1993; Borradaile and Henry 1997; Bouchez 1997; Cagnoli and Tarling 1997; Borradaile and Jackson 2004), however data must be scrutinised and cross checked preferably with directly observable field evidence. Outcrop scale fabric measurements, crystal preferred orientation analysis, x-ray imaging, petrographic microstructural investigation, comparison to map scale structural interpretations and regional scale models are all useful means to check the validity of AMS and other magnetic data.

It is crucial to understand the mineralogy of each specimen under examination (Thompson and Oldfield 1986; Rochette *et al.* 1992; Tarling and Hrouda 1993; Dunlop and Ozdemir 1997). This may be achieved partially by standard transmitted and reflected light microscopy which must be supplemented by some form of rock magnetic analysis. As a minimum, bulk susceptibility measurements derived from standard AMS analysis can sometimes suffice but this may only give a very vague indication of the grain scale contributors to the bulk AMS ellipsoid (Tarling and Hrouda 1993). In order to gain a better idea of the mineralogical controls over the AMS data, and fully contemplate the relationship between magnetic fabrics and those observed in the field, it is necessary to carry out some rock magnetic experiments. Such work is desirable in all cases but is critical in scenarios in which magnetic fabrics contradict or remain ambiguous with other data.

References;

Akimoto, S. (1962), 'Magnetic properties of FeO-Fe_2O_3-TiO system as a basis of rock magnetism', *Journal of physics Society Japan,* 17 (suppl. B1), 706-10.

Almqvist, B. S. G., Herwegh, M., Schmidt, V., Pettke, T., and Hirt, A. M. (2010), 'Magnetic susceptibility as a tool to study deformed calcite with variable impurity content', *Geochem. Geophys. Geosyst.,* 11 (1), Q01Z09.

Ameglio, L., Vigneresse, J. L., and Bouchez, J. L. (1997), 'Granite Pluton geometry and emplacement mode inferred from combined fabric and gravity data', *In: Bouchez, J.L., Hutton, D.H.W., Stephens, W.E., (eds.), Grantie: From Segregation of Melt to Emplacement Fabrics, Kluwer Academic Publishers, Dordrecht*, 199-214.

Améglio, L. and Vigneresse, J. L. (1999), 'Geophysical imaging of the shape of granitic intrusions at depth: a review', *In Castro, A. Gernandez, C. Vigneresse, J.L. (eds) Understanding Granites: Integrating New and Classical Techniques, Geological Society of London, Special Publication,* 168, 39-54.

Archanjo, C. J., Launeau, P., and Bouchez, J. L. (1995), 'Magnetic fabric vs. magnetite and biotite shape fabrics of the magnetite-bearing granite pluton of Gameleiras (Northeast Brazil)', *Physics of the Earth and Planetary Interiors,* 89 (1–2), 63-75.

Archanjo, C. J. and Launeau, P. (2004), 'Magma flow inferred from preferred orientations of plagioclase of the Rio Ceará-Mirim dyke swarm (NE Brazil) and its AMS significance', *Geological Society, London, Special Publications,* 238 (1), 285-98.

Argyle, K. S. and Dunlop, D. J. (1990), 'Low-Temperature and High-Temperature Hysteresis of Small Multidomain Magnetites (215-540 nm)', *J. Geophys. Res.,* 95 (B5), 7069-82.

Arzi, A. A. (1978), 'Critical phenomena in the rheology of partially melted rocks', *Tectonophysics,* 44 (1–4), 173-84.

Aubourg, C. and Robion, P. (2002), 'Composite ferromagnetic fabrics (magnetite, greigite) measured by AMS and partial AARM in weakly strained sandstones from western Makran, Iran', *Geophysical Journal International,* 151 (3), 729-37.

Bailey, M. E. and Dunlop, D. J. (1983), 'Alternating field characteristics of pseudo-single-domain (2–14 µm) and multidomain magnetite', *Earth and Planetary Science Letters,* 63 (3), 335-52.

Balsley, J. R. and Buddington, A. F. (1960), 'Magnetic Susceptibility Anisotropy and Fabric of some Adirondack Granite and Orthogneisses', *American Journal of Science, Bradley Volume,* 258-A, 6-20.

Bathal, R. S. (1971), 'Magnetic anisotropy in rocks', *Earth Science Review,* 7, 227-53.

Beausoleil, N., Lavallee, P., Yelon, A., Ballet, O., and Coey, J. M. D. (1983), 'Magnetic properties of micas', *Journal of Applied Physics,* 54, 906-15.

Benn, K. (2010), 'Anisotropy of magnetic susceptibility fabrics in syntectonic plutons as tectonic strain markers: the example of the Canso pluton, Meguma Terrane, Nova Scotia', *Geological Society of America Special Papers,* 472, 147-58.

Blenkinsop, T. G. (2000), 'Deformation microstructures and mechanisms in minerals and rocks', *Dordrecht: Kluwer*.

Bolle, O., Diot, H., and Trindade, R. I. F. (2003), 'Magnetic fabrics in the Holum granite (Vest-Agder, southern most Norway): implications for the late evolution of the Sveconorwegian (Grenvillian) orogen of SW Scandinavia', *Precambrian Research,* 121, 221-49.

Borradaile, G. (1987), 'Anisotropy of magnetic susceptibility: rock composition versus strain', *Tectonophysics,* 138 (2–4), 327-29.

--- (2001), 'Anisotropy of magnetic susceptibility, Measurement schemes', *Geophysical Research Letters,* 22, 1957-60.

Borradaile, G. and Lagroix, F. (2001), 'Magnetic fabrics reveal upper mantle flow fabrics in the Toordos ophiolite complex, Cyprus.', *Journal of Structural Geology,* 23, 1299-317.

Borradaile, G. (2003), 'Statistics of Earth Science Data', *Springer-Verlag*, 351.

Borradaile, G. J. and Tarling, D. H. (1981), 'The influence of deformation mechanisms on magnetic fabrics in weakly deformed rocks', *Tectonophysics,* 77 (1–2), 151-68.

Borradaile, G. J. and Puumala, M. A. (1989), 'Synthetic magnetic fabrics in a plasticene medium', *Tectonophysics,* 164 (1), 73-78.

Borradaile, G. J. and Werner, T. (1994), 'Magnetic anisotropy of some phyllosilicates', *Tectonophysics,* 235 (3), 223-48.

Borradaile, G. J. and Stupavsky, M. (1995), 'Anisotropy of magnetic susceptibility: Measurement schemes', *Geophys. Res. Lett.,* 22 (15), 1957-60.

Borradaile, G. J. and Henry, B. (1997), 'Tectonic applications of magnetic susceptibility and its anisotropy', *Earth-Science Reviews,* 42 (1–2), 49-93.

Borradaile, G. J. and Jackson, M. (2004), 'Anisotropy of magnetic susceptibility (AMS): magnetic petrofabrics of deformed rocks', *Geological Society, London, Special Publications,* 238 (1), 299-360.

--- (2010), 'Structural geology, petrofabrics and magnetic fabrics (AMS, AARM, AIRM)', *Journal of Structural Geology,* 32 (10), 1519-51.

Bouchez, J. L., Gleizes, G., Djouadi, T., and Rochette, P. (1990), 'Microstructure and magnetic susceptibility applied to emplacement kinematics of granites: the example of the foix pluton (French pyrenees)', *Tectonophysics,* 184 (2), 157-71.

Bouchez, J. L. (1997), 'Granite is never isotropic: an introduction to AMS studies of granitic rocks.', *In: Bouchez, J.L., Hutton, D.H.W., Stephens, W.E., (eds.), Grantie: From Segregation of Melt to Emplacement Fabrics, Kluwer Academic Publishers, Dordrecht*, 95-112.

Bouchez, J. L., Nguema, T. M. M., Esteban, L., Siqueira, R., and Scrivener, R. (2006), 'The tourmaline-bearing granite pluton of Bodmin (Cornwall, UK): magnetic fabric study and regional inference', *Journal of the Geological Society,* 163 (4), 607-16.

Brokate, M. and Sprekels, J. (1996), 'Hysteresis and Phase Transitions', *Springer-Verlag New Your, Inc.,* 121.

Butler, R. F. (1982), 'Magnetic Mineralogy of Continental Deposits, San Juan Basin, New Mexico, and Clark's Fork Basin, Wyoming', *J. Geophys. Res.,* 87 (B9), 7843-52.

Cagnoli, B. and Tarling, D. H. (1997), 'The reliability of anisotropy of magnetic susceptibility (AMS) data as flow direction indicators in friable base surge and ignimbrite deposits: Italian examples', *Journal of Volcanology and Geothermal Research,* 75 (3–4), 309-20.

Callot, J. P. and Guichet, X. (2003), 'Rock texture and magnetic lineation in dykes: a simple analytical model', *Tectonophysics,* 366 (3–4), 207-22.

Callot, J. P., Gurevitch, E., Westphal, M., and Pozzi, J. P. (2004), 'Flow patters in the Siberian traps deduced from magnetic fabric studies', *Geophysical Journal International,* 156 (3), 426-30.

Cañón-Tapia, E. (1996), 'Single-grain versus distribution anisotropy: a simple three-dimensional model', *Physics of the Earth and Planetary Interiors,* 94 (1–2), 149-58.

--- (2001), 'Factors affecting the relative importance of shape and distribution anisotropy in rocks: theory and experiments', *Tectonophysics,* 340 (1–2), 117-31.

Cawood, P. A. and Pisarevsky, S. A. (2006), 'Was Baltica right-way-up or upside-down in the Neoproterozoic?', *Journal of the Geological Society,* 163 (5), 753-59.

Chadima, M., Cajz, V., and Týcová, P. (2009), 'On the interpretation of normal and inverse magnetic fabric in dikes: Examples from the Eger Graben, NW Bohemian Massif', *Tectonophysics,* 466 (1–2), 47-63.

Chappell, B. W. and White, A. J. R. (1974), 'Two contrasting granite types', *Pacific Geology,* 8, 173-74.

Cifelli, F., Mattei, M., Chadima, M., Lenser, S., and Hirt, A. M. (2009), 'The magnetic fabric in "undeformed clays": AMS and neutron texture analyses from the Rif Chain (Morocco)', *Tectonophysics,* 466 (1–2), 79-88.

Collinson, D. W. (1983), 'Methods in rock magnetism and palaeomagnetism: techniques and instrumentation', *Chapman & Hall*.

Constable, C. and Tauxe, L. (1990), 'The Bootstrap for Magnetic Susceptibility Tensors', *J. Geophys. Res.,* 95 (B6), 8383-95.

Cruden, A. R., Tobisch, O. T., and Launeau, P. (1999), 'Magnetic fabric evidence for conduit-fed emplacement of a tabular intrusion: Dinkey Creek Pluton, central Sierra Nevada batholith, California', *J. Geophys. Res.,* 104 (B5), 10511-30.

Daly, L. and Zinsser, H. (1973), 'Etude comparative des anisotropies de susceptibiliteet d'aimantation remanente isotherme: Consequences pour l'analyse structurale et le paleomagnetisme', *Ann. Geophys.,* 29, 189-200.

Day, R., Fuller, M., and Schmidt, V. A. (1977), 'Hysteresis properties of titanomagnetites: Grain-size and compositional dependence', *Physics of the Earth and Planetary Interiors,* 13 (4), 260-67.

Debacker, T. N., Robion, P., and Sintubin, M. (2004), 'The anisotropy of magnetic susceptibility (AMS) in low-grade, cleaved pelitic rocks: influence of cleavage/bedding angle and type and relative orientation of magnetic carriers', *Geological Society, London, Special Publications,* 238 (1), 77-107.

Dewey, J. F. (2005), 'Orogeny can be very short', *Proceedings of the National Academy of Sciences of the United States of America,* 102 (43), 15286-93.

Dewey, J. F., Dutton, B., Ryan, P.D. (1997), 'Transpression in the Irish Caledonides and the Silurian evolution of basins, plutons, fabrics and cleavage sequences', *Abstracts: Continental Transpressional and Transtensional Tectonics. Tectonic Studies Group Meeting, London*.

Dunlop, D. J. (1971), 'Magnetic properties of fine particle hematite', *Ann. Geophys.,* 27, 269-93.

--- (1972), 'Magnetic Mineralogy of Unheated and Heated Red Sediments by Coercivity Spectrum Analysis*', *Geophysical Journal of the Royal Astronomical Society,* 27 (1), 37-55.

Dunlop, D. J., Hanes, J. A., and Buchan, K. L. (1973), 'Indices of Multidomain Magnetic Behavior in Basic Igneous Rocks: Alternating-Field Demagnetization, Hysteresis, and Oxide Petrology', *Journal of geophysical Research,* 78, 1387-93.

Dunlop, D. J. (1986), 'Hysteresis Properties of Magnetite and their Dependence on Particle Size: A Test of Pseudo-Single-Domain Remanence Models', *J. Geophys. Res.,* 91 (B9), 9569-84.

Dunlop, D. J. (1990), 'Developments in Rock Magnetism', *Reports on Progress in Physics,* 53, 707-92.

Dunlop, D. J. and Ozdemir, O. (1997), 'Rock Magnetism: Fundamentals and Frontiers', *Cambridge University Press*.

Edgardo, C.-T. (2001), 'Factors affecting the relative importance of shape and distribution anisotropy in rocks: theory and experiments', *Tectonophysics,* 340 (1–2), 117-31.

Edwards, J. (1984), 'Partial anhysteretic remanent magnetizations produced in rotating samples, and comparisons with corresponding rotational remanent magnetizations', *Geophysical Journal of the Royal Astronomical Society,* 77 (3), 619-37.

Einstein, A. (1905), 'Zur Elektrodynamik bewegter Körper', *Annalen der Physik, Bern*, 891-921.

--- (1923), 'On the Electrodynamics of moving Bodies', *In: The Principle of Relativity (english translation of Einsteins' 1905 Zur Elektrodynamik bewegter Körper), Methuen and Company, Ltd. of London*.

Ellwood, B. B. and Wenner, D. B. (1981), 'Correlation of magnetitic susceptibility with $^{18}O/^{16}O$ data in late orogenic granites of the southern Appalachian Piedmont', *Earth and Planetary Science Letters,* 54 (2), 200-02.

Ellwood, B. B., Balsam, W., Burkart, B., Long, G. J., and Buhl, M. L. (1986), 'Anomalous Magnetic Properties in Rocks Containing the Mineral Siderite: Paleomagnetic Implications', *J. Geophys. Res.,* 91 (B12), 12779-90.

Ellwood, B. B., Burkart, B., Rajeshwar, K., Darwin, R. L., Neeley, R. A., McCall, A. B., Long, G. J., Buhl, M. L., and Hickcox, C. W. (1989), 'Are the Iron Carbonate Minerals, Ankerite and Ferroan Dolomite, Like Siderite, Important in Paleomagnetism?', *J. Geophys. Res.,* 94 (B6), 7321-31.

Ellwood, B. B., Terrell, G. E., and Cook, W. J. (1993), 'Frequency dependence and the electromagnetic susceptibility tensor in magnetic fabric studies', *Physics of the Earth and Planetary Interiors,* 80 (1–2), 65-74.

Esmaeily, D., Bouchez, J. L., and Siqueira, R. (2007), 'Magnetic fabrics and microstructures of the Jurassic Shah-Kuh granite pluton (Lut Block, Eastern Iran) and geodynamic inference', *Tectonophysics,* 439 (1–4), 149-70.

Fanjat, G., Camps, P., Shcherbakov, V., Barou, F., Sougrati, M. T., and Perrin, M. (2012), 'Magnetic interactions at the origin of abnormal magnetic fabrics in lava flows: a case study from Kerguelen flood basalts', *Geophysical Journal International,* 189 (2), 815-32.

Feely, M., Selby, D., Hunt, J., and Conliffe, J. (2010), 'Long-lived granite-related molybdenite mineralization at Connemara, western Irish Caledonides', *Geological Magazine,* 147 (6), 886-94.

Femenias, O., Diot, H., Berza, T., Gauffriau, A., and Demaiffe, D. (2004), 'Asymmertical to symmetrical magnetic fabric of dikes: Paleo-flow orientations and Paleo-stresses recorded on feeder-bodies from the Motru Dyke Swarm (Romania)', *Journal of Structural Geology,* 26, 1401-218.

Ferré, E. C. (2002), 'Theoretical models of intermediate and inverse AMS fabrics', *Geophys. Res. Lett.,* 29 (7), 1127.

Flinn, D. (1965), 'On the Symmetry Principle and the Deformation Ellipsoid', *Geological Magazine,* 102 (01), 36-45.

Friedman, M. and Higgs, N. G. (1981), 'Calcite fabrics in experimental shear zones in mechanical behavior of crustal rocks', *American Geophysical Union Monograms,* 24, 11-27.

Fuller, M. D. (1963), 'Magnetic Anisotropy and Paleomagnetism', *J. Geophys. Res.,* 68 (1), 293-309.

Gaillot, P., de Saint-Blanquat, M., and Bouchez, J.-L. (2006), 'Effects of magnetic interactions in anisotropy of magnetic susceptibility: Models, experiments and implications for igneous rock fabrics quantification', *Tectonophysics,* 418 (1–2), 3-19.

Gee, D. G. (1975), 'A tectonic model for the central part of the Scandinavian Caledonides.', *American Journal of Science,* 275A, 48.

Getzlaff, M. (2007), 'Fundamentals of Magentism', *Springer Berlin Heidelberg New York*.

Girdler, R. W. (1961), 'The Measurement and Computation of Anisotropy of Magnetic Susceptibility of Rocks', *Geophysical Journal of the Royal Astronomical Society,* 5 (1), 34-44.

Goodenough, K. M., Evans, J. A., and Krabbendam, M. (2006), 'Constraining the maximum age of movements in the Moine Thrust Belt: dating the Canisp Porphyry', *Scottish Journal of Geology,* 42 (1), 77-81.

Graham, J. W. (1954), 'Magnetic susceptibility anisotropy, an unexploited petrofabric element', *Geologcial Society of America Bulletin,* 65, 1257-58.

--- (1966), 'Significance of magnetic anisotropy in Appalachian sedimentary rocks', *In: Steinhart, J.S. and Smith, T.J. (eds.) The Earth Beneath the Continents. American Geophysical Union Geophysical Monograph* 10, 627-48.

Granar, L. (1958), 'Magnetic measurements on Swedish varved sediments', *Arkiv Fur Geofysik,* 3, 1-40.

Grégoire, V., de Saint Blanquat, M., Nédélec, A., Bouchez, J., and Luc (1995), 'Shape anisotropy versus magnetic interactions of magnetite grains: Experiments and application to AMS in granitic rocks', *Geophys. Res. Lett.,* 22 (20), 2765-68.

Grégoire, V., Darrozes, J., Gaillot, P., Nédélec, A., and Launeau, P. (1998), 'Magnetite grain shape fabric and distribution anisotropy vs rock magnetic fabric: a three-dimensional case study', *Journal of Structural Geology,* 20 (7), 937-44.

Grocott, J., Arévalo, C., Welkner, D., and Cruden, A. (2009), 'Fault-assisted vertical pluton growth: Coastal Cordillera, north Chilean Andes', *Journal of the Geological Society,* 166 (2), 295-301.

Hamilton, T. D., Borradaile, G. J., and Lagroix, F. (2004), 'Sub-fabric identification by standardization of AMS, an example of inferred neotectonic structures from Cyprus', *In: Martin-Hernandes, F., Lunenburg, C.M., Aubourg, C., Jackson, A. (eds.). Magnetic Fabrics. Geological Society of London Special Publications,* 238, 527-40.

Hargraves, R. B., Johnson, D., and Chan, C. Y. (1991), 'Distribution anisotropy: The cause of AMS in igneous rocks?', *Geophys. Res. Lett.,* 18 (12), 2193-96.

Hartz, E. H. and Torsvik, T. H. (2002), 'Baltica upside down: A new plate tectonic model for Rodinia and the Iapetus Ocean', *Geology,* 30 (3), 255-58.

Heider, F., Dunlop, D. J., and Soffel, H. C. (1992), 'Low-Temperature and Alternating Field Demagnetization of Saturation Remanence and Thermoremanence in Magnetite Grains (0.037 μm to 5 mm)', *J. Geophys. Res.,* 97 (B6), 9371-81.

Henry, B. and Daly, L. (1983), 'From qualitative to quantitative magnetic anisotropy analysis: The prospect of finite strain calibration', *Tectonophysics,* 98 (3–4), 327-36.

Henry, B. (1985), 'Magnetic fabrics and superimposed deformations: example of Dalradian rocks from the southwest Highlands of Scotland', *Physics of the Earth and Planetary Interiors,* 40 (3), 187-200.

--- (1988), 'The magnetic fabrics of the Egletons granite (France): separation and structural implications', *Physics of the Earth and Planetary Interiors,* 51 (4), 253-63.

Henry, B., Jordanova, D., Jordanova, N., Souque, C., and Robion, P. (2003), 'Anisotropy of magnetic susceptibility of heated rocks', *Tectonophysics,* 366 (3–4), 241-58.

Hext, G. R. (1963), 'The estimation of second-order tensors, with related tests and designs', *Biometrika,* 50 (3-4), 353-73.

Hippertt, J. F. M. (1993), '‘V’-pull-apart microstructures: a new shear-sense indicator', *Journal of Structural Geology,* 15 (12), 1393-403.

Hirt, A. M., Lowrie, W., Clendenen, W. S., and Kligfield, R. (1988), 'The correlation of magnetic anisotropy with strain in the Chelmsford Formation of the Sudbury Basin, Ontario', *Tectonophysics,* 145 (3–4), 177-89.

Housen, B. A., Richter, C., and van der Pluijm, B. A. (1993), 'Composite magnetic anisotropy fabrics: experiments, numerical models and implications for the quantification of rock fabrics', *Tectonophysics,* 220 (1–4), 1-12.

Hrouda, F., Chlupáčová, M., and Rejl, L. (1971), 'The mimetic fabric of magnetite in some foliated granodiorites, as indicated by magnetic anisotropy', *Earth and Planetary Science Letters,* 11 (1–5), 381-84.

Hrouda, F. and Jelínek, V. (1990), 'Resolution of ferrimagnetic and paramagnetic anisotropies in rocks, using combined low-field and high-field measurements', *Geophysical Journal International,* 103 (1), 75-84.

Hrouda, F. (1992), 'Separation of a component of tectonic deformation from a complex magnetic fabric', *Journal of Structural Geology,* 14 (1), 65-71.

Hrouda, F., Jelínek, V., and Zapletal, K. (1997), 'Refined technique for susceptibility resolution into ferromagnetic and paramagnetic components based on susceptibility temperature-variation measurement', *Geophysical Journal International,* 129 (3), 715-19.

Hrouda, F. (2002), 'The use of the anisotropy of magnetic remanence in the resolution of the anisotropy of magnetic susceptibility into its ferromagnetic and paramagnetic components', *Tectonophysics,* 347 (4), 269-81.

--- (2003), 'Indices for Numerical Characterization of the Alteration Processes of Magnetic Minerals Taking Place During Investigation of Temperature Variation of Magnetic Susceptibility', *Studia Geophysica et Geodaetica,* 47 (4), 847-61.

Hrouda, F., Chlupáčová, M., and Mrázová, Š. (2006), 'Low-field variation of magnetic susceptibility as a tool for magnetic mineralogy of rocks', *Physics of the Earth and Planetary Interiors,* 154 (3–4), 323-36.

Hrouda, F. (2010), 'Modelling Relationship Between Bulk Susceptibility and AMS in Rocks Consisting of Two Magnetic Fractions Represented by Ferromagnetic and Paramagnetic Minerals – Implications for Understanding Magnetic Fabrics in Deformed Rocks', *Journal Geological Gociety of India,* 75, 254-66.

Hunt, C. P. and Moskowitz, B. P. (1995), 'Magnetic properties of rocks and minerals', *In: Ahrens, T.J. (ed.). Rock Physics and Phase Relations: A Handbook of Physical Constants. American Geophysical Union,* 3, 189-204.

Hutton, D. H. W. (1988), 'Granite emplacement mechanisms and tectonic controls: inferences from deformation studies', *Earth and Environmental Science Transactions of the Royal Society of Edinburgh,* 79 (2-3), 245-55.

Ising, G. (1942), 'On the magentic properties of varved clay', *Arkiv for Matematik, Astronomi och Fysik,* 29A, 1-37.

Jackson, M. (1991), 'Anisotropy of magnetic remanence: A brief review of mineralogical sources, physical origins, and geological applications, and comparison with susceptibility anisotropy', *Pure and Applied Geophysics,* 136 (1), 1-28.

Jackson, M. J. and Tauxe, L. (1991), 'Anisotropy of magnetic susceptibility and remanence, developments in the characterization of tectonic, sedimentary and igneous fabric', *Revies of Geophysics, IUGG Report-Contributions in Geomagnetism, Paleomagnetism),* 29, 371-76.

Jelinek, V. (1977), 'The statistical theory of measuring anisotropy of magnetic susceptibility of rocks and its aplication', *Geophyzika, Brno*.

--- (1981), 'Characterization of the magnetic fabric of rocks', *Tectonophysics,* 79 (3–4), T63-T67.

Jelínek, V. (1981), 'Characterization of the magnetic fabric of rocks', *Tectonophysics,* 79, 63-67.

Jelínek, V. and Pokorný, J. (1997), 'Some new concepts in technology of transformer bridges for measuring susceptibility anisotropy of rocks', *Physics and Chemistry of The Earth,* 22 (1–2), 179-81.

Just, J., Kontny, A., and Dewall, H. (2003), 'Magnetic Fabric Development During Hydrothermal Alteration And Brittle Deformation In Granite From The EPS-1 Drilling, (Soultz-sous-Forets, France)', *American Geophysical Union, Fall Meeting 2003, Abstract*.

Just, J., Kontny, A., De Wall, H., Hirt, A. M., and Martín-Hernández, F. (2004), 'Development of magnetic fabrics during hydrothermal alteration in the Soultz-sous-Forêts granite from the EPS-1 borehole, Upper Rhine Graben', *Geological Society, London, Special Publications,* 238 (1), 509-26.

Just, J. and Kontny, A. (2012), 'Thermally induced alterations of minerals during measurements of the temperature dependence of magnetic susceptibility: a case study from the hydrothermally altered Soultz-sous-Forêts granite, France', *International Journal of Earth Sciences,* 101 (3), 819-39.

Kanaori, Y., Kawakami, S.-I., and Yairi, K. (1991), 'Microstructure of deformed biotite defining foliation in cataclasite zones in granite, central Japan', *Journal of Structural Geology,* 13 (7), 777-85.

Kelso, P. R., Tikoff, B., Jackson, M., and Sun, W. (2002), 'A new method for the separation of paramagnetic and ferromagnetic susceptibility anisotropy using low field and high field methods', *Geophysical Journal International,* 151 (2), 345-59.

Khan, M. A. (1962), 'The Anisotropy of Magnetic Susceptibility of Some Igneous and Metamorphic Rocks', *J. Geophys. Res.,* 67 (7), 2873-85.

King, R. F. (1966), 'The magnetic fabric of some Irish Granites', *Geological Journal,* 5 (1), 43-66.

Kletetschka, G., Wasilewski, P. J., and Taylor, P. T. (2000), 'Hematite vs. magnetite as the signature for planetary magnetic anomalies?', *Physics of the Earth and Planetary Interiors,* 119, 259-67.

Lagroix, F. and Borradaile, G. J. (2000a), 'Magnetic fabric interpretation complicated by inclusions in mafic silicates', *Tectonophysics,* 325 (3–4), 207-25.

--- (2000b), 'Tectonics of the circum-Troodos sedimentary cover of Cyprus, from rock magnetic and structural observations', *Journal of Structural Geology,* 22 (4), 453-69.

Lambert, R. S. J. and McKerrow, W. S. (1977), 'The Grampian Orogeny', *Scottish Journal of Geology,* 12 (4), 271-92.

Landau, L. D. and Lifschitz, E. M. (1935), 'On the theory of th edispersion of magnetic permeability in ferromagnetic bodies (translation from Russian)', *Phys. Z. Sowjetunion,* 8, 153-69.

Lattard, D., Engelmann, R., Kontny, A., and Sauerzapf, U. (2006), 'Curie temperatures of synthetic titanomagnetites in the Fe-Ti-O system: Effects of composition, crystal chemistry, and thermomagnetic methods', *Journal of Geophysical Research,* 111 (B12S28).

Launeau, P. and Robin, P. Y. F. (1996), 'Fabric analysis using the intercept method', *Tectonophysics,* 267 (1–4), 91-119.

Launeau, P. and Robin, P.-Y. F. (2005), 'Determination of fabric and strain ellipsoids from measured sectional ellipses—implementation and applications', *Journal of Structural Geology,* 27 (12), 2223-33.

Lienert, B. R. (1991), 'Monte Carlo Simulation of Errors in the Anisotropy of Magnetic Susceptibility: A Second-Rank Symmetric Tensor', *J. Geophys. Res.,* 96 (B12), 19539-44.

López de Luchi, M. G., Rapalini, A. E., Siegesmund, S., and Steenken, A. (2004), 'Application of magnetic fabrics to the emplacement and tectonic history of Devonian granitoids in central Argentina', *Geological Society, London, Special Publications,* 238 (1), 447-74.

Lowrie, W. and Fuller, M. (1971), 'On the Alternating Field Demagnetization Characteristics of Multidomain Thermoremanent Magnetization in Magnetite', *J. Geophys. Res.,* 76 (26), 6339-49.

Lowrie, W. and Heller, F. (1982), 'Magnetic properties of marine limestones', *Rev. Geophys.,* 20 (2), 171-92.

Lowrie, W. (1990), 'Identification of ferromagnetic minerals in a rock by coercivity and unblocking temperature properties', *Geophysical Research Letters,* 17 (2), 159-62.

--- (2007), 'Fundamentals of Geophysics', *Cambridge University Press,* 2.

Lui, Q., Torrent, J., Yu, Y., and Deng, C. (2004), 'Mechanism of the parasitic remanence of aluminous

goethite [α-(Fe, Al)OOH]', *Journal of Geophysical Research,* 109 (B12106).

Lüneburg, C. M., Lampert, S. A., Lebit, H. D., Hirt, A. M., Casey, M., and Lowrie, W. (1999), 'Magnetic anisotropy, rock fabrics and finite strain in deformed sediments of SW Sardinia (Italy)', *Tectonophysics,* 307 (1–2), 51-74.

Magee, C. (2011), 'Emplacement of sub-volcanic cone sheet intrusions', *Ph.D. thesis, University of Birmingham*.

Magee, C., Stevenson, C. T. E., O'Driscoll, B., and Petronis, M. S. (2012), 'Local and regional controls on the lateral emplacement of the Ben Hiant Dolerite intrusion, Ardnamurchan (NW Scotland)', *Journal of Structural Geology,* 39 (0), 66-82.

Mamtani, M. A. and Greiling, R. O. (2005), 'Granite emplacement and its relation with regional deformation in the Aravalli Mountain Belt (India)—inferences from magnetic fabric', *Journal of Structural Geology,* 27 (11), 2008-29.

Martin-Hernandez, F. and Hirt, A. M. (2003a), 'The anisotropy of magnetic susceptibility in biotite, muscovite and chlorite single crystals', *Tectonophysics,* 367 (1–2), 13-28.

--- (2003b), 'The anisotropy of magnetic susceptibility in biotite, muscovite and chlorite single crystals', *Tectonophysics,* 367, 13-28.

Martin-Hernandez, F. and Ferre, E. C. (2006), 'Separation of paramagnetic and ferrimagnetic anisotropies: A review', *Journal of Geophysical Research,* 112 (B03105), 1-16.

Maxwell, J. C. (1865), 'A Dynamical Theory of the Electromagnetic Field', *Philosophical Transactions of the Royal Society of London,* 155, 459-512.

McKerrow, W. S., MaC Niocaill, C., and Dewey, J. F. (2000), 'The Caledonian Orogeny redefined', *Journal of the Geological Society,* 157 (6), 1149-54.

Mees, F., Swennen, R., Van Geet, M., and Jacobs, P. (2003), 'Applications of X-ray computed tomography in the geosciences', *Geological Society, London, Special Publications,* 215, 1-6.

Mintsa Mi Nguema, T., Trindade, R. I. F., Bouchez, J. L., and Launeau, P. (2002), 'Selective thermal enhancement of magnetic fabrics from the Carnmenellis granite (British Cornwall)', *Physics and Chemistry of the Earth, Parts A/B/C,* 27 (25–31), 1281-87.

Morin, J. (1950), 'Magnetic susceptibility of αFe_2O_3 and ΥFe_2O_3 ', *Physical Review,* 78, 819-20.

Moskowitz, B. M. (1981), 'Methods for estimating Curie temperatures of titanomagnetites from experimental Js-T data', *Earth planet Sci. Lett.,* 53 (84-88).

Moskowitz, B. M. (1993), 'High-Temperature Magnetostriction of Magnetite and Titanomagnetites', *J. Geophys. Res.,* 98 (B1), 359-71.

Moskowitz, B. P. (Unpublished), 'Hitchiker's Guide to Magnetism', *Environmental Magnetism Workshop, 5th-8th June 1991, Institue for Rock Magnetism, University of Minnesota, U.S.A.* .

Nagata, T. (1961), 'Rock Magnetism', *Maruzen, Tokyo*.

Nagata, T. and Kinoshita, H. (1967), 'Effect of hydrostatic pressure on magnetostriction and magnetocrystalline anisotropy of magnetite', *Physics of the Earth and Planetary Interiors,* 1 (1), 44-48.

Neel, L. (1955), 'Some theoretical aspects of rock magnetism', *Advances in Physics,* 5 (14), 191-243.

Neilson, J. C., Kokelaar, B. P., and Crowley, Q. G. (2009), 'Timing, relations and cause of plutonic and volcanic activity of the Siluro-Devonian post-collision magmatic episode in the Grampian Terrane, Scotland', *Journal of the Geological Society,* 166 (3), 545-61.

Nettleton, L. L. (1971), 'Gravity and Magnetics for Geologists and Seismologists', *SEG Books*.

Neves, S. P., Araujo, A. M. B., Correia, P. B., and Mariano, G. (2003), 'Magnetic fabrics in the Cabanas Granite (NE Brazil): interplay between emplacement and regional fabrics in a dextral transpressive regime', *Journal of Structural Geology,* 25, 441-53.

Nye, J. F. (1957), 'Physical properties of crystals', *Oxford University Press*, 322.

O'Driscoll, B., Stevenson, C. T. E., and Troll, V. R. (2008), 'Mineral Laminations in Layered Gabbro', *Journal of Petrology,* 49 (6), 1221.

O'Reilly, W. (1984), 'Rock and mineral magnetism', *Blackie*.

O'Driscoll, B., Stevenson, C. T. E., and Troll, V. R. (2008), 'Mineral Lamination Development in Layered Gabbros of the British Palaeogene Igneous Province: A Combined Anisotropy of Magnetic Susceptibility, Quantitative Textural and Mineral Chemistry Study', *Journal of Petrology,* 49 (6), 1187-221.

Olivier, P., Ameglio, L., Richen, H., and Vadeboin, F. (1999), 'Emplacement of the Aya Variscan granitic pluton (Basque Pyrenees) in a dextral transcurrent regime inferred from a

combined magneto-structural and gravimetric study', *Journal of the Geological Society,* 156 (5), 991-1002.

Ono, T., Hosomi, Y., Arai, H., and Takagi, H. (2010), 'Comparison of petrofabrics with composite magnetic fabrics of S–C mylonite in paramagnetic granite', *Journal of Structural Geology,* 32 (1), 2-14.

Owens, W. H. (1974), 'Mathematical model studies on factors affecting the magnetic anisotropy of deformed rocks', *Tectonophysics,* 24 (1–2), 115-31.

Owens, W. H. and Bamford, D. (1976), 'Magnetic, Seismic, and other Anisotropic Properties of Rock Fabrics', *Philosophical Transactions of the Royal Society of London. Series A, Mathematical and Physical Sciences,* 283 (1312), 55-68.

Owens, W. H. and Rutter, E. H. (1978), 'The development of magnetic susceptibility anisotropy through crystallographic preferred orientation in a calcite rock', *Physics of the Earth and Planetary Interiors,* 16 (3), 215-22.

Owens, W. H. (2000a), 'Error estimates in the measurement of anisotropic magnetic susceptibility', *Geophysical Journal International,* 142 (2), 516-26.

--- (2000b), 'Statistical analysis of normalized and unnormalized second‐rank tensor data, with application to measurements of anisotropy of magnetic susceptibility', *Geophys. Res. Lett.,* 27 (18), 2985-88.

Parés, J. M. and van der Pluijm, B. A. (2002a), 'Evaluating magnetic lineations (AMS) in deformed rocks', *Tectonophysics,* 350, 283-98.

--- (2002b), 'Phyllosilicate fabric characterization by Low-Temperature Anisotropy of Magnetic Susceptibility (LT-AMS)', *Geophys. Res. Lett.,* 29 (24), 2215.

Parés, J. M. (2004), 'How deformed are weakly deformed mudrocks? Insights from magnetic anisotropy', *Geological Society, London, Special Publications,* 238 (1), 191-203.

Passchier, C. W. and Trouw, R. A. J. (2005), 'Microtectonics', *Springer Berlin Heidelberg New York,* 2.

Paterson, S. R., Vernon, R. H., and Tobisch, O. T. (1989), 'A review of criteria for the identification of magmatic and tectonic foliations in granitoids', *Journal of Structural Geology,* 11 (3), 349-63.

Paterson, S. R., Fowler Jr, T. K., Schmidt, K. L., Yoshinobu, A. S., Yuan, E. S., and Miller, R. B. (1998), 'Interpreting magmatic fabric patterns in plutons', *Lithos,* 44 (1–2), 53-82.

Paterson, S. R., Pignotta, G. S., and Vernon, R. H. (2004), 'The significance of microgranitoid enclave shapes and orientations', *Journal of Structural Geology,* 26 (8), 1465-81.

Perarnau, A. and Tarling, D. H. (1985), 'Thermal enhancement of magnetic fabric in Cretaceous sandstones', *Journal of the Geological Society,* 142 (6), 1029-34.

Petronis, M. S., Hacker, D. B., Holm, D. K., Geissman, J. W., and Harlan, S. S. (2004), 'Magmatic flow paths and palaeomagnetism of the Miocene Stoddard Mountain Laccolith, Iron Axis Region, Southwestern Utah, USA.', *In: Martin-Hernandez, F., Luneburg, C.M., Aubourg, C. & Jackson, M. (eds) Magnetic Fabric: Methods and Applications. Geological Society, London, Special Publications,* 238, 251-84.

Petronis, M. S., O'Driscoll, B., and Lindline, J. (2011), 'Late stage oxide growth associated with hydrothermal alteration of the Western Granite, Isle of Rum, NW Scotland', *Geochem. Geophys. Geosyst.,* 12 (1), Q01001.

Petronis, M. S., O'Driscoll, B., Stevenson, C. T. E., and Reavy, R. J. (2012), 'Controls on emplacement of the Caledonian Ross of Mull Granite, NW Scotland: Anisotropy of magnetic susceptibility and magmatic and regional structures', *Geological Society of America Bulletin,* 124, 906-27.

Petrovský, E., Kapi, and ka, A. (2006), 'On determination of the Curie point from thermomagnetic curves', *J. Geophys. Res.,* 111 (B12), B12S27.

Pharaoh, T. C., Brewer, T. S., and Webb, P. C. (1993), 'Subduction-related magmatism of Late Ordovician age in eastern England', *Geological Magazine,* 130 (5), 647-56.

Pharaoh, T. C. (1999), 'Palaeozoic terranes and their lithospheric boundaries within the Trans-European Suture Zone (TESZ): a review', *Tectonophysics,* 314 (1–3), 17-41.

Philpotts, A. R. and Asher, P. M. (1994), 'Magmatic flow-direction indicators in a giant diabase feeder dike, Connecticut', *Geology,* 22 (4), 363-66.

Pignotta, G. S. and Benn, K. (1999), 'Magnetic fabric of the Barrington Passage pluton, Meguma Terrane, Nova Scotia: a two-stage fabric history of syntectonic emplacement', *Tectonophysics,* 307 (1–2), 75-92.

Pitcher, W. S. (1982), 'Granite type and tectonic environment', *In: Hsu, K.J. (ed.) Mountain Building Processes. Academmic Press, London*, 19-40.

Porath, H. and Chamalaun, F. H. (1966), 'The magnetic anisotropy of hematite bearing rocks', *Pure and Applied Geophysics,* 64 (1), 81-88.

Potter, D. K. and Stephenson, A. (1988), 'Single domain particles in rocks and magnetic fabric analysis', *Geophys. Res. Lett.,* 15 (10), 1097-100.

Ramsay, J. G. (1967), 'Folding and Fracturing of Rocks ', *McGraw Hill, New York*.

Raposo, M. I. B., Chaves, A. O., Lojkasek-Lima, P., D'Agrella-Filho, M. S., and Teixeira, W. (2004), 'Magnetic fabrics and rock magnetism of Proterozoic dike swarm from the southern Sao Francisco Craton, Minas Gerais State, Brazil', *Tectonophysics,* 378 (1), 43-63.

Revol, J., Day, R., and Fuller, M. (1978), 'Effect of Uniaxial Stress upon Remanent Magnetisation: Stress Cycling and Domain State Dependence', *Journal of Geomagnetism and Geoelectricity,* 30 (5), 593-605.

Richter, C., Ratschbacher, L., and Frisch, W. (1993a), 'Magnetic Fabrics, Crystallographic Preferred Orientation, and Strain of Progressively Metamorphosed Pelites in the Helvetic Zone of the Central Alps (Quartenschiefer Formation)', *J. Geophys. Res.,* 98 (B6), 9557-70.

Richter, C., van der Pluijm, B. A., and Housen, B. A. (1993b), 'The quantification of crystallographic preferred orientation using magnetic anisotropy', *Journal of Structural Geology,* 15 (1), 113-16.

Robin, P.-Y. F. (2002), 'Determination of fabric and strain ellipsoids from measured sectional ellipses — theory', *Journal of Structural Geology,* 24 (3), 531-44.

Robion, P., Averbuch, O., and Sintubin, M. (1999), 'Fabric development and metamorphic evolution of lower Palaeozoic slaty rocks from the Rocroi massif (French–Belgian Ardennes): new constraints from magnetic fabrics, phyllosilicate preferred orientation and illite crystallinity data', *Tectonophysics,* 309 (1–4), 257-73.

Rochette, P. (1987), 'Magnetic susceptibility of the rock matrix related to magnetic fabric studies', *Journal of Structural Geology,* 9 (8), 1015-20.

--- (1988), 'Inverse magnetic fabric in carbonate-bearing rocks', *Earth and Planetary Science Letters,* 90 (2), 229-37.

Rochette, P. and Fillion, G. (1988), 'Identification of multicomponent anisotropies in rocks using various field and temperature values in a cryogenic magnetometer', *Physics of the Earth and Planetary Interiors,* 51 (4), 379-86.

Rochette, P., Jackson, M. J., and Aubourg, C. (1992), 'Rock magnetism and the interpretation of anisotropy of magnetic susceptibility', *Reviews of Geophysics,* 30, 209-26.

Rochette, P., Aubourg, C., and Perrin, M. (1999), 'Is this magnetic fabric normal? A review and case studies in volcanic formations', *Tectonophysics,* 307 (1–2), 219-34.

Rosenberg, C. L. and Handy, M. R. (2005), 'Experimental deformation of partially melted granite revisted: implications for the continental crust', *Journal of Metamorphic Geology,* 23, 19-28.

Rozenson, I., Spiro, B., and Zak, I. (1982), 'Transformation of Iron-bearing Kaolinite to Iron-free Kaolinite, Goethite and Hematite', *Clays and Clay Minerals,* 30 (3), 207-14.

Schulmann, K., Jezek, J., and Venera, Z. (1997), 'Perpendicular linear fabrics in granite: markers of combined simple shear and pure shear flows?', *In: Bouchez, J.L., Hutton, D.H.W., Stephens, W.E., (eds.), Grantie: From Segregation of Melt to Emplacement Fabrics, Kluwer Academic Publishers, Dordrecht*, 159-76.

Scotese, C. R. and McKerrow, W. S. (1990), 'Revised World maps and introduction', *Geological Society, London, Memoirs,* 12 (1), 1-21.

Shelley, D. (1993), 'Igneous and metamorphic rocks under the microscope.', *Chapman & Hall*.

Soper, N. J. and Hutton, D. H. W. (1984), 'Late Caledonian sinistral displacements in Britain: Implications for a three-plate collision model', *Tectonics,* 3 (7), 781-94.

Soper, N. J., Webb, B. C., and Woodcock, N. H. (1987), 'Late Caledonian (Acadian) transpression in north-west England: timing, geometry and geotectonic significance', *Proceedings of the Yorkshire Geological Society,* 46 (3), 175-92.

Soper, N. J., Strachan, R. A., Holdsworth, R. E., Gayer, R. A., and Greiling, R. O. (1992), 'Sinistral transpression and the Silurian closure of Iapetus', *Journal of the Geological Society,* 149 (6), 871-80.

Stacey, F. D. (1960), 'Magnetic Anisotropy of Rocks', *Journal of Geophysical Research,* 54, 2429-42.

Stacey, F. D. (1963), 'The physical theory of rock magnetism', *Advances in Physics,* 12 (45), 45-133.

Stacey, F. D. and Banerjee, S. K. (1974), 'The physical principles of rock magnetism', *Amsterdam, New York, Elsevier Scientific Pub. Co.. Developments in solid earth geophysics,* 5.

Steenken, A., Siegesmund, S., and Heinrichs, T. (2000), 'The emplacement of the Rieserferner Pluton (Eastern Alps, Tyrol): constraints from field observations, magnetic fabrics and microstructures', *Journal of Structural Geology,* 22 (11–12), 1855-73.

Stephenson, A. (1994), 'Distribution anisotropy: two simple models for magnetic lineation and foliation', *Physics of the Earth and Planetary Interiors,* 82 (1), 49-53.

Stevenson, C. T. E., Owens, W. H., and Hutton, D. H. W. (2007), 'Flow lobes in granite: The determination of magma flow direction in the Trawenagh Bay Granite, northwestern Ireland, using anisotropy of magnetic susceptibility', *Geological Society of America Bulletin,* 119 (11-12), 1368-86.

Stevenson, C. T. E. (2008), 'A Revised intrusion sequence for the Donegal Batholith: evidence from its aureole in Lettermacaward', *Irish Journal of Earth Sciences,* 26, 33-43.

Stevenson, C. T. E., Hutton, D. H. W., and Price, A. R. (2008a), 'The Trawenagh Bay Granite and a new model for the emplacement of the Donegal Batholith', *Earth and Environmental Science Transactions of the Royal Society of Edinburgh,* 97 (4), 455-77.

Stevenson, C. T. E., O'Driscoll, B., Holohan, E. P., Couchman, R., Reavy, R. J., and Andrews, G. D. M. (2008b), 'The structure, fabrics and AMS of the Slieve Gullion ring-complex, Northern Ireland: testing the ring-dyke emplacement model', *Geological Society, London, Special Publications,* 302 (1), 159-84.

Stevenson, C. T. E. (2009), 'The relationship between forceful and passive emplacement: The interplay between tectonic strain and magma supply in the Rosses Granitic Complex, NW Ireland', *Journal of Structural Geology,* 31 (3), 270-87.

Stevenson, C. T. E. and Bennett, N. (2011), 'The emplacement of the Palaeogene Mourne Granite Centres, Northern Ireland: new results from the Western Mourne Centre', *Journal of the Geological Society,* 168 (4), 831-36.

Strangway, D. W., McMahon, B. E., and Honea, R. M. (1967), 'Stable Magnetic Remanence in Antiferromagnetic Goethite', *Science,* 158 (3802), 785-87.

T.G., B. (2000), 'Deformation microstructures and mechanisms in minerals and rocks', *Kluwer Academic Publishers, Dordrecht*, 150.

Takahashi, M., Anamaki, S., and Ishikawa, S. (1980), 'Magnetite series/ilmenite series vs. Itype/S type granitoids', *In: Ishikawa, S. and Takenouchi, S. (eds.). Granitic Magmatism and Related Mineralisation. Special issue Mining Geology Japan,* 8, 13-28.

Takahashi, M. and Noguchi, S. (2003), 'Three-dimensional fabric and texture analysis in granitic rocks using microfocus Xray-CT', *American Geophysical Union, Fall Meeting 2003, Abstract*.

Tarasov, L. P. (1939), 'Dependence of ferromagnetic anisotropy on the field strength', *Physics Review,* 56 (12), 1224-30.

Tarling, D. H. (1983), 'Palaeomagnetism: principles and applications in geology, geophysics and archaeology', *Chapman & Hall*.

Tarling, D. H. and Hrouda, F. (1993), 'The Magnetic Anisotropy of Rocks', *Chapman & Hall*.

Tauxe, L. (1998), 'Paleomagnetic principles and practice', *Kluwer Academic Publishers, Dordrecht*, 299.

--- (2002), 'Paleomagentic Principles and Practice', *Springer Berlin Heidelberg New York*.

Thompson, R. and Oldfield, P. (1986), 'Environmental Magnetism', *Allen & Unvin, London*.

Torsvik, T. H., Smethurst, M. A., Meert, J. G., Van der Voo, R., McKerrow, W. S., Brasier, M. D., Sturt, B. A., and Walderhaug, H. J. (1996), 'Continental break-up and collision in the Neoproterozoic and Palaeozoic — A tale of Baltica and Laurentia', *Earth-Science Reviews,* 40 (3–4), 229-58.

Trench, A. and Torsvik, T. H. (1992), 'The closure of the Iapetus Ocean and Tornquist Sea: new palaeomagnetic constraints', *Journal of the Geological Society,* 149 (6), 867-70.

Trindade, R. I. F., Bouchez, J.-L., Bolle, O., Nédélec, A., Peschler, A., and Poitrasson, F. (2001), 'Secondary fabrics revealed by remanence anisotropy: methodological study and examples from plutonic rocks', *Geophysical Journal International,* 147 (2), 310-18.

Usui, Y., Nakamura, N., and Yoshida, T. (2006), 'Magnetite microexsolutions in silicate and magmatic flow fabric of the Goyozan granitoid (NE Japan): Significance of partial remanence anisotropy', *J. Geophys. Res.,* 111 (B11), B11101.

Valley, P. M., Hanchar, J. M., and Whitehouse, M. J. (2011), 'New insights on the evolution of the Lyon Mountain Granite and associated Kiruna-type magnetite-apatite deposits, Adirondack Mountains, New York State', *Geosphere,* 7 (2), 357-89.

Van der Molen, I. and Paterson, M. S. (1979), 'Experimental deformation of partially-melted granite', *Contributions to Mineralogy and Petrology,* 70 (3), 299-318.

van Staal, C. R., Dewey, J. F., Niocaill, C. M., and McKerrow, W. S. (1998), 'The Cambrian-Silurian tectonic evolution of the northern Appalachians and British Caledonides: history of a complex, west and southwest Pacific-type segment of Iapetus', *Geological Society, London, Special Publications,* 143 (1), 197-242.

Varga, R. J., Gee, J. S., Staudigel, H., and Tauxe, L. (1998), 'Dike surface lineations as magma flow indicators within the sheeted dike complex of the Troodos Ophiolite, Cyprus', *J. Geophys. Res.,* 103 (B3), 5241-56.

Vegas, N., Naba, S., Bouchez, J., and Jessell, M. (2008), 'Structure and emplacement of granite plutons in the Paleoproterozoic crust of Eastern Burkina Faso: rheological implications', *International Journal of Earth Sciences,* 97 (6), 1165-80.

Vernon, R. H. (2004), 'A practical guide to Rock Microstructure', *Cambridge University Press*, 43-165.

Verwey, E. J. W. (1939), 'Electronic Conduction of Magnetite (Fe3O4) and its Transition Point at Low Temperatures', *Nature,* 144, 327-28.

Verwey, E. J. W. and Haayman, P. W. (1941), 'Electronic conductivity and transition point of magnetite ("Fe3O4")', *Physica,* 8 (9), 979-87.

Vigneresse, J.-L., Tikoff, B., and Améglio, L. (1999), 'Modification of the regional stress field by magma intrusion and formation of tabular granitic plutons', *Tectonophysics,* 302 (3–4), 203-24.

Vigneresse, J. L. (1990), 'Use and misuse of geophysical data to determine the shape at depth of granitic intrusions', *Geological Journal,* 25 (3-4), 249-60.

Vincenz, S. A. (1965), 'Frequency Dependence of Magnetic Susceptibility of Rocks in Weak Alternating Fields', *J. Geophys. Res.,* 70 (6), 1371-77.

Waters, A. C. (1960), 'Determining Direction of Flow in Basalts', *American Journal of Science,* 258-A, 350-66.

Whittaker, E. T. (1951), ' A History of the Theories of Aether and Electricity', *Dover Publications*, 34.

Williams, H. J. (1937), 'Magnetic properties of single crystals of silicon iron', *Physics Review,* 52, 747-51.

Wolff, J. A., Ellwood, B. B., and Sachs, S. D. (1989), 'Anisotropy of magnetic susceptibility in welded tuffs: application to a welded-tuff dyke in the tertiary Trans-Pecos Texas volcanic province, USA', *Bulletin of Volcanology,* 51 (4), 299-310.

Xu, S. and Dunlop, D. J. (1995), 'Toward a better understanding of the Lowrie-Fuller test', *J. Geophys. Res.,* 100 (B11), 22533-42.

Žák, J., Hrouda, F., and Holub, F. V. (2010), 'Plane-confined magnetic lineations in mingled mafic and felsic magmas, the Sázava pluton, Bohemian Massif', *Journal of Volcanology and Geothermal Research,* 190 (3–4), 312-24.